Molecular Design of Side Group Liquid Crystal Polymers: Understanding Their Interactions with Small-Molecule Liquid Crystal Solvent

Thesis by

Zuleikha Kurji

In Partial Fulfillment of the Requirements

for the Degree of

Doctor of Philosophy

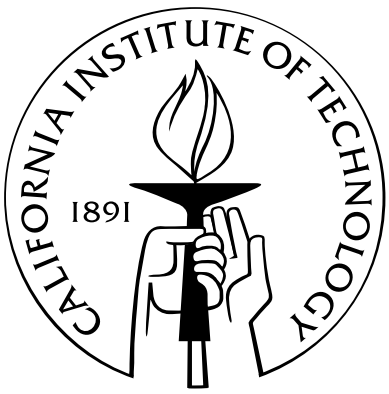

California Institute of Technology

Pasadena, California

2013

(Defended June 10, 2013)

Dedicated to my parents, Amin and Zarina Kurji.

Acknowledgements

This thesis would not have been possible without the aid and support of countless people over the years, and I take immense pleasure in being able to thank them here.

In my case, I feel like I would be remiss in not thanking my thesis committee first: Professors Bill Goddard, Bob Grubbs, Dave Tirrell, and my advisor, Julie Kornfield, who were always available when I had questions or needed advice. I particularly want to thank my original candidacy committee, Bob, Bill, and Julie, who saw me through a pretty rough beginning but had enough faith in me to let me continue. I hope that I've justified their decision.

I need to thank my advisor, Julia A. Kornfield. From Julie, I also learned how to be a better scientist: how to listen when data is speaking to you and how to place our research into the big picture. Julie has also, time and time again, has gone above and beyond the call of advisorly duty for me, and I am beyond grateful for her help throughout my graduate career. One of Julie's favorite life lessons that she passes down is to "avoid Icky People." Not only is it good advice that has served me well throughout my graduate career, and, I expect, beyond, but: Julie, you are the farthest from an icky person that I've ever known, and I'm proud to have graduated from your group. If I'm ever in a position to manage or mentor others, I hope I can do it with even half the compassion and support that you have. Thank you, Julie, for the time, effort, and energy that you put into my scientific development and my graduate career.

The work in this thesis would not have been possible without Dr. Michael D. Wand of LC Vision. Along

with intellectual collaboration, material assistance in synthesis, and use of his laboratory equipment, Michael also participated, along with Julie and me, in the writing of three collaborative NSF grant proposals, which, when they were funded, became my primary means of support for the last half of my graduate years.

Paul Pirogovsky and Dr. Rohan Hule also made intellectual contributions to this thesis. Paul, Rohan and I worked together on the neutron scattering project(s) described here. Paul also helped design, build, and put together a number of instruments that made this thesis possible, in particular, the temperature controller that I used for my x-ray scattering experiments along with the temperature controller that Paul, Rohan, and I used for our neutron scattering experiments. Dr. Neal R. Scruggs and Dr. Rafael Verduzco overlapped with me on this project during my first years at Caltech, I learned polymer synthesis and deuterated solvent synthesis from them both. I also went on my first neutron scattering trips with Neal and Rafael, where they taught me the ropes during their experiments. Neal and Rafael also initiated the diblock copolymer project that Paul, Rohan and I picked up and ran with – we even used material that Neal and Rafael synthesized during their tenures as graduate students in Julie's group (Chapter 5). In this vein, I'd also like to thank Dr. Mike Kempe, who I've never met, but am grateful to nonetheless, for initiating the SGLCP project in the Kornfield group.

Professionally, I'd also like to thank Jyotsana Lal and Ed Lang at Argonne National Lab's IPNS, Boualem Hammouda and John Barker at NIST's NCNR, Ken Littrel, Lisa Debeer-Schmit, and Kathy Bailey at Oak Ridge National Laboratory's High Flux Isotope Reactor, Rex Hjelm and Monika Hartl at Los Alamos National Laboratory's LANSCE, Alex Hexemer and Lawrence Berkeleys Advanced Light Source, and Xiaobing Zuo at Argonne National Labs Advanced Photon Source for their assistance and mentoring at the various scattering experiments that I've carried out over the years. Professor Noel Clark, at the University of Colorado at Boulder, Professor George Rossman at Caltech, Torsten Hegmman at the University of Manitoba in Canada, Professor Phillip Chen at National Chaio Tung University,

in Taiwan, and Professor Soo-Young Park at Kyungpook National University, in Korea also gave assistance and advice up to and including experiments performed in their laboratories.

The Kornfield group has been a place of scientific growth and support for me, and I'm grateful to past and present graduate students and postdocs: Dr. Eric A. Pape, Dr. Charles S. Nickerson, Dr. Derek W. Thurman, Dr. Lucia Fernandez-Ballester, Dr. Neal R. Scruggs, Dr. Rafael Verduzco, Dr. Michael J. Mackel, Dr. Matthew S. Mattson, Dr. R. L. Ameri David, Dr. Ryan Turner, Dr. Shuicui Kimata, Dr. Yan Xia, Dr. Diana Smirnova, Dr, Joyce Huynh, Jeremy Wei, Dr. Keesu Jeon, Dr. Bahar Bingol, Dr. Bradley D. Olsen, Dr. Rohan Hule, Dr. Ladan Foose, Dr. Ruoyu Zhang, Paul Pirogovsky, Iman Hajimorad, Zachary Williams, Artemis Ailianou, Amy Fu, Dennis Ko, Wendy Gu, Boyu Li and Joey Kim. We've also been fortunate to work with some talented visitors: Professor Robert Tanner, Professor Soo-Young Park, Dr. Yasutoyo Kawashima, Dr. Manabu Kato, Vanessa Rodriguez, Dr. Dong-yul Lee, Dr. Markus Cudaj, Dr. Adelia Grzbowski, Dr. Wei Sun and Yuchen Zhou. (If I've missed any past or present member of the Kornfield group, I sincerely apologize, its not due to your lack of support, it's just because I've been here so long that I've overlapped with so many people).

During my graduate career, I had the pleasure of mentoring four Summer Undergraduate Research Fellows (SURFs): Neal Bansal, Lita Yang, Heejae Kim, and Nick Mackay. Not only did each my SURFs contribute to the science that I was able to do, in order to give them meaningful projects, I was required to clarify my understanding of both the big picture and the small details of experiments. This clarity has been incredibly valuable to my research career. Spending time trying to keep undergrads engaged in science was also some of the most fun I've had over an oft-difficult career.

I'd also like to thank Mike Roy and Steve Olson in the chemistry machine shop for making equipment for nearly every chapter of this thesis, in particular the heating units that I've used in x-ray and neutron scattering experiments. Thanks also to Steve Gould and his staff in Purchasing for handling the multi-

tude of chemical order forms that I've sent their way; Joe Drew, Ron Koen, and everyone in Chemistry Shipping and Receiving; Rick from the glass shop, Tom Dunn from the electrical shop; Dr. Scott Ross and Dr. David VanderVelde in the Liquid NMR Facility, and Suresh Gupta.

Over the course of my graduate career, I've been very grateful for the administrative support from Dian Buchness, Agnes Tong, Laura Lutz-King, Karen Baumgartener and Kathy Bubash. Keeping Julie's group running smoothly is no small feat, and I'm very grateful for Anne Hormann, Marcy Fowler, and Andrea Arias for, in their turn, keeping the Kornfield lab moving. In particular, Marcy Fowler, whose tenure in Julie's group overlapped the most with mine, and has become a friend in truth, over the years.

Participating in the Prufrock Cooking and Eating Group, the Caltech Dance Troupe, the Caltech Ballet Club, the Caltech Project for Effective Teaching, and the Caltech Women's Center have all enriched my life during my tenure as a graduate student here. Thanks are also due to Candace Rypisi, Felicia Hunt, and Portia Harris for their help, friendship, and support during (and after) their tenures as director of the Caltech Women's Center. The Women's Center, and especially the Graduate Women's Discussion Group (affectionately called "Women's Lunch," by most of us), was a great emotional stabilizer for me. Thank you also to Lee Coleman for the further emotional support when I needed it.

Along with professional mentorship, personal friendships are necessary for success in graduate school. I don't think I would have made it through graduate school without Teresa Emery, Chi Wang, Nathalie Vriend, Harmony Gates, Artemis Ailianou, Heather McCaig, and Ryan Turner. In so many different ways, the people listed here have been, and still are, examples to me. Without them, life at Caltech would have been very different for me. It was chance that put me in the same suite as Teresa in my first year, but without that chance, my whole life would have been different. I may never have met Chi Wang (one of the greatest friends I'll ever have), joined Prufrock (where the cooking, eating, and socializing kept me sane), or met Chris W. Teresa, I guess I have you to thank for my friendships, my sanity, AND

my love life. I'm not sure how I can ever thank you enough.

So much gratitude to Chris Walker, too, for always being there, even when he was far away. Thanks for the endless understanding and support because, not only did I need every ounce of it, but I appreciated it all so much.

My siblings, Ayisha (the original Dr. Kurji in our family) and Adil (also soon-to-be a Dr. Kurji, if he stays on the path he's on at the time of this writing), and my brother-in-law, Naheed (neither a Kurji nor a Dr., but we love him anyway), have all laughed with me, been silly with me, and just make me so darn happy most of the time. When I was in undergrad, my Psych 101 professor gave us a thought excercize: choose two people from our lives that we'd most want in the hospital bed next to us if we were both immobilized and could never get away from them. It turns out that this exercise was a way of telling you who in your life that you most want to be like, and I always thought it was telling that I chose Ayisha and Adil. Nowadays, I'd add Naheed and Chris to that list without question.

Finally, I have to thank my parents. I have never felt anything but support from them both. When I was having trouble in graduate school, they never suggested that I do anything but what was right for me, even if it meant quitting. Their quiet faith in me and in my ability to know myself is a support that has never felt like silent pressure, only like a buoy holding me up. Mom and Dad, for a lot of my life, I've wanted nothing more than to make you proud, and it humbled me when I realized that I don't have to be anything other than what I am to make you proud. With this kind of launch pad, I can't imagine how high I can go.

Abstract

Liquid crystal (LC) gels – the combination of macromolecules with small molecule LCs – couple the elasticity and mechanical strength of polymers to the order inherent to LCs and are attractive to many researchers hoping to marry liquid crystals' optical and electro-optical responsiveness with polymers' mechanical strength and ease of processing. In particular, side-group liquid crystal polymers (SGLCPs) are flexible-chain polymers that are functionalized with LC side-groups. Here we introduce the concept of polymer dopants: homogenously dissolved LC-containing SGLCP homopolymers that are molecularly designed for solubility in and coupling to small molecule LC solvents. Using polymer analogous chemistry (changing the molecular makeup of the side groups and their linkers, while keeping backbone molecular weight, polydispersity index, and degree of polymerization constant), we've targeted the effect of side-group orientation, dipole position and strength, spacer length and linking-group type on polymer solubility and bulk material properties. We've shown that, at low concentration, these dopants can have significant effects on the bulk material properties of two types of LCs: ferroelectric and vertically aligned nematic LCs.

Contents

List of Figures

List of Schemes

List of Tables

Chapter 1

Introduction

1.1 Background

1.1.1 Liquid Crystals

Liquid crystal phases (Figure 1.1, center) are intermediate phases of matter that fall between the solid, or crystal, phase and the isotropic liquid phase. The crystalline phase (Figure 1.1, left) and the liquid phase (Figure 1.1, right) are two of the three most familiar states of matter: in a crystalline solid the constituent molecules are constrained in both their orientation and position, while in a liquid they lack both the orientational constraint and long-range correlation [1]. Molecules in a solid thus possess both orientational and positional order, while the molecules in a liquid have neither. The lack of rigid arrangement of molecules in the liquid phase means they are free to randomly diffuse, allowing liquids to flow, take the shape of their container, and be deformed in response to weak outside forces [1]. The molecules in liquid crystal phases also flow, like the molecules in a liquid, but possess a small amount of additional order, like the molecules in a solid (Figure 1.1) [1].

The solid-to-liquid crystalline phase transition generally requires much more energy than a typical liquid crystalline-to-liquid phase transition, implying that most of the order present in the solid phase is lost

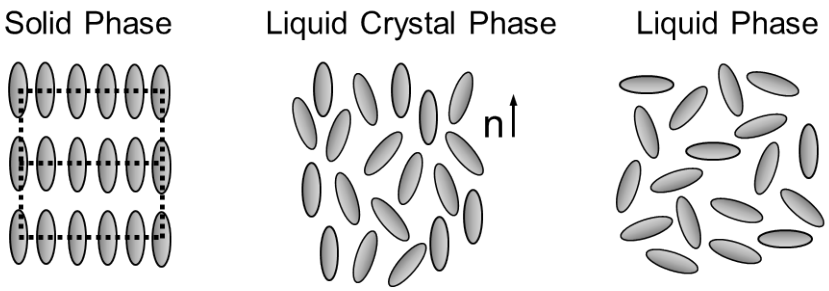

Figure 1.1. In the solid phase, the molecules (represented here by gray rods) have both orientational and positional order. When heated, certain molecules pass through a progression of partially ordered liquid crystalline phases, one of which is shown here: in this case losing positional order, but remaining oriented in a preferred direction called the director, *n*. After further heating, the molecules become liquid – having neither long-range positional order nor orientational correlations.

in the transition to the liquid crystal phase. This small amount of additional order retained in the liquid crystalline phase is then lost at the liquid crystal-to-liquid phase transition

Certain molecules, or families of molecules, are more likely to have liquid crystalline phases. Specifically, two conditions are generally satisfied for a molecule to display an LC phase: a rigid, anisotropic core gives the molecule order while flexible tail group(s) allow the molecules to flow. Calamitic liquid crystals, for example, are rigid, rod-shaped molecules with an elongated conformation (*i.e.*, significantly longer than they are wide) that allows for preferential alignment of their long axes along one spatial direction. The average direction of the long axes of the molecules in an LC phase is called the director (*n*) (Figure 1.1, middle). Energetically, when elongated molecules are aligned parallel to each other they tend to have stronger attractive forces

An elongated structure can be accomplished by connecting two or more rigid cyclic units (*i.e.*, phenyl groups) in a manner that results in an overall planar conformation. For example, these cyclic units are often linked together with moieties that tend to restrict the molecules overall freedom of rotation (*i.e.*, multiple bonds: -(CH=N)-, -N=N-, -(CH=CH)n-, -CH=N-N=CH-, etc.). Multiple bonds also contribute pi-electrons that can conjugate with the phenylene rings and enhance the overall anisotropic polarizability of the molecule . Figure 1.2 shows the molecular structure of 4'-*n*-pentyl-4-cyanobiphenyl ("5CB"),

which has an LC phase at room temperature, making it a frequently studied LC. 5CB, made up of a rigid biphenyl core, a flexible hydrocarbon tail, and a permanent dipole moment (contributed by the cyano-moiety), has an anisotropic, rodlike structure with a long axis of 20 Å and a short axis of 5 Å.

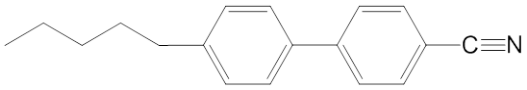

Figure 1.2. 5CB, calamitic (rodlike) liquid crystal widely used in laboratory studies, contains a rigid core and a flexible tail and is in a liquid crystalline phase at room temperature. 5CB is anisotropic: one axis (called the "long axis") is longer than the other (called the "short axis"). Calamitic LCs like 5CB are often represented as rod-like cartoons in schematic representations.

There are many liquid crystalline phases, but there are three, in particular, that are relevant to this thesis, the nematic, the smectic A (SmA) and the smectic C (SmC) phases (Figure 1.3). Molecules in the nematic LC phase (Figure 1.3, left), the simplest LC phase, only have orientational order: the nematic molecules point on average along a common axis, the director (n). Smectic liquid crystalline phases have orienational order, but also possess positional order: the molecules are arranged in layers. In the SmA phase (Figure 1.3, center) the molecules in the layers point, on average, parallel to the layer normal, while in the SmC phase (Figure 1.3, right) they are tilted off that axis. Unlike some other smectic phases, the molecules in the SmA and SmC phases can randomly diffuse within each plane – no positional order thus exists within these planes [1].

The molecular orientation of LC molecules around the director is not perfect. Rather, the director can be thought of as an indication of the average orientation of LC molecules at a given moment in time (or the time-averaged orientation of a single molecule). The distribution of molecular orientations is characterized by a thermodynamic order parameter, S, which quantitatively specifies the orientational order of an LC system: a perfectly ordered system has an order parameter of 1, while a completely isotropic system has an order parameter of 0 [2]. For example, in a nematic LC, the angle between the director and the local orientation of the molecules is typically around 30°, while the angle in a

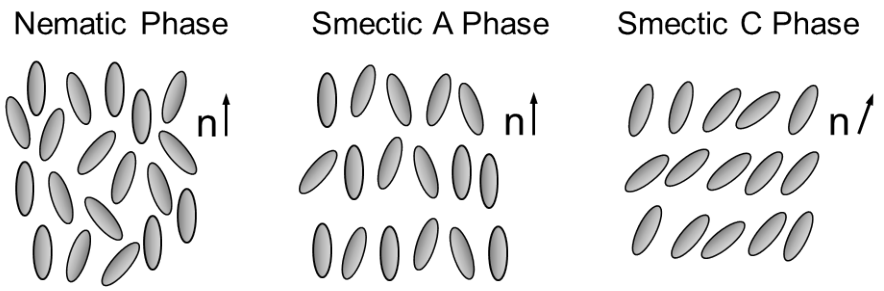

Figure 1.3. Molecules in the nematic liquid crystalline phase display orienational order. The director, n, is parallel to the average direction of molecular alignment. Smectic liquid crystalline phases are found at lower temperatures than the nematic phase and are defined by the formation of well-defined layers (positional order) as well as having their molecules point on average in a one direction (orientational order). In the smectic A phase, the director is paralell to the layer normal, while in the smectic C phase, the director is tilted.

smectic LCs is typically around 20°, corresponding to order parameters of 0.6 and 0.8, respsectively. The strength of LC order, and hence the value of the order parameter, is related to the anisotropy of physical properties displayed by LCs, such as birefringence or dielectric anisotropy [2].

Because LCs are composed of anisotropic molecules, their interactions with external fields and surfaces can strongly influence their properties. For example, LCs exhibit dielectric anisotropy ($\Delta\epsilon$) -where the dipole moment along the long axis that does not equal the dipole moment along the short axis - making them susceptible to electric fields. The breaking of isotropic symmetry also gives rise to optical birefringence (anisotropic refractive indices), diamagnetic anisotropy, and orientational elasticity. LC's anisotropic optical properties, for example, can be exploited in temperature sensitive applications: birefringence disappears at the LCs nematic-to-isotropic phase transition temperature inherent to LCs, enabling nematic LCs to change from bright (birefringent) to dark under crossed polars at a threshold temperature (the LC phase transition temperature) [3]. When the LC molecules are chiral, a color change with temperature is seen throughout the materials' LC phase. This effect has been used in several commercial applications including mood rings [1], swimming pool and fish tank thermometers [4], disposable medical thermometers [4] and hotspot detectors for the failure analysis of integrated circuits [5] [6].

Liquid crystal displays (LCDs), arguably the most well-known application of LCs, are made possible due to the coupling of order to fluidity: the LCs anisotropic dielectric properties make LC's anisotropic optical properties accessible, while LC fluidity allows for the orienting electric fields to be small (*i.e.*, readily accessible) [7]. In these cases, the alignment of the bulk LC in the applied electric field is dictated by a combination of the interactions between the LC and the field, the aligning surface and the elastic interactions with other LC molecules [7]. A more detailed description of commercial LCDs can be found in section 1.1.3.

1.2 Side-Group Liquid Crystal Polymers

Side-group liquid crystal polymers (SGLCPs) are flexible-chain polymers that are functionalized with liquid crystalline (LC) side-groups. Because the side-groups contain a liquid crystal mesophase-forming group, called a mesogen, the SGLCP exhibits unique properties that arise from the coupling of the orientational order inherent in the LC side group to the entropically driven flexibility of the polymer backbone [8]. Ideally, then, SGLCPs can combine the functionality of conventional LCs with the advantages of polymer systems [8] [9] [10] [11]. SGLCPs are soluble in LC phases, while random-coil polymers are typically not [12]. This allows SGLCPs to be used as additives in LCs to stabilize structure, or enhance electro-optical response.

In contrast to random coil polymers in good solvents (Figure 1.4, left), SGLCPs adopt an anisotropic conformation upon dissolution in a small-molecule LC (Figure 1.4, center, right) [13]. The extent of the anisotropy depends on the LC order parameter, which in turn depends on the temperature of the system. The ability to control polymer conformation using temperature has led to a number of possible applications including shape-memory LCs systems [14] [15] [16] [17] [18].

There are three structural features of SGLCPs that can have significant impact on the polymers' mate-

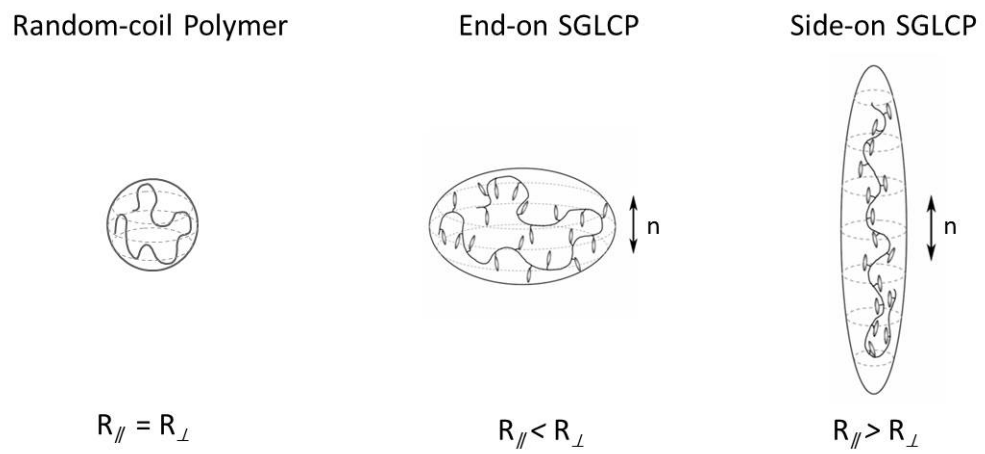

Figure 1.4. When dissolved in small molecule nematic liquid crystal, random-coil polymers (left) display isotropic conformations ($R_{\|} = R_{\perp}$), while end-on SGLCPs, with mesogens perpendicular to the polymer backbone (center), typically show an oblate conformation ($R_{\|} < R_{\perp}$), and side-on SGLCPs, with mesogens parallel to the polymer backbone (right), typically show a prolate conformation ($R_{\|} > R_{\perp}$).

rial properties: the polymer backbone, the mesogenic side group –both its chemical structure and the manner in which it is attached to the backbone (emphe.g., either at the center or the end of the mesogen) and, finally, the chemical structure and length of group that links the side groups to the polymer backbone. One of the most common (and historical) ways to make an SGLCP is the functionalization of a polysiloxane backbone, a system first devised by Finkelmann *et al.* [19]. Mesogenic side groups are grafted onto already synthesized polyalkylsiloxane backbones (for example poly(methylhydrosiloxane)) using platinum catalyzed hydrosilation to attach a side group to as many silane hydrogens as desired, often resulting in a mesoenic group in nearly every repeat group. Polysiloxane SGLCPs are generally transparent and have low glass transition temperatures, making them ideal for many applications [20].

Grafting side groups onto an already polymerized backbone is called polymer analogous chemistry. This method allows one to predetermine the molecular weight and degree of polymerization of an SGLCP – a particularly useful tool when targeting the effect of side group structure on material properties: polymers with different side groups but the same backbone characteristics can be synthesized. In addition to the polyalkylsiloxane backbone, polymer analogous chemistry has also been used to make SGLCPs with

hydrocarbon backbones: 1,2-polybutadiene's pendant vinyl group, for example, can be modified with mesogenic side groups using a variety of chemistries [9] [21] [22]. The polybutadiene is polymerized by anionic polymerization, making high molecular weight and low polydispersity index SGLCPs accessible. Increasing polymer molecular weight generally allows for the use of lower polymer concentrations to achieve similar effects, without the concomitant increase in rotational viscosity (and hence lower switching speed) that comes with increasing polymer concentration [23]. Polymer analogous chemistry using the 1,2-polybutadiene polymer backbone is thus the synthetic method of choice for the SGLCPs reported in this thesis.

Mesogen-containing monomers with polymerizable groups can also be directly polymerized into SGLCPs. Polyacrylates and polyolefins are common hydrocarbon backbones polymerized this way. This method yields lower molecular weight polymer (on the order of 2 to 20 kg/mol), but offers a broader choice of side group and spacers.

Rodlike mesophase-forming side groups can be attached to the polymer backbone, either terminally, giving "end-on" SGLCPs, or at their center, giving "side-on" SGLCPs. The molecular structure of the side groups is chosen both to confer liquid crystalline behavior to the SGLCP and to be soluble in small molecule LC solvents. Much like small molecule LCs, SGCLP side groups are typically made up of rigid core combined with a flexible part either an alkyl spacer or an alkyl tail, or both. A common method to achieve good solubility in small molecule LC solvents is to use side groups with structures similar to that of the solvent [19]. For example, the Kornfield group has used cyanobiphenyl-based side groups in SGLCPs designed to dissolve in 5CB [8] [9] [13] [22] [24] [12].

The mesogenic side groups are attached to the polymeric backbones by means of a linking group that often includes a flexible alkyl spacer. These flexible spacers decouple the dynamics of the polymer backbone from that of the mesogenic side groups, allowing the polymer to display liquid crystalline phases

in the bulk [10]. Decoupling the motions of the mesogens from the backbone gives greater entropy to the system, making the LC mesophases more thermally accessible and decreasing the polymer's glass transition temperature (T_g). In addition, the increased mobility leads to a greater entropy of solvation, making SGLCPs more soluble in small molecule LCs than their analogous main chain LCPs [23].

When dissolved in an LC solvent, the thermodynamic behavior of the polymer backbone is quite different from that of the mesogenic side groups: the backbone is driven by maximization of conformational entropy to be disordered and coil-like, while side groups are driven by maximization of their enthalpic interactions to self-assemble into ordered structures [10]. When an SGLCP is dissolved in a liquid crystal solvent, the order of the LC along with interactions between adjacent side groups can affect flexibility and orientation of the polymer chain segments [23]. For example, in a nematic solvent, the mesogens in end-on SGLCP typically lie perpendicular to the polymer backbone, resulting in the polymer having a larger radius of gyration in the direction perpendicular to the director (Figure 1.4, center). This disclike, spheroid conformation is called "oblate." A side-on SGLCP (with mesogens parallel to the backbone), on the other hand, adopts a prolate ellipsoidal, or egg-shaped, conformation (Figure 1.4, right).

When systems include both macromolecules and small molecule LCs, they are called "LC gels," and are attractive to many researchers that hope to marry liquid crystals' optical and responsive properties with polymers' mechanical strength and ease-of-processing. LC gels that also show fast reorientation dynamics, and good optical uniformity, are attractive targets for the LCD industry [25], [26], [27]. Other potential applications of LC gels include miniactuators [28], [29], [30], sensors [31] [32] and optical data storage [33].

Block copolymers (BCPs) are chemically different polymers linked by covalent bonds that, by definition, tend to minimize contact surfaces between immiscible blocks by aggregating into domains [34]. Self-assembly in classical block copolymers is a known to be a compromise between the miscibility of

the blocks and the solvent and the penalty associated with the stretching of the polymer chain across the interface. As a result, the domain size is set by the molecular weight of each block and can easily be in the 10 nm range [35].

Flexible coil polymers are generally insoluble in LCs, and thus provide a driving force for phase segregation when covalently linked to SGLCPs. Coil-SGLCP block copolymers (BCPs) exhibit ordered morphologies that reflect the interplay of microphase segregation and LC order. Just as with conventional block copolymers, unfavorable thermodynamic interactions between the two blocks cause them to form microstructures that minimize the insoluble block's contact with the LC solvent. When the other block is liquid crystalline, the swollen material can show order at many length scales: from the nanometer scale (interaction on the molecular level) to upwards of hundreds of nanometers (BCP self-assembly).

Block copolymer self-assembly in LC solvent has been investigated for producing LC gels. For example, the Kornfield group has produced LC gels using the association of the end blocks of a polystyrene-SGLCP-polystyrene triblock copolymer in a small molecule nematic LC solvent as the driving force for gelation [9]. Because of their intrinsic nematic order, the SGLCP midblocks are soluble in the small molecule LC solvent, while the polystyrene end groups are less soluble and tend to aggregate together to reduce contact with the solvent – leading to a three-dimensional polymer network in the LC solvent. The macromolecular structure of these physical gels is produced in a controlled way, resulting in materials with regular and thermally reversible

1.3 Liquid Crystal Displays

LCDs have been on the commercial market since the late 1970s [4], appearing first in digital watches and calculators, then in computer monitors, televisions, and more recently in personal electronic devices like smart phones and tablet computers. In nearly all cases, the cross section of the LCD is quite simi-

lar, regardless of application (Figure 1.5). A generic LC electro-optic cell is made up of LC molecules sandwiched between two parallel glass plates spaced from 1 to 25 μm apart, using uniform spacer beads (Figure 1.5). The inner surfaces of the glass substrates are first treated with indium tin oxide (ITO), creating a transparent electrode. When a voltage is applied across the two ITO electrodes, the dipoles of LC molecules will align in the direction of the electric field, reorienting the LC molecules from their voltage-off state. In fact, it was, in part, the discovery of ITOs use as a transparent electrode during the second world war that made modern LCDs possible: previously, because of their opacity, metal electrodes could only apply a field perpendicular to the direction of the light, greatly limiting potential opto-electronic applications [4]. After the ITO layer is added, a very thin polymer alignment layer is spin-coated onto the electrode (or transistor array) and is physically rubbed in one direction: this treatment confers macroscopic orientational order to the LCs in their voltage-off state. Depending on the polymer and the surface treatment, the LCs can orient either parallel to the surface (homogenous' or "planar" alignment, Figure 1.6a), or perpendicular to the surface (homeotropic or "vertical alignment (VA)" Figure 1.6b). The cooperative ordering of LCs amplifies molecular level orientation at the anchoring surface, conferring the desired alignment to the bulk. In fact, the main differences in the various types of commercial LCDs are the type of LC material and the type and direction of the alignment layer.

Nearly 95% of LCDs on the market use nematic LCs [36]. At present, there are two main approaches used in the manufacture of nematic liquid crystal displays: the twisted nematic (TN) LCD, which uses homogenous alignment (HA, Figure 1.6a), and vertically aligned nematic (VAN) LCDs (Figure 1.6b). Another type of LCD that has shown promise in the laboratory but has yet to be widely commercialized, uses ferroelectric liquid crystals (FLC) LCD which, instead of nematic LCs, uses homogeneously aligned LCs in the smectic C phase.

TN-LCDs were the first LCDs to be manufactured [36] and, with refinements, have continued to be used today, in digital watches, cell phones, computer monitors, laptops, signage, and more [2]. In a

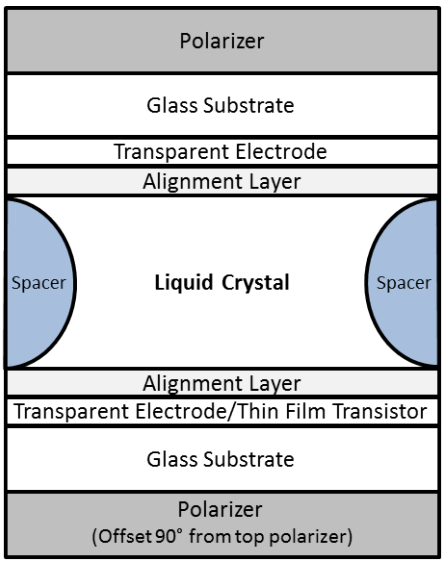

Figure 1.5. A schematic representation of a typical electro-optic LC cell. The LC layer is sandwiched between substrates that are treated with a transparent electrode, followed by a polymer alignment layer that constrains the LC to desired alignment. In a commercial LCD the bottom electrode layer is replaced by a thin-film transistor array that addresses each pixel electronically. A color filter is also placed in between the top electrode and the glass substrate to provide color to the pixels of a commercial LCD.

TN display, the alignment layers on both the top and the bottom substrate promote parallel/homogenous alignment (Figure 6a, left). However, instead of having their rubbing directions lying parallel, the top substrate is rotated 90° relative to the bottom one, orienting the LC molecules into a twisted, helix-like orientation in the bulk. When no voltage is applied, the parallel, birefringent LC molecules in the helix rotate plane polarize light, and thus appears bright when sandwiched between crossed polars (Figure 1.6). Thus, in the voltage-off state, the TN device is in the bright state. When a voltage is applied, the LCs untwist and, because their dipoles are along the long axis of the molecule, align in the direction of the electric field (perpendicular to the glass substrates). The untwisted molecules are now in homeotropic alignment, and thus not birefringent in the viewing direction, resulting in a dark state (Figure 1.6a, right). This thesis presents a strategy to improve two alternatives to TN displays: vertically aligned (VA) nematic displays, and ferroelectric (FLC) displays. Specifically using soluble SGLCP homopolymers at low concentrations to improve alignment without disrupting necessary bulk properties.

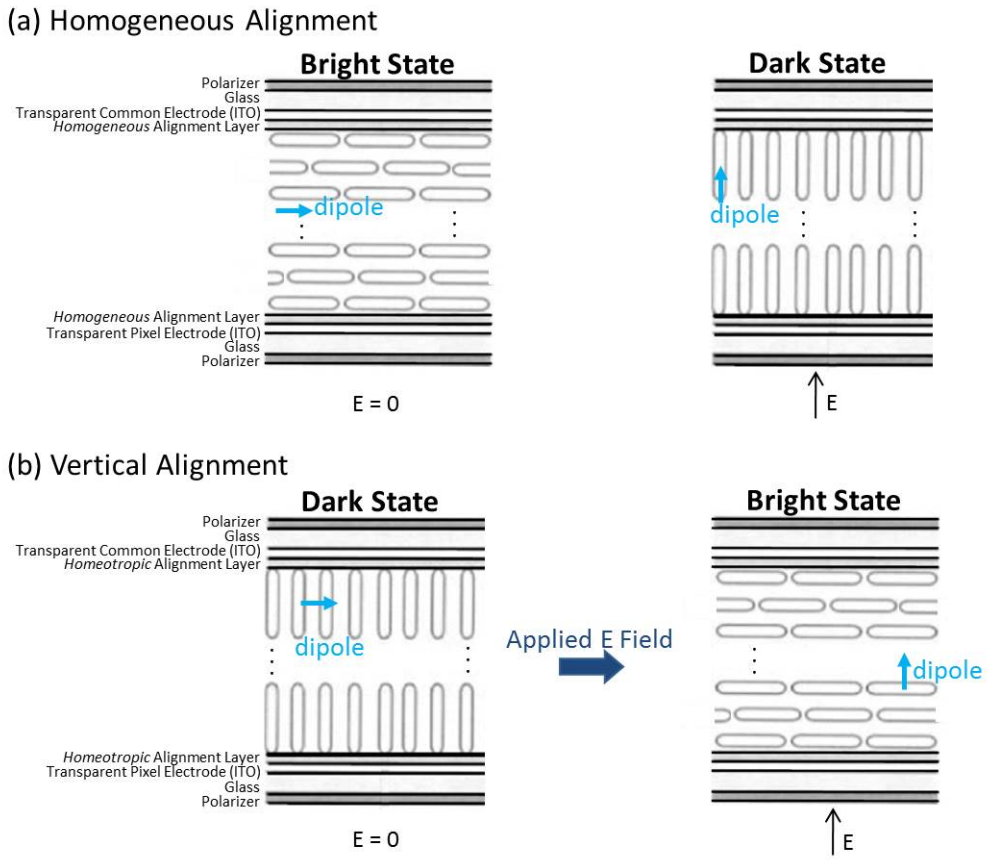

Figure 1.6. (a) Schematic of a typical homogenously aligned LC cell. In the voltage-off state, the cell is in the bright state, and when voltage is applied the molecules reorient to align their dipoles (blue arrows) in the direction of the field, resulting in homeotropic alignment, and an optical dark state. A commercial twisted nematic (TN) display, is very similar to this, but the molecules in the voltage-off state (right) are arranged in a helix, instead of the simplified version shown here. The helix untwists and aligns homeotropically (as shown here, right) when voltage is applied. (b) A vertically aligned nematic (VAN) displays voltage-off state, on the other hand, consists of homeotropically aligned molecules, resulting in a dark state. When a voltage is applied, the molecules reorient to align their dipoles in the direction of the applied field. Because the VAN molecules dipoles are transverse to the molecular axis, this leads to a homogeneous (parallel) alignment, resulting in the bright state when voltage is applied.

1.3.1 Vertically Aligned Nematic LCDs

In a vertically aligned cell, the opposite configuration relative to TN cells occurs: at rest, these LC molecules align homoetropically (typically compelled so by a hydrophobic polymer alignment layer), rendering the system into the dark state (Figure 1.6b, left). A different type of nematic liquid crystal, referred to as negative $\Delta\epsilon$ nematic, because the dielectric constant along the short axis of the LC molecule is larger than along the long axis (a negative dielectric anisotropy, $\Delta\epsilon$), called a “transverse dipole,” is

used in VA nematic displays. In contrast to homogeneously aligned nematic cells, the dipole of these LC molecules is perpendicular to their molecular axis (thus perpendicular to the glass surface). When an electric field is applied, the LC molecules reorient such that their dipoles rotate toward the direction of the electric field (*i.e.*, their molecular axes rotate toward being parallel to the glass plates), resulting in a state that is birefringent under crossed polars: the bright state (Figure 1.6b, right, note arrows labeled dipole and E).

The major commercial advantage of the VA mode, is that VA nematic displays have high contrast (large difference between light transmission in the dark state relative to that in the light state), because the LC is almost completely vertically at zero voltage, giving the cell an excellent dark state under crossed polarizers (Figure 1.6a, right). However, the very high contrast of VAN-LCDs comes at expense of the response time of the display: a pixel in a current VA nematic display takes on the order of 100 ms [2] to switch (rise time + fall time), compared to less than 20 ms for a TN display [37].

On a molecular level, the key to successful VAN devices is the transverse dipole (Scheme 1.1). The addition of groups that give transverse dipoles, for example the 2,3-difluorphenyl group (Scheme 1.1), also tends to increase the melting temperature of the system, for example, The structures shown in Scheme 1, for example have strongly negative dipoles (ranging from -2.7 for **3** to -8.6 for **8**) but many of them are crystalline solids at room temperature with melting points range from 45°C for 1 to 99°C for **7** (adding a transverse dipole tends to increase the melting temperature). When the pure compounds do have a room temperature nematic phase, they tend also to have high viscosity, leading to slow switching speeds. Synthesis of negative $\Delta\epsilon$ nematic LCs with low viscosity (*e.g.*, **8** in Scheme 1) was a breakthrough attributed to Merck [38] [39].

In Chapter 3, we show that liquid crystal polymers with negative $\Delta\epsilon$ side-groups can improve switching speed of VA LCs without harming contrast or viscocity.

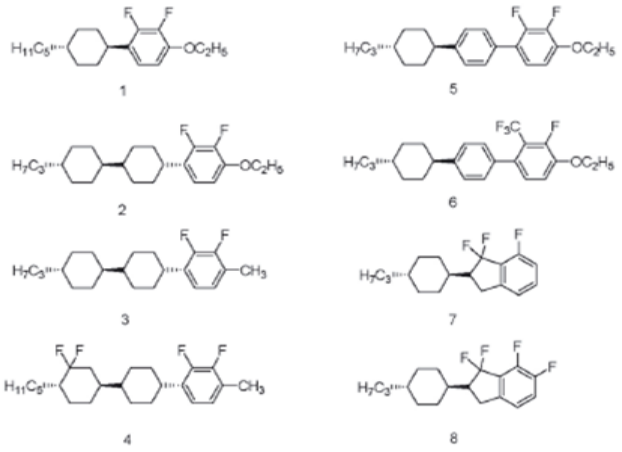

Scheme 1.1. Placing electron-withdrawing fluorine groups asymmetrically on rings that lie along the long axis of the molecules creates transverse dipole, giving negative $\Delta\epsilon$ nematic LCs.

1.3.2 Ferroelectric LCDs

In addition to LCDs that use nematic LCs, ferroelectric liquid crystals (FLCs) can also be used in LCDs. A ferroelectric material is defined as one that possesses a spontaneous electric polarization in the absence of an external electric field (Figure 1.7, pink arrow). Because of this property, ferroelectric liquid crystals have significantly faster switching speeds, dramatically lower power consumption and superior resolution when compared to nematic LCDs [40]. Chiral molecules in the Smectic C phase (tilted, layered orientation, Figure 1.3, left) have a reduced symmetry that lead to a spontaneous polarization.

When molecule in the chiral Smectic C phase are constrained to homogeneous alignment and thin spacings (on the order of 10 μm between glass plates), each molecule ends up in one of two orientations, both parallel to the aligning surface: one with the spontaneous polarization pointing “down” (parallel to the layer normal), and one with the polarization pointing “up” (Figure 1.7). Because the molecules in an FLC LCD “on-state” and “off-state” are in the same plane (as opposed to rotating to another plane, as seen in HA and VA cells) (Figure 1.7), LCDs made from FLCs do not suffer the same viewing angle problems as nematic displays. The main technical obstacles to widespread commercial application of FLCs are the manufacture of properly aligned cells, and then the further stabilization of this alignment

for the lifetime of the display device. Cells in poor alignment are marked by the formation of "zigzag defects," a light-leaking defect that renders the cell effectively useless in an LCD. The difficulty in achieving perfectly aligned FLC cells limits the size and yield of available FLC displays.

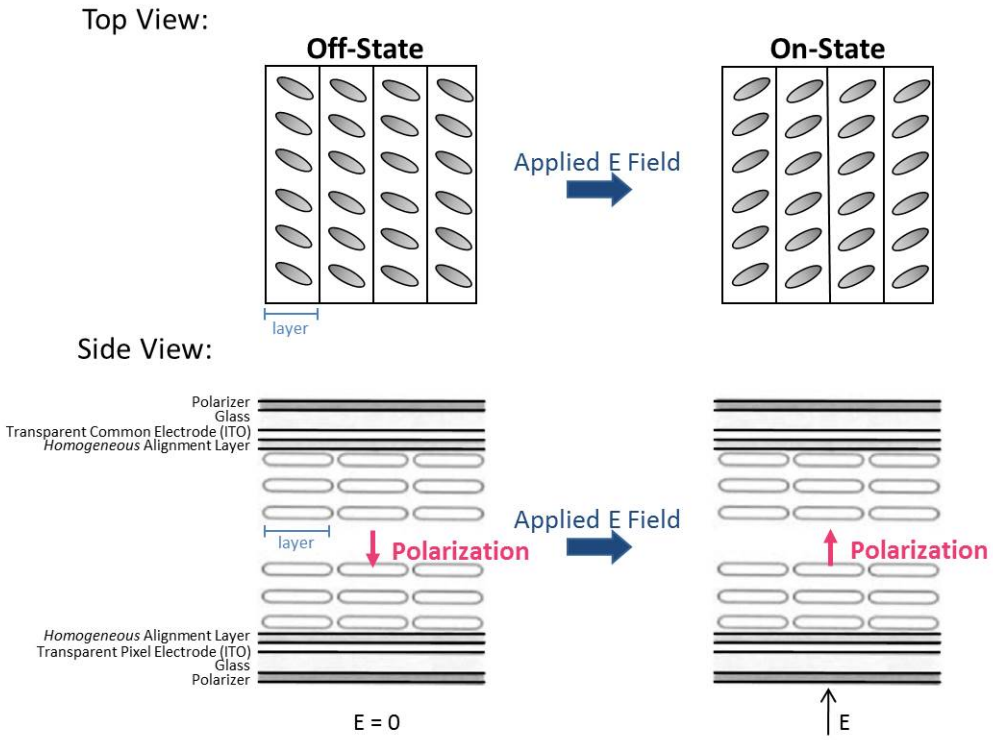

Figure 1.7. A schematic representation of the top and side view of an FLC cell. When chiral molecules in the Smectic C phase (a tilted, layered orientation) are confined in an FLC cell with homogenous alignment, they exhibit a spontaneous polarization. When a vertical electric field is applied, their polaization aligns parallel to the field and the molecules switch orientations to the opposite tilt. Because this switching occurs in the same plane, "dark" and "bright" states can be determined by placement of the polarizer. In-plane switching also results in a very good viewing angle.

Many groups have also attempted to utilize polymers to stabilize FLCs by *in situ* polymerization of monomers in an FLC host [41] [27] [42]. *In situ* polymerization of FLC stabilizing elastomers generally uses anywhere from 5% to 25% polymer to stabilize the alignment. Polymerization occurs while the monomer is aligned, typically with an applied electric field, an additional, and often onerous, manufacturing step. The presence of the cross-linked network often leads to an increase in switching speed and an increase in driving voltage required to switch the cross-linked network [42].

In Chapter 2, we will show that homogenously dissolvend SGLCPs at low concentrations make good

dopants in FLC host, suppressing zigzag defects without sacrificing speed or optical uniformity.

1.4 Motivation

This work aims to further the molecular-level understanding of LC-polymer interactions, by examining the changes in bulk LC properties upon very specific modifications to side-group chemistry. The structure, conformation, and material property enhancement of a variety of types of LCs upon addition of soluble SGLCP homopolymers was investigated, This work has lead to the concept of using homogenously dissolved SGCLP homopolymers at low concentration as“dopants” that can enhance the optic and electro-optic properties of a variety of LC types. Among the targeted structure modifications are molecular weight, side-on *vs.* end-on attachment, linking group type, alkyl spacer length, dipole direction, dipole strength and polymer endgroup.

Chapters 2 and 3 examine the effect of soluble SGLCP homopolymers in two display-relevant systems: FLC and VA nematic LCs. In Chapter 4 we examine the structure and conformation of end-on and side-on SGLCP homopolymers in aligned nematic solvent using neutron scattering. When these homopolymers are attached to an LC-phobic polystyrene block, we can examine the self-assembly of the resulting diblock copolymers in aligned nematic solvents (Chapter 5).

Bibliography

[1] Peter J. Collings. *Liquid Crystals*. Princeton University Press, Princeton, NJ, 1 edition, 1990.

[2] Deng-Ke Yang and Shin-Tson Wu. *Fundamentals of Liquid Crystal Devices*. John Wiley & Sons Ltd, Chichester, 2006.

[3] Yiqun Bai and Nicholas L. Abbott. Recent advances in colloidal and interfacial phenomena involving liquid crystals. *Langmuir: The ACS Journal of Surfaces and Colloids*, 27(10):5719–5738, May 2011.

[4] Timothy J. Sluckin, David A. Dunmur, and Horst Stegemeyer. *Crystals that Crystals, Flow: Classic papers from the history of liquid crystals*. Taylor & Francis, London, 2004.

[5] H. Lin, M. Khan, and T. Giao. Dynamic Liquid Crystal Hot Spot Examination of Functional Failures on Production Testers. In *Proceedings from the 20th International Symposium for Testing and Failure Analysis*, page 81, 1994.

[6] David Burgess. Liquid Crystal Hotspot Detection. http://www.acceleratedanalysis.com/LC_hotspotdetection_

[7] Scott J. Woltman, Gregory D. Jay, and Gregory P. Crawford. Liquid-crystal materials find a new order in biomedical applications. *Nature Materials*, 6(12):929–38, December 2007.

[8] Michael D. Kempe and Julia A. Kornfield. Shear alignment behavior of nematic solutions induced by ultralong side-group liquid crystal polymers. *Physical Review Letters*, 90(11):19–22, March 2003.

[9] Michael D. Kempe, Neal R. Scruggs, Rafael Verduzco, Jyotsana Lal, and Julia A. Kornfield. Self-assembled liquid-crystalline gels designed from the bottom up. *Nature Materials*, 3(3):177–82, March 2004.

[10] Jun-Feng Zheng, Zhen-Qiang Yu, Xin Liu, Xiao-Fang Chen, Shuang Yang, and Er-Qiang Chen. Side-chain liquid-crystalline polymers based on flexible rod-like mesogen directly attached to backbone. *Journal of Polymer Science Part A: Polymer Chemistry*, 50(24):5023–5031, December 2012.

[11] Xuzhou Yan, Feng Wang, Bo Zheng, and Feihe Huang. Stimuli-responsive supramolecular polymeric materials. *Chemical Society Reviews*, 41(18):6042–65, September 2012.

[12] Neal R. Scruggs and Julia A. Kornfield. Synergistic ordering of side-group liquid crystal polymer and small molecule liquid crystal: order and phase behavior of nematic polymer solutions. *Macromolecular Chemistry and Physics*, 208(1920):2242–2253, October 2007.

[13] Michael D. Kempe, Julia A. Kornfield, and Jyotsana Lal. Chain anisotropy of side-group liquid crystalline polymers in nematic solvents. *Macromolecules*, 37(23):8730–8738, 2004.

[14] Sawa Yoshiki, Kenji Urayama, and Toshikazu Takigawa. Temperature-responsive bending of nematic elastomers with hybrid molecular alignment. *Molecular Crystals and Liquid Crystals*, 549(1):106–112, October 2011.

[15] Marc Behl and Andreas Lendlein. Actively moving polymers. *Soft Matter*, 3(1):58, 2007.

[16] Andreas Lendlein, Annette M Schmidt, and Robert Langer. Segments showing shape-memory properties. *Proceedings of the National Academy of Sciences*, 98(3):842–847, 2001.

[17] Andreas Lendlein. Progress in actively moving polymers. *Journal of Materials Chemistry*, 20(17):3332, 2010.

[18] Suk-kyun Ahn and Rajeswari M. Kasi. Exploiting microphase-separated morphologies of side-chain liquid crystalline polymer networks for triple shape memory properties. *Advanced Functional Materials*, 21(23):4543–4549, December 2011.

[19] H Finkelman, H.-J. Kock, and G Rehage. Phase studies of liquid crystalline side chain polymers mixed with low molar mass liquid crystals of similar structure. *Mol*, 89:23–26, 1982.

[20] Hong Yang, Ming-Xia Liu, Yue-Wei Yao, Ping-Yang Tao, Bao-Ping Lin, Patrick Keller, Xue-Qin Zhang, Ying Sun, and Ling-Xiang Guo. Polysiloxane–based liquid crystalline polymers and elastomers Prepared by thiol–ene chemistry. *Macromolecules*, 46:3406–3416, 2013.

[21] Michael D Kempe, Julia A. Kornfield, Christopher K. Ober, and Steven D. Smith. Synthesis and phase behavior of side-group liquid crystalline polymers in nematic solvents. *Macromolecules*, 37:3569–3575, 2004.

[22] R. L. Ameri David and Julia A. Kornfield. Facile, efficient routes to diverse protected thiols and to their deprotection and addition to create functional polymers by thiol–ene coupling. *Macromolecules*, 41(4):1151–1161, February 2008.

[23] Michael David Kempe. *Rheology and dynamics of side-group liquid crystalline polymers in nematic solvents*. Phd thesis, California Institute of Technology, 2003.

[24] Rafael Verduzco, Neal R. Scruggs, Samuel Sprunt, Peter Palffy-Muhoray, and Julia A. Kornfield. Director dynamics in liquid-crystal physical gels. *Soft Matter*, 3(8):993, 2007.

[25] Czung-Yu Ho, Fa-Hsin Lin, Yu-Tai Tao, and Jiunn-Yih Lee. Improvement in device performance from a mixture of a liquid crystal and photosensitive acrylic prepolymer with the photoinduced vertical alignment method. *Science and Technology of Advanced Materials*, 12(6):065002, December 2011.

[26] Chi-Yen Huang, Wen-Yi Jhuang, and Chia-Ting Hsieh. Switching of polymer-stabilized vertical alignment liquid crystal cell. *Optics express*, 16(6):3859–64, March 2008.

[27] Hideo Fujikake, Tahito Aida, Jun Yonai, Hiroshi Kikuchi, Masahiro Kawakita, and Kuniharu Takizawa. Rigid formation of aligned polymer fiber network in ferroelectric liquid crystal. *Japanese Journal of Applied Physics*, 38(9):5212–5213, 1999.

[28] M.-H. Li, P. Keller, J. Yang, and P.-A. Albouy. An artificial muscle with lamellar structure based on a nematic triblock copolymer. *Advanced Materials*, 16(21):1922–1925, November 2004.

[29] H. Meng. A brief review of stimulus-active polymers responsive to thermal, light, magnetic, electric, and water/solvent stimuli. *Journal of Intelligent Material Systems and Structures*, 21(9):859–885, May 2010.

[30] Christian Ohm, Christophe Serra, and Rudolf Zentel. A continuous flow synthesis of micrometer-sized actuators from liquid crystalline elastomers. *Advanced Materials*, 21(47):4859–62, December 2009.

[31] Michael I Kinsinger, Maren E Buck, Nicholas L Abbott, and David M Lynn. Immobilization of polymer-decorated liquid crystal droplets on chemically tailored surfaces. *Langmuir: The ACS Journal of Surfaces and Colloids*, 26(12):10234–42, June 2010.

[32] Dong-Yul Lee, Jung-Min Seo, Waliullah Khan, Julia A. Kornfield, Zuleikha Kurji, and Soo-Young Park. pH-responsive aqueous/LC interfaces using SGLCP-b-polyacrylic acid block copolymers. *Soft Matter*, 6(9):1964, 2010.

[33] Aya Saishoji, Daisuke Sato, Atsushi Shishido, and Tomiki Ikeda. Formation of Bragg gratings with large angular multiplicity by means of the photoinduced reorientation of azobenzene copolymers. *Langmuir: The ACS Journal of Surfaces and Colloids*, 23(1):320–6, January 2007.

[34] Anne de Cuendias, Roger C. Hiorns, Eric Cloutet, Laurence Vignau, and Henri Cramail. Conjugated rod-coil block copolymers and optoelectronic applications. *Polymer International*, 59(11):1452–1476, November 2010.

[35] Yuefei Tao, Bryan McCulloch, Suhan Kim, and Rachel A. Segalman. The relationship between morphology and performance of donor-acceptor rod-coil block copolymer solar cells. *Soft Matter*, 5(21):4219, 2009.

[36] Peter J. Collings and Michael Hird. *Introduction to Liquid Crystals: Chemistry and Physics*. Taylor & Francis, London, 2001.

[37] Type of LCD Panel Technology. http://guide2lcdtv.com/2010/07/lcd-tv-panel-technology-comparison/, 2010.

[38] Matthias Bremer and Lars Lietzau. 1,1,6,7-Tetrafluoroindanes: improved liquid crystals for LCD-TV applicationw. *New Journal of Chemistry*, 29:72–74, 2005.

[39] Krause J. Plach H. J. Weber G. Reiffenrath, V. New liquid-crystalline compounds with negative dielectric anisotropy. *Liquid Crystals*, 5(1):159–170, 1989.

[40] Sven T. Lagerwall. *Ferroelectric and Antiferroelectric Liquid Crystals*. Wiley-VCH, Weinheim, 1999.

[41] Kyehun Lee and Sin-Do Lee. Fast linear electro-optical switching ferroelectric liquid crystals properties of polymer-dispersed. *Applied Physics Letters*, 64(6):718–720, 1994.

[42] Takeshi Murashige, Hideo Fujikake, Hiroto Sato, Hiroshi Kikuchi, Taiichiro Kurita, and Fumio Sato. Polymer alignment behavior with molecular switching of ferroelectric liquid crystal. *Japanese Journal of Applied Physics*, 46(2):L37–L39, January 2007.

Chapter 2

Polymer-Doped Ferroelectric Liquid Crystals

Michael D. Wand of LC Vision contributed to the experiments discussed in this chapter by formulating the FLC hosts. I synthesized the polymers. Together we analyzed them optically and electro-optically at LC Vision. We also thank Noel Clark for his insight into FLC physics and two members of his group, Chenhui Zhu and Yongqiang Shen, for advice about surface stabilized x-ray cells. Torsten Hegmann and his group at the University of Manitoba carried out the capillary (polydomain) x-ray experiments. We are also grateful to the Tirrell lab for use of their spin-coater.

For their help with x-ray scattering experiments. I also thank Alexander Hexemer, Eric Schaible, Peter Reichert, Steven A. Alvarez-Rivera, and Eun Lim at Lawrence Berkeley's Advanced Light Source, as well as Xiaobing Zuo and Soenke Seifert at Argonne National Lab's Advance Photon Source. Paul Pirogovsky helped with both the design and fabrication of the temperature stage and temperature controller we used for x-ray experiments, he also wrote the software that we used to integrate the temperature controller to the beamlines' software. Artemis Ailianou, Paul Pirogovsky, Diana Smirnova, and Iman Hajimorad are the Kornfield group members who helped me during my actual ALS and APS x-ray scattering beamtimes.

2.1 Abstract

A family of polymer dopants for Ferroelectric Liquid Crystals (FLCs) has been discovered that overcomes the main technical obstacles to large-scale application of FLC devices: manufacturing and stabilizing properly aligned cells. Side-on and end-on side-group liquid crystal polymers that were soluble in an FLC host were identified. These polymer-doped FLCs suppressed zigzag defects yet retained the fast electro-optic responses, good contrast and appropriate tilt angle required for display devices. Side-on SGLCPs were also demonstrated to rapidly and robustly adopt an alignment that enabled bistable switching providing the first glimpse into the consequences of orientational coupling in chiral smectic LCs.

2.2 Introduction

2.2.1 Background

A ferroelectric material is defined as one that possesses a spontaneous electric polarization in the absence of an external electric field. Ferroelectricity can be achieved when *chiral* LC molecules self-organize into a chiral Smectic C phase (SmC*), a tilted, layered organization (Figure 2.1b). The tilt of the long axis of the molecules is necessary for a spontaneous dipole to occur in the bulk: if the long axis of the molecules simply points along the layer normal, there is no spontaneous dipole in the plane of the layers. The reduced symmetry of chirality allows for the discrimination between two different tilted states that have opposite dipole directions [1].

Spontaneous polarization is symmetry-allowed in the SmC* phase, but not in the SmC, SmA or nematic phases: The symmetry elements of the point group of a material must be included among the symmetry

elements of every property of the material (Neumann's principle) [1]. Spontaneous polarization in a liquid crystal phase must thus share the same symmetry elements as the liquid crystal phase. In the SmC* phase, because the chiral mesogens are oriented in tilted layers, the system possesses only a unique twofold rotation axis, C_{2y} (chirality eliminates the mirror plane, (Figure 2.1, right) and the inversion center that are present in an smectic C phase). If one imagines the three components of the polarization vectors (Figure 2.1a,b), a 180° rotation about the C_2-axis, in this case the y-axis, would reverse the signs of the components in the x and z directions. Since both the SmC and SmC* phases *are* symmetric about this axis, the polarization in these two directions must be zero (Figure 2.1). However, polarization in the y direction is invariant with respect to this rotation, and, thus, a non-zero P_y symmetry is allowed. Because the molecules in the SmC* phase are chiral, there are no other symmetry operations that in turn disallow the polarization in the y direction (Figure 2.1b, right), in contrast to the SmC phase for which reflection symmetry across the xz plane disallows the polarization in the y direction (Figure 2.1a, right). The reduced symmetry of SmC* thus allows for the existence of a permanent dipole moment parallel to its C_2-axis. In turn, the permanent dipole can be switched by reversing the polarity of an applied electric field [2].

Although each molecule in the SmC* phase posseses an inherent polarization, forcing adjacent layers to point their dipoles in the same direction costs free energy, so, the system instead adopts a helical arrangement, where both the director and the dipole direction precess about a cone, called the "smectic cone," resulting in no net macroscopic dipole in the bulk (Figure 2.2). In order to achieve a uniform orientation of the dipoles, confinement to a gap smaller than the pitch of the helix is required so that surface effects dominate over bulk effects. Tailoring the anchoring surfaces such that the molecules have a strong incentive to lie parallel to the walls of the celleliminates all but two director positions on the smectic cone, specifically: two energetically equal positions, one with the polarization vector pointing up, and one with the polarization vector pointing down. This insight is behind the concept of a

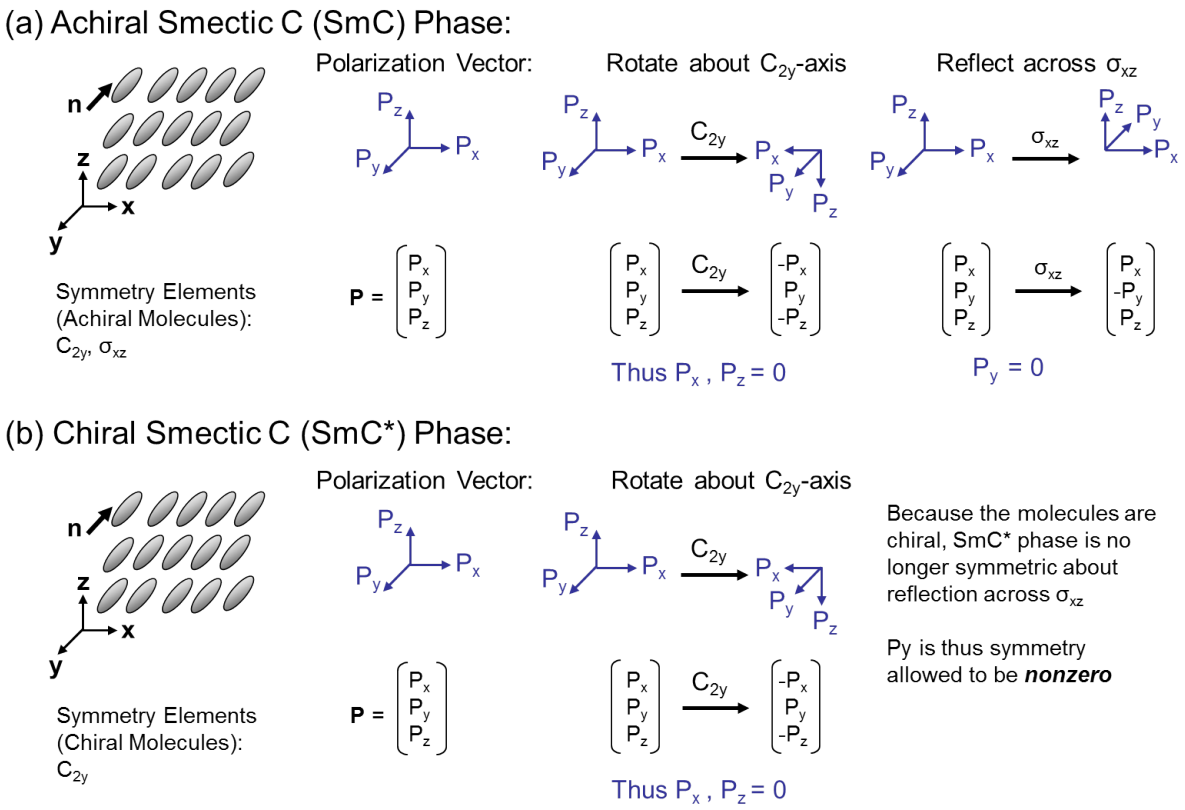

Figure 2.1. (a) The achiral SmC phase has orientational and positional order (moleclues are organized into tilted layers). Symmetry arguments show that polarization is not permitted in this phase. (b) Chirality reduces the SmC* phase's symmetry to one C_2-axis. Spontaneous polarization in the plane of the C_2-axis is thus permitted by symmetry.

surface stabilized ferroelectric liquid crystal (SSFLC), conceived by Noel Clark and Sven Lagerwall in 1980 [3].

The ideal FLC display layer structure is "bookshelf geometry," where the layers are orthogonal to walls of the cell (like books on a single shelf), and the molecules in the layers are, on average, oriented parallel to the walls of the cell (Figure 2.3a). The LC director is then forced to align parallel to the surface, in one of two discrete orientations that satisfy its required tilt relative to the layer normal (Figure 2.3b and c). A consequence of perfect bookshelf alignment is that an electric field can be used to "pop" the director orientation into one or the other of the two "allowed" orientations. After the field is removed, the director does not reorient (Figure 2.3c), so it is stable when voltage stops being applied. This is commonly referred to as bistability. Soon after the discovery of SSFLC, however, it was realized that it

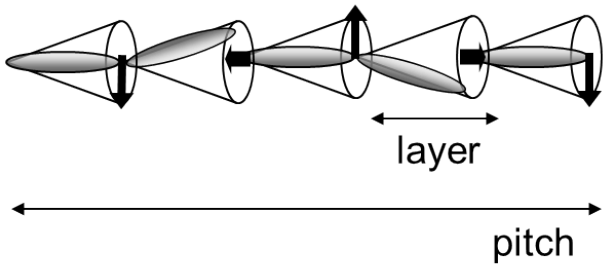

Figure 2.2. Chirality causes the molecules in the SmC* phase to adopt a helical arrangement with their dipoles precessing about a cone. Constraining the sample thickness to smaller than the helical pitch with surface conditions will unwind the helix, resulting in two energetically equal orientations.

is no simple matter to align as SmC* in the bookshelf geometry [1] [4].

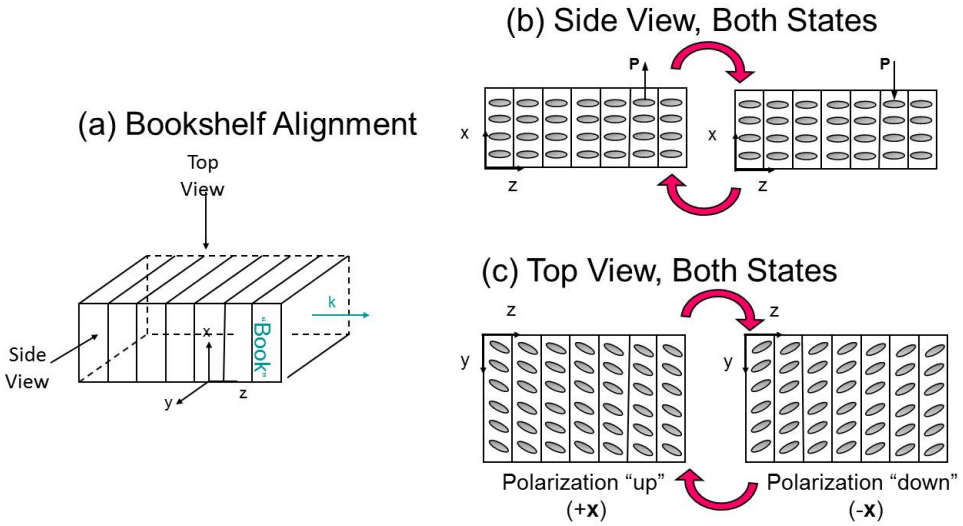

Figure 2.3. (a) The optimal alignment of smectic layers for a bistable FLC if for the layers to arrange like books on a single bookshelf, (b) a side view of the bookshelf alignment shows that the two stable states have dipoles pointing in opposite directions, allowing a brief application of a small voltage across the cell to switch the cell from one state to the other, (c) a top view shows that switching reorients the optical axes in the plane of the device, giving rise to the FLC electro-optic effects that are exploited in displays.

2.2.2 FLC Challenges

In practice, FLC layers are often oriented in configurations called chevrons, with two sets of layers that tilt symmetrically away from the bookshelf orientation (Figure 2.5, right) [5]. This is a serious problem for FLC devices, because without bookshelf geometry, it is difficult to obtain bistability. In fact, the

few FLC devices on the market today do not use bistable operation, and instead use a continuously imposed electric field to hold the molecules in a chosen optic axis state. Current FLC devices thus forfeit one of the great advantages of FLC's – low power consumption, limiting the range of potential applications [6]. A more significant issue arises: zigzag defects tend to form during processing and use of chevron devices. Zigzag defects are visible boundaries between domains with different chevron directions that result in leakage of light, resulting in bright lines when the FLC cell is viewed through crossed polarizers (Figure 2.9) [5] [7]. Such optical defects are present even upon application of an electric field and thus render a device useless as a display [8] [4].

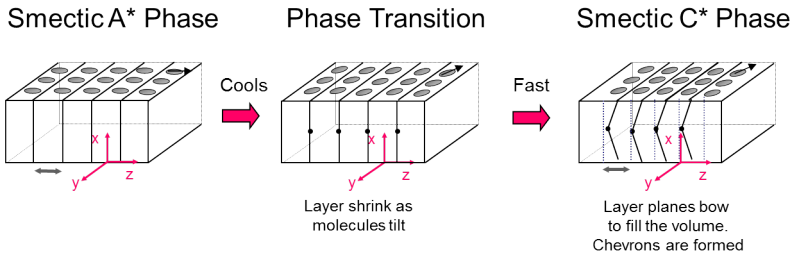

Figure 2.4. Manufacturing steps to produce bookshelf alignment in the (non ferroelectric) Smectic A (SmA) phase are known (left). Unfortunately, upon cooling into the requisite (ferroelectric) Smectic C* (SmC*) phase, the desired alignment structure becomes unstable due to the decrease in smectic layer spacing of the tilted smectic phase relative to the SmA. Kinetically, the system can rapidly decrease its free energy by splitting into two orientations that meet at the center of the cell forming a "chevron" defect.

To eliminate chevrons it is useful to understand how and why they form. During processing, it is relatively easy to produce the bookshelf alignment in a smectic phase that has no spontaneous dipole in the layer plane (the Smectic A phase, Figure 2.5). Upon cooling into the tilted SmC* phase, the average layer thickness decreases. To retain the desired bookshelf orientation, it is necessary to nucleate additional layers (more, thinner layers are required to fill the space in bookshelf orientation, Figure 2.5). But it takes time to nucleate additional layers; the kinetically favoredway to fill the required volume with layers of the reduced layer spacing is to increase the area of each layer by reorienting it, specifically the layers kink to fill more space (Figure 2.5) [5]. Once the chevrons have formed, the driving force to form additional layers and achieve the bookshelf geometry is lost.

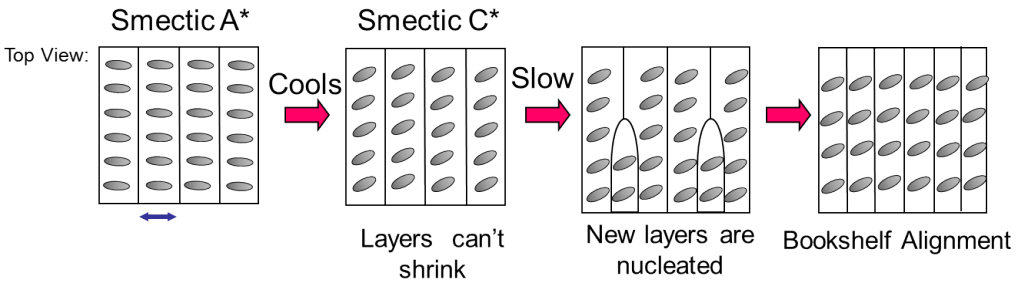

Figure 2.5. Upon cooling to SmC* from SA* (top view), if the driving force to form chevrons is reduced, for example, if polymer dopants can slow the formation of chevrons, new layers can nucleate, resulting in bookshelf geometry.

The difficulty of attaining bookshelf geometry has been recognized for over 20 years and numerous strategies have been pursued attain it. For example, Kobayashi *et al.* used obliquely deposited amorphous silicon as an alignment layer to force the smectic layers into bookshelf geometry [9]. However, because the silicon must be deposited in a vacuum chamber, this method is expensive and difficult to generalize to different cell configurations. Takezoe and co-workers applied a high voltage, low frequency electric field across a cell that had the undesired chevron geometry to induce quasi-bookshelf geometry, but this technique sacrifices switching speed and, because the orientation is not thermodynamically stable, the alignment will be lost if the device is heated past its transition temperature, to another LC or isotropic phase [7] [8].

Other groups have attempted to utilize polymers to stabilize FLCs by *in situ* polymerization of monomers in an FLC host [10] [11] [12]. Specifically, soluble monomers with cross-linkable tails are dissolved in the FLC along with a photoinitiator. The mixure is then loaded into the cell, an electric field is applied to align the system, and UV light is used to photoinitiate polymerization of the aligned monomers throughout the bulk. Because the polymerization takes place in an aligned liquid crystal, the resulting three-dimensional polymeric structure is itself aligned in the direction of the field. Polymerization in the SmC* phase *has* led to zigzag-free SSFLC cells, however, they often suffer from an unacceptable increase in the driving voltage required to switch the cross-linked network [11] as well as scatter a

new source of leakage: the phase-separated polymer networks typically scatter light because they have different refractive indices and birefringenc than the FLC host.

The ideal solution to the challenge of attaining bookshelf geometry would be to have a material that, using an ordinary rubbed polymer as an alignment layer and a relatively brief cooling time, spontaneously forms layers with a bookshelf geometry. Specifically, our approach uses side-group liquid crystal polymers (SGLCPs), *i.e.*, polymers with pendant LC groups that can undergo changes in orientational order along with the LC solvent. For a chosen LC host, we hypothesize that the pendant side groups can be designed to confer solubility in the LC phase(s). In nematic solvents, we have found that small quantities of polymer have only a small effect on the switching speed, a consequence of the orientational coupling between the polymer and the LC [13]. In smectic systems, the switching occurs within the SmC* layerswithout moving the layers themselves. Therefore, it is hoped that that switching may occur without distorting the polymer, so the FLCs switching speed remains fast.

We thus designed a suite of both end-on (terminally-attached) and side-on (laterally-attached) SGLCPs, targeting the effect of side group orientation and dipole strength on orientation and properties of FLCs. Specifically, we synthesized side-on SGLCPs with neutral (no dipole) side groups, along with one SGLCP with a very strong transverse dipole (using four fluorine atoms). Asymmetric molecules are generally more soluble in FLCs, than symmetric ones, so this design serves two purposes: stronger coupling of the pendant mesogents to the neighboring FLC molecules for enhanced control over the LC director, and increased stability of SGLCP solubility in an FLC host. We also synthesized a set of phenylpyrimidine-based end-on SGLCPs. The phenylpyrimidine moiety has a weak dipole along its molecular axis, giving it the same dipole direction relative to the polymer backbone as the transverse dipole is on the side-on SGLCP. The FLC hosts we used are predominantly made of phenylpyrimidine-based mesogens, so this moeity was chosen to promote solubility of the SGCLPs in the FLC hosts. It is also easy to modify the alkyl spacer and/or the linking chemistry (*e.g.*, siloxane or thioether) of end-

on SGLCPs. In this manner, we are able to target the effect of side group orientation, dipole position and strength, spacer length and linking group type on polymer solubility in FLC hosts, zigzag defect suppression, bistability and switching speed.

2.3 Experimental

2.3.1 Materials and Instrumentation

4-(5-decylpyrimidin-2-yl)phenol was purchased by LC Vision from Roman Dabrowskis laboratory at the Military Institute in Warsaw. Polybutadiene (98% 1,2 content) of size 1.07 x 10^3 g/mol and (polydispersity index 1.07) were synthesized by Dr. Steven Smith of Procter and Gamble Co. Polybutadiene (85%, 1,2 content) of size 4.8 x 10^2 g/mol and (polydispersity index 1.07) was used as received from Polymer Source (Montreal, Quebec). Platinum catalysts were obtained from United Chemical Technologies in Bristol, PA and used as received. Boron-rich capillary tubes (0.01 mm wall thickness, a 1 mm outer diameter) were obtained from Charles Supper Company in Natick, MA. Uniform silica spacer beads were obtained from Bangs Laboratories in Fishers, IN and used as received. Sapphire wafers (10 mm x 10 mm x 0.5 mm) with both sides polished were obtained from MTI corporation in Richmond, CA. Elvamide 8023R® was obtained as a sample from DuPont Engineering Polymers. Optically activated glue, NOA68, was obtained from Norland Optical Products in Cranbury, NJ. All reagents were purchased and used as received from Sigma Aldrich, unless otherwise noted.

Reaction temperatures were controlled by an IKAmag RET basic temperature modulator. Thin-layer chromatography (TLC) was performed using J. T. Baker silica gel IB and visualized by short wave UV (254 nm), EMD Silica gel (particle size 0.040-0.063 mm) was used for flash column chromatography.

^{1}H NMR spectra were obtained using an Inova 500MHz NMR spectrometer, recorded in $CDCl_3$ and

referenced to tetramethylsilane. In some cases, a 300MHz Varian NMR spectrometer was used to collect ^{13}F NMR spectra to characterize the fluorination of the side groups provided by LC Vision.

Polymer molecular weight measurements were obtained by gel permeation chromatography in tetrahydrofuran (THF) at 25°C eluting at 0.9 mL/min through four PLgel 10 μm analytical columns (Polymer Labs, 10^6 to 10^3 Å pore size) connected to a Waters 410 differential refractometer detector (λ = 930 nm). The molecular weight measurements were analyzed based on calibrations using polystyrene standards.

Ferroelectric material properties (optical rise time, spontaneous polarization, dielectric constant and viscosity) were measured at LC Vision using the Liquid Crystal Analysis System, LCAS-3, an automated capacitance-based device developed by LC Vision to measure nematic and ferroelectric LC properties. Electro-optic behaviorwas characterized using transient electric fields generated by LC Vision's LCAS-3 instrument appliedto a cell in an optical train with crossed polarisers and photo-detector (either a Thor labs DET10A or a Thorlabs PDA 100A photodetector) connected to a data acquisition system (either a HP 54503A Digital oscilloscope or the same LCAS instrument).

Initial lab-scale x-ray scattering data, on polydomain FLCs, was acquired in Torsten Hegmanns laboratory at the University of Manitoba using a Rigaku 3 pinhole camera (S-MAX3000) equipped with a Rigaku MicroMax+002 microfocus sealed tube (Cu Kα radiation at 1.54 Å) and Confocal Max Flux (CMF) optics operating at 40 W.

Small Angle X-ray Scattering (SAXS) experiments on aligned FLCs were conducted at beamline 7.3.3 at Lawrence Berkeley National Laboratory's Advanced Light Source and beamline 12-ID-B at Argonne National Laboratory's Advanced Photon Source.

2.3.2 Methods

2.3.3 Synthesis of Side-on SGLCP Homopolymers

The side-on homopolymer (1), has a laterally attached butoxy benzoate side group (Figure 2.7), attached to 1,2 polybutadiene via silane coupling as described by Rafael Verduzco [13] [14]. The first batch of Polymer **1** used in these experiments was synthesized by Rafael Verduzco, I prepared later batches and all other polymers.

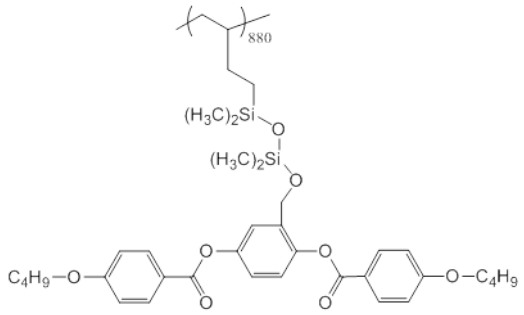

(1)

Figure 2.6. The structure of the side-on polymer, Polymer **1**.

2.3.3.1 Synthesis of Aldehyde-Containing Butoxybenzoate Mesogen for Siloxane Coupling

4-Butoxybenzoic acid (25 g, 128 mmol) was reacted with an excess of thionyl chloride (50 mL, 685 mmol, though it should be noted that a two-fold excess than has proved to be sufficient) for one hour at 59°C in a 100 mL round-bottom flask filled with argon and capped with a drying tube containing drierite to capture the acid generated by the reaction (Scheme 2.1). When TLC confirmed the reaction was complete, the excess thionyl choloride was removed by evaporation, leaving approximately 40 mL of yellow liquid. In a separate 100mL round-bottom flask, 2,5-dihydroxy benzaldehyde (7.028 g, 50.88 mmol), was dissolved in 50 mL anhydrous dichloromethane and 20mL anhydrous pyridine. To

this green tinted solution, the crude butoxy-benzyl chloride was added, whereupon the mixture turned opaque yellow (Scheme 2.1). Dry argon gas was blown over the top of the mixture for five minutes, and the flask was then capped with a Teflon septum and reacted overnight at room temperature, yielding a dark purple reaction mixture.

The reaction mixture was poured onto 1N HCl to remove the pyridine. The organic layer was reserved and dicloromethane was used to extract any product dissolved in the HCl phase. This liquid-liquid extraction dichloromethane was repeated three times, followed by washing with a saturated $NaHCO_3$ solution three times. The combined organic layers were evaporated, and the product, 3,5-di(4-butoxybenzoate)-benzaldehde, was purified by recrystallization from hot ethanol into slightly pinkish crystals (12.28 g, 98.4% yield).

2.3.3.2 Siloxane Coupling and 1,2 Polybutadiene Functionalization of Aldehyde-Containing Butoxybenzoate

The following is a general procedure describing the synthesis of the siloxane intermediate and the subsequent polybutadiene functionalization using the side-on butoxybenzoate side group: 3,5-di(4-butoxybenzoate)-benzaldehde (2.97 g, 6.18 mmols) and a small amount of Wilkinsons catalyst (chlorotris(triphenylphosphine)rhodium(I), 25.7 mg) were dissolved in anhydrous toluene with a 14-fold excess of 1,1,3,3-tetramethyl disiloxane, TMDS, (15mL, 85 mmols). The reaction flask was filled with dry Argon gas, sealed with a teflon se and reacted at 60°C for 1 hour. After verifying reaction completion with thin layer chromatography, the excess TMDS and solvent were then evaporated at 80°C under vacuum from the orange-colored reaction mixture, which was then purified via anhydrous column chromatography yielding 1,2-bis(4-butoxybenzoate)-2-methyl[(1,1,3,3,-tetramethyl-disiloxane)oxy]-benzene, or "SiBB" (3.08 g, 81% yield).

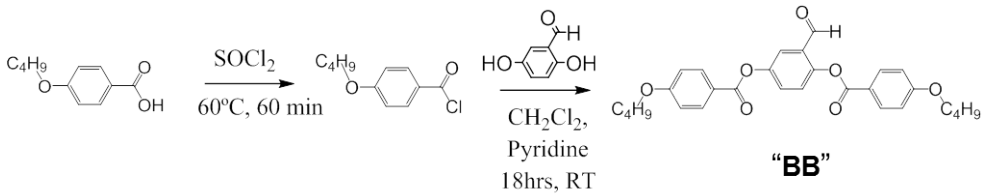

Scheme 2.1. The synthesis of the 3,5-di(4-butoxybenoate)-benzaldehde side group, "BB."

The siloxane-linked mesogen was then attached to the pendant vinyl groups of 1,2-polybutadiene via platinum catalyzed hydrosilation (Scheme 2.2). Polybutadiene (0.0352 g, 0.6 mmols) was dissolved in 10 mL of anhydrous tetrahydrofuran (THF) under inert atmosphere. A three-fold excess of freshly purified SiBB and one drop of platinum catalyst (PC085, platinum cyclovinyl complex in vinylmethyl-siloxanes) were added, and the mixture was heated at 50°C for four to six days. Reaction progress was monitored by ^{1}H NMR. When the reaction was complete it was quenched with excess styrene (about 3 Pasteur pipettefuls, ∼4.5 mL) and heated at 50°C overnight. The polymer was then purified by evaporating all but the last 5 mL of solvent under vacuum, followed by repeated precipitation (sometimes up to 5 times) from THF solutions with cold methanol containing 10 ppm BHT (Butylated hydroxy-toluene or 2,6-di-tert-butyl-4-methylphenol), followed by drying to constant weight under vacuum at room temperature.

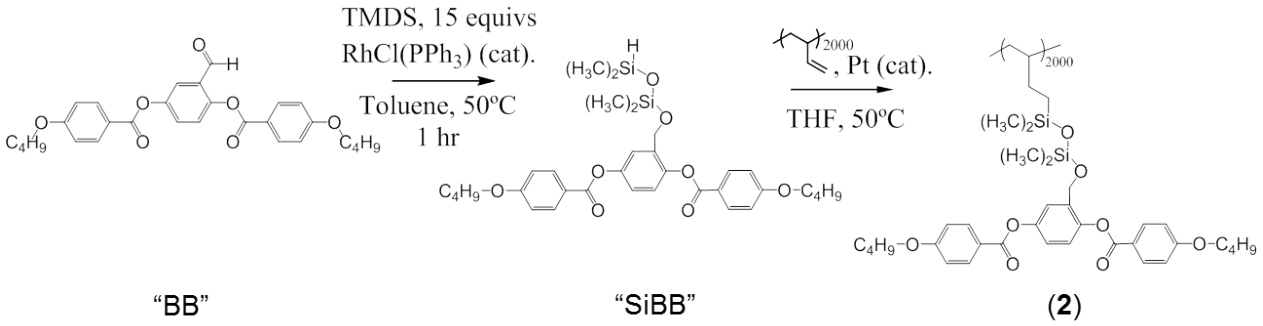

Scheme 2.2. The "BB" side group is grafted onto the pendant vinyl groups of 1,2-polybutadiene by platiunm catalyzed hydrosilation of its aldehyde group. Attaching the mesogen at a middle point in the molecule leads to a side-on SGLCP.

2.3.4 Synthesis of End-on SGLCP Homopolymers

2.3.4.1 Synthesis of Vinyl-Terminated Phenyl Pyrimidines for Siloxane Coupling

Vinyl-teminated phenyl pyrimidines with different spacer lengths were synthesized from 4-(5-decylpyrimidin-2-yl)phenol for siloxane coupling to 1,2 polybutadiene. A general procedure for this synthesis is as follows: 4-(5-decylpyrimidin-2-yl)phenol (1.89 g, 6.05 mmols), a bromoalkene (7-bromo hept-1-ene, 8-bromooct-1-ene or 10-bromododec-1-ene, 8mmol) and Cs_2CO_3 (2.56 g, 8 mmols) were stirred at room temperature in 40 mL of dimethyl formamide overnight, resulting in near-quantitative conversion to the ether (Scheme 2.3), monitored by thin-layer chromatography. The reaction mixture was extracted three times with 50 mL of dichloromethane. The combined organic extracts were washed three times with water and dried with $MgSO_4$. The crude product was recrystallized in hot 95% ethanol, resulting in analytically pure white crystals of 5-decyl-2-(4-(hept-6-enyloxy)phenyl)pyrimidine, 5-decyl-2-(4-(oct-7-enyloxy)phenyl)pyrimidine, or 5-decyl-2-(4-(dec-9-enyloxy)phenyl)pyrimidine (1.20 g, 2.09 g, 1.69 g and 48.0%, 83.6%, or 66.02% overall yield, respectively).

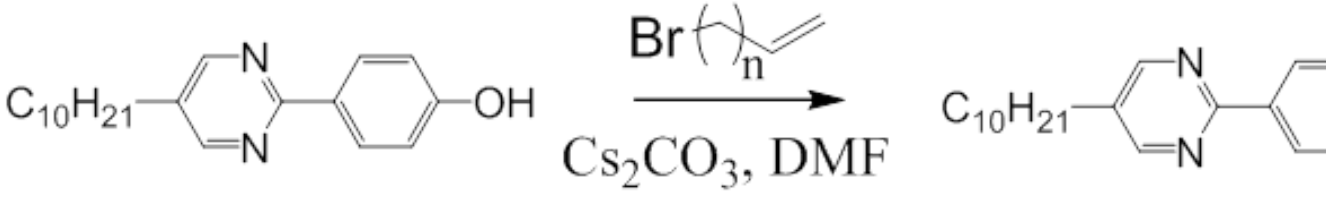

Scheme 2.3. Williamson ether synthesis of end-on phenyl pyrimdine mesogenic side groups.

2.3.4.2 Siloxane coupling and 1,2 Polybutadiene Functionalization of Vinyl-Terminated Phenyl Pyrimidines

A siloxane linking group is added to the alkene-terminated phenyl pyrimidine mesogens by hydrosilation (Scheme 2.4). The following is a general procedure describing the synthesis using one of the vinyl-

terminated mesogens: A tenfold excess of 1,1,3,3-tetramethyldisiloxane (TMDS) (3 mL, 17 mmol) and the mesogens, *e.g.*, C8PPC10V (0.693 g, 1.69 mmol) were dissolved in 20 mL anhydrous toluene. A drop of platinum catalyst (PC072 platinum divinyl complex in xylene) was added and the mixture was stirred at 50°C for 2 days. This reaction was monitored by thin layer chromatography, and, when completed, the solvent and excess TMDS are evaporated at 80°C under vacuum and the product ("SiC8PPC10") was purified by anhydrous column chromatography (0.639 g, 69.1% yield).

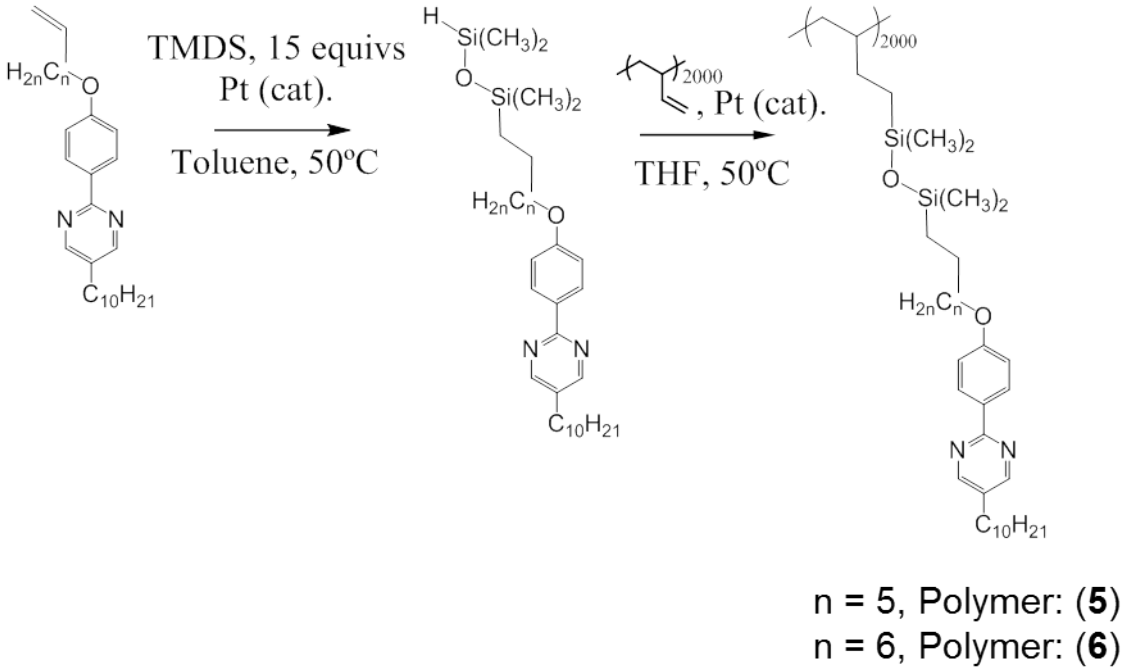

Scheme 2.4. Siloxane coupling, first to vinyl-terminated mesogen, then to 1,2-polybutadiene.

The siloxane-linked mesogen was then attached to the pendant vinyl groups of 1,2-polybutadiene, also by platinum catalyzed hydrosilation (Scheme 2.4). Polybutadiene (0.035 g, 0.6 mmols) was dissolved in 10 mL of anhydrous tetrahydrofuran (THF) under inert atmosphere. A one-and-a-half-fold excess of freshly purified SiC8PPC10 and one drop of platinum catalyst (PC085, platinum cyclovinyl complex in vinylmethylsiloxanes) was added and the mixture was heated at 50°C for four to six days. Reaction progress was monitored by ^{1}H NMR. When the reaction was complete it was quenched with excess styrene and heated at 50°C overnight. The polymers (5 and 6) were then purified by evaporating all but the last 5 mL of solvent under vacuum, then repeated precipitation from THF solutions with cold

methanol containing 10 ppm BHT, followed by drying to constant weight under vacuum at room temperature.

2.3.5 Synthesis of Benzoyl-Protected Thiols, for Thiol-Ene Coupling

Benzoyl-protected thiols were synthesized from 4-(5-decylpyrimidin-2-yl)phenol for thiol-ene coupling to 1,2 polybutadiene. 4-(5-decylpyrimidin-2-yl)phenol (1.89 g, 6.05 mmols), 1-bromo-6-chloro-hexane (1.57 g, 8 mmol) and $CsCO_3$ (2.56 g, 8 mmols) were stirred at room temperature in 40 mL of dimethyl formamide overnight, resulting in near-quantitative conversion of the ether (Scheme 2.5). The reaction mixture was extracted three times with 50 mL of dichlormethane. The organic extracts were washed three times with water and dried with Mg_2SO_4. The crude product was recrystallized in hot 95% ethanol, resulting in analytically pure white crystals (1.92 g; 76.56% overall yield) of 2(4-(5-chlorohexyloxy)phenyl)-5-decylpyridine.

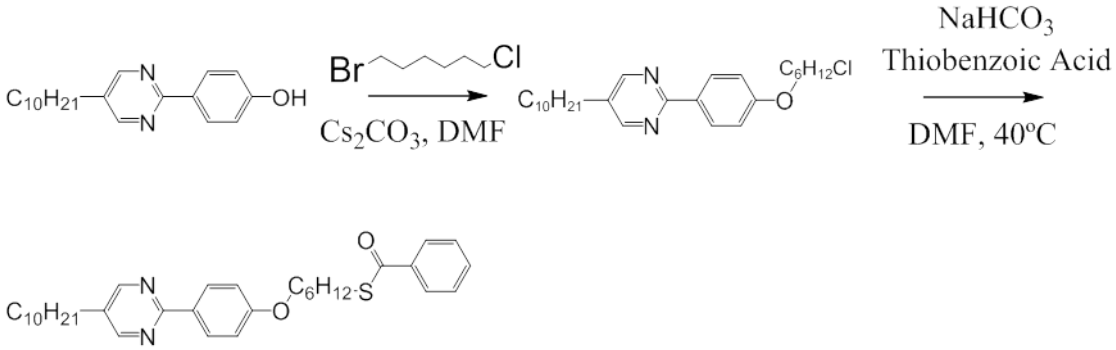

Scheme 2.5. The synthesis of the protected thiol mesogenic phenyl pyrimidine side group.

2.3.5.1 Thioester cleavage and 1,2-Polybutadiene Functionalization.

The thioesters in the benzoyl-protected thiols were cleaved and the resulting thiol terminated mesogens were coupled to 1,2-polybutadiene by radical initiated thiol-ene coupling (Scheme 2.6). The thioester (1 g, 1.9 mmol) was first dissolved in 25-75 mL DMF (dimethylformamide) with hydrazine monochloride

(0.13 g, 1.9 mmol) and sodium acetate (0.13 g 1.9 mmol). The reaction mixture was purged with argon for 10 minutes and stirred for 6 hours at room temperature. The thiol product was extracted into 30mL of chloroform, washed 3 times with water and transferred into a flask containing 1,2-polybutadiene (0.03 g, 0.6 mmol) and AIBN (50 mg, 0.30 mmol) dissolved in 10 mL of chloroform. This mixture was then degassed in 2 freeze-pump-thaw cycles and then allowed to react at 55°C overnight. The final polymer product (4) was then purified by evaporating all but the last 5mL of solvent under vacuum, followed by repeated precipitation from THF solutions with cold methanol containing 10 ppm BHT, then drying to constant weight under vacuum at room temperature.

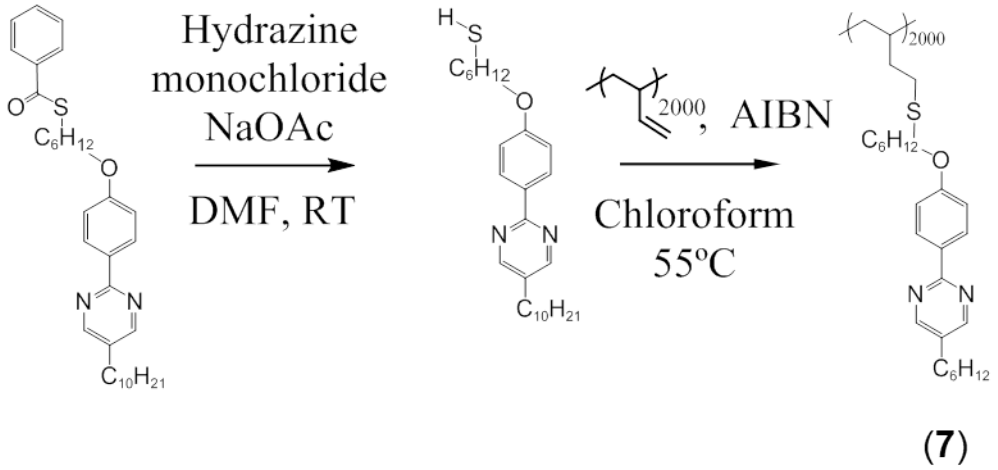

(**7**)

Scheme 2.6. Thioester cleavage into thiol, followed by direct radical-catalyzed thiol-ene coupling with 1,2-polybutadiene.

2.3.5.2 Polymer Characterization

Proton nuclear magnetic resonance spectroscopy (^{1}H NMR). ^{1}H spectra (16 or 32 scans) of solutions of polymer (with concentrations of approximately 10 to 20 mg/mL) in $CDCl_3$ were recorded at room temperature on an Inova 500 MHz NMR spectrometer. The percent conversion of the pendent vinyl groups was determined by comparing the integrated area for the peaks corresponding to both the 1,2-polybutadiene and mesogen at 4.7-4.9 ppm, with peaks corresponding to the alkyl spacers on the mesogen.

Gel permeation chromatography (GPC). The side group liquid crystal polymers relative molecular weight and molecular weight distributions (PDI = M_w/M_n), were measured using gel permeation chromatography (GPC) calibrated with monodisperse PS standards.

2-7 mg polymer was dissolved $\sim$1 mL of tetrahydrofuran (THF) and shaken for at least 30 min with a mechanical shaker. These solutions were filtered with a 0.45 μm syringe filter prior to being injected into the GPC. The total time to traverse all four columns was approximately 45 minutes.

Polymer-FLC solutions. Polymers were dissolved in FLC hosts prepared by our collaborator, Michael Wand, at LC Vision in Boulder, CO.

2.3.5.3 FLC Hosts

The proprietary hosts (FLC-A, FLC-B, FLC-C, Table 2.1) provided by LC Vision are eutectic mixtures of approximately 10 components, including mesogens (generally with phenylpyrimidine cores) and chiral dopants. Each mixture was characterized by broad SmC* temperature ranges accessible isotropization temperature and narrow windows of SmA and nematic phases, weak-to-moderate spontaneous polarization ($\sim$20 nC/cm^2), and differing significantly in helical pitch and rise time.

Table 2.1. Three FLC hosts were designed by LC Vision to have polarization around $\sim$20nC/cm^2, and similar viscosity and dielectric constants, but varying in pitch.

FLC Host	Phase Transitions (°C)	Polarization (nC/cm^2)	Viscocity (mPas)	$\Delta\epsilon$	Pitch (μm)
FLC-A	I 107.6 N 97.8 A 93.3 C*	26.7	76	3.90	11
FLC-B	I 109 N 97 A 89 C*	25.4	66	4.14	5
FLC-C	I 106.5 N* 93.5 A 86.5 C*	19.7	79	3.90	-

2.3.5.4 Solutions of Polymers in FLC Hosts

Known weights of SGLCPS were dissolved in known weights of FLC host materials by repeated iterated heating to the isotropic phase followed by centrifugation and vortex mixing. (No solvent was used to disperse the polymers in the host so as not to introduce any impurities that might detrimentally affect FLC properties.)

The polymer-FLC solutions were loaded in to test cells with an active area of 1 cm^2 and an approximate thickness of 1.85 μm at temperatures $>$100°C (FLC solutions flow very poorly unless they are in the isotropic phase). The polymer-doped FLC cells were then placed on the bench to cool from the isotropic phase to room temperature (SmC* phase) without controlled cooling. Cells were not annealed under an applied electric field.

2.3.5.5 Polarized Light Microscopy

Phase transition temperatures were measured using polarized light microscopy. First small droplets are sandwiched between a glass slide and coverslip were examined using a Zeiss Universal optical microscope equipped with a Mettler FP82 hot stage and crossed polarizers. Each sample was heated and cooled at a rate of 1 or 2 °C from room temperature to 115-120 °C while the optical texture was observed and the phase transition temperatures were recorded.

2.3.6 Optical and Electro-optic Measurements

2.3.6.1 FLC Properties

We evaluated FLC material properties (electronic rise time, polarization, dielectric anisotropy and viscosity) of appropriate polymer dopant concentrations in FLC hosts using the LCAS-3 provided by LC Vision. The system first measures and nulls any parasitic capacitance of the cables and LCAS system without a cell in it. The empty cells resistance and capacitance are then measured and nulled. The cell is filled with the sample of interest and its capacitance is measured, electronic rise time, polarization, viscosity, and dielectric constant are determined based on known relationships to the measured cell capacitance. Finally, the data is normalized by previously measured cell thickness information.

By using the attached "CoolNHot box" that accompanies the LCAS instrument, which holds the sample in a thermal chamber equipped with electrodes to measure capacitance, determination of FLC material properties over a wide range of temperatures was acheivable.

2.3.6.2 Rise Time and Bistability

The rise time and contrast were measured by driving the cells at with a 100 Hz square wave at 5 or 8 V. Initial measurements were taken at LC Vision with the following setup: the cells were placed in a polarized optical microscope with crossed polars and a photodetector attached to the top. The photodetector was connected to an ocilliscope. A more rigorous version of this setup was also constructed at LC Vision: The sample was aligned between crossed polars (45°, approximately the angle of the FLCs bright and dark state when filling direction is aligned parallel to the floor) in the path of A red HeNe laser (633 nm) followed by a photodetector, which was connected to the LCAS instrument that generated the wave forms, for simultaneous monitoring of the pulse and the response. The rise time was calculated

to as the time it took for the light transmission to go from 10% to 90% of the transmission generated by the square wave, while the contrast was calculated by dividing the brightest state voltage (relative to the darkest state: with crossed polars and no sample cell in the microscope, thus being as dark as the setup could be) by the dark states voltage (also relative to the darkest state). Bistabilty was measured by driving the same cells with a DC balanced bipolar pulse at 100 Hz and 20 Hz and monitoring the transmission loss (relative to a square wave at the corresponding frequency) after the switching pulse stopped.

2.3.7 Small Angle X-ray Scattering of Polydomain FLC Samples

Initial 1-D x-ray layer spacing determinations were collected in collaboration with Torsten Hegmanns laboratory (then at the University of Manitoba). FLC samples were loaded into thin-walled glass boron-rich capillary tubes and flame-sealed (with a lab propane torch). Boron-rich glass has a higher x-ray transparency relative to conventional glass, and is easier to seal relative to quartz capillary (which is more x-ray transparent). Scattering data of these polydomain samples was acquired using a Rigaku 3 pinhole camera (S-MAX3000) and the Hegmann lab completed the data reduction according to established procedures [15].

Because the FLC host has a layered structure at both SmA and SmC* temperatures, a Bragg peak representing the layer spacing is easily seen in the temperature-dependant scattering patterns. The wave vector (q) at the maximum of the Bragg peak:

$$q_{max} = 2\pi/d \tag{2.1}$$

where d is the layer spacing. The tilt angle of the molecules SmC* temperatures can be determined from

the simple equation:

$$cos\theta = d_C/d_A, \tag{2.2}$$

where theta is the the tilt angle from the layer normal, d_C is the layer spacing in the Smectic C phase, and d_A is the layer spacing in the Smectic A phase (assumed to correlate closely with the molecular length). The position of the Bragg peak in the SmA phase is insesitive to temperature (hence d_A is approximately constant) and shifts with temperature in the SmC* phase (i.e. d_C rises with temperature, increasing with subcooling with respect to the A to C* transition).

2.3.8 Small Angle X-ray Scattering of Aligned Cells

Small-angle x-ray scattering (SAXS) of aligned FLCs in surface-stabilized cells was carried out to measure the smectic layer spacing and chevron angles as a function of temperature, cooling rate, polymer stucture and concentration. The collection of rocking curves (SAXS patterns aqcuired with the aligned FLC cell tilted relative to the beam (Figure 2.12)) reveal chevron formation and characterize chevron angle.

2.3.8.1 Sample Cells

Sample cells containing homogeneously aligned SGLCP solutions were prepared by sandwiching 1.5 μm silica spacer beads between 500 μm thick sapphire wafers that had been pretreated with a layer of rubbed nylon (Elavamide®) to induce uniform alignment of the LC director. (The alignment layer was created by spin coating the sapphire with 0.5% Elvamide® solution in methanol, followed by rubbing with a natural hair brush for more than 50 strokes). Polished sapphire was chosen for its optical transparency (to give the ability to compare texture observed in the microscope with SAXS patterns) and its thermal conductivity. The spacer beads were suspended in UV-polymerizable glue and distributed on

the ends of the cell, perpendicular to the rubbing direction and clamped with binder clips. The clamped assembly was then irradiated with long wave UV (354 nm) for at least half an hour to cure the adhesive, then the clips were removed the cell was irradiated for at least one further hour.

Polymer solutions were loaded into the sapphire cells at elevated temperatures ($\sim$115°C) in the isotropic phase so that the sample flowed into the cells by capillary action. Filled cells were then sandwiched between two 1"x 1" aluminum plates with 3mm holes drilled out of the center of each plate (for passing the x-ray beam).

2.3.8.2 Temperature Controlled Sample Environment

Homogeneously aligned SGLCP solutions were mounted in our home-built transmission-geometry, temperature-controlled Peltier-based sample environment that enabled precise, rapid, bidirectional temperature changes (designed by Paul Pirogovsky). The inside of the front and back plates of the heating/cooling unit consisted of 4, high-temperature Peltier heating units spaced to make a hole for the x-ray beam. U-shaped water channels (water temp = 70°C) provided the heat sink for the Peltier units. High temperature Peltier units were necessary in order to heat the samples to isotropic phase of FLC-C ($\sim$110°C), to erase thermal history. This unit also enabled us to cool at a variety of cooling rates. The heating unit was mounted on a triple axis goniometer stage on the x-ray beamline.

2.3.8.3 Small Angle X-ray Scattering

Small-angle x-ray scattering (SAXS) experiments were performed at beamline 7.3.3 at the Lawrence Berkeley National Laboratory's Advanced Light Source (ALS), using x-rays with a wavelength of 1.240 Å (10 keV), and at beamline 12-ID-B at Argonne National Laboratory's Advanced Photon Source using x-rays with a wavelength of 0.886 Å (14 keV). Two-dimensional scattering patterns were collected at

each angle from -30° to 30° at a detector distance of 1.3 m (ALS) and 2 or 2.7m (APS) using a Pilatus 1M (ALS) and 2M (APS) CCD detector, respectively. (Because the Bragg peak representing the FLC layer spacing occurs at relatively high q, a number of sample-to-detector distances were used.) The sample-to-detector distance was calibrated using a silver behenate standard. Silver behenate is a silver salt of behenic acid ($CH_3(CH_2)_{20}COOAg$, "AgBe") that has a large number of well-defined diffraction peaks in the low-angle range, making it a common calibrant for small angle x-ray scattering [16].

Rocking curves at temperatures near the SmA-SmC* transition were collected by first heating the sample to isotropic temperatures, ($> 115°$C), holding for at least 5-10 minutes, then cooling (at either 1, 4, 10, or 20 °C/min) until the desired temperature was reached. A 0.1 or 0.3 s exposure was acquired for each one degree increments from -30° to -30°, followed by acquisition of a control image at 0° to check for any changes (either from radiation damage or temperature fluctuations) during the acquisition of the rocking curve. Radiation damage was seen at exposure times longer than 1 s, hence this precaution. Rocking curves are only discussed here if there was no change in the initial exposure at 0° and this control exposure.

The scattering patterns were analyzed using the Nika software package for Igor pro, developed at Argonne National Labs Advanced Photon Source [17]. Two-dimensional scattering patterns were sector-averaged for easier visualization. At Smectic A temperatures, data at specific scattering vectors, q, within $\pm 40°$ of the equatorial (horizontal) direction were averaged. The equatorial axis was approximately 0°, but was quantitatively determined to control for sample cells being tilted in their aluminum holders – a 1-D line profile of the 2-D bookshelf arcs was taken and the from the q_y and q_z of the most intense spots on the profile, the angle of the bookshelf peaks, or horizontal direction was determined. The raw data were converted to absolute coherent scattering intensities, I, as a function of q using corrections for detector inhomogeneity and sensitivity according to standard procedures [17].

2.4 Results

2.4.1 Polymer Characteristics

We synthesized a series of side-on and end-on SGLCP homopolymers designed to isolate the effects of molecular weight (Polymer 1 vs 2), tail length (Polymers **1** and **2** vs.**3**), dipole (Polymers **4** vs **1**-**3**), spacer length (Polymer **5** vs **6**) and linking group type (*i.e.*, siloxane (Polymers **5** and **6**), or thioether (Polymer **7**)) on the solubility in and stabilization of FLCs (Figure 2.8).The side-on SGLCP homopolymers are rubbery and liquid crystalline at room temperature. The low T_g of the side-on polymers can be attributed to the presence of tetramethyl-disiloxane linker in the polymer. Similar polymers without siloxane typically have higher T_g. The siloxane-linked end-on homopolymers were also rubbery and liquid crystalline polymers, while the thiol-linked end-on homopolymers were more brittle, but still liquid crystalline.

2.4.2 Solubility in the FLC matrix

Very little is known about the solubility of polymers in an FLC matrix, a necessary criterion for polymeric additives for use in FLC displays. At low concentrations, six of the seven synthesized polymers were soluble in the FLC hosts. Side-on Polymers (**1**) and (**2**), and end-on Polymers **5** and **7** were tested in all three hosts (FLC A-C), and Polymers **3** and **4** were tested in FLC-B and FLC-C. In all cases that were tested, solublity in one of the FLCs was accompanied by solubility in every other FLC. End-on Polymer **6** was insoluble in FLC-A at ambient temperature. At this low concentration, the polymer has no discernable effect on the phase transition temperatures of the host FLC which is impotatnt because it preserves the broad SmC* temperature range). Of the pair-of siloxane-coupled phenylpyrimidine-based end-on polymers, Polymer **5** was soluble at both 1.5% and 0.75% by weight. On the other hand, Poly-

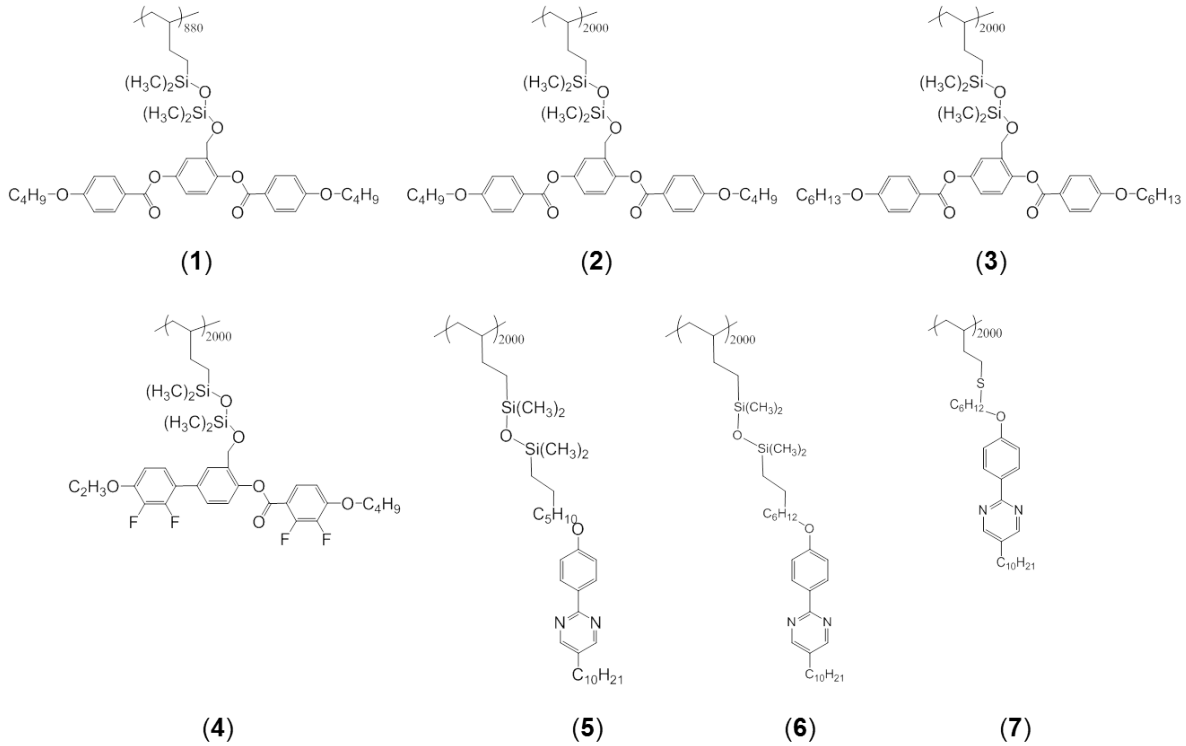

Figure 2.7. Side-on polymers 1, 2 and 3 have no net dipole, while side-on polymer 4 has a strong transverse dipole, end-on polymers 5 and 6 have siloxane-linked, phenylpyrimidine side groups but different spacer lengths while polymer 7 contains thio-ether linked, phenylpyrimidine side groups. The phenylpyrimidine side groups were designed to confer solubility to the phenylpyrimidine-containing FLC hosts.

mer **6** was not soluble at either of these concentrations, suggesting an even-odd effect of spacer length. The thiol-linked, phenylpyrimidine-based end-on polymer, Polymer, **7**, was soluble at all concentrations tested (3% and lower). These results indicate that SGLCPs can be sesigned to favor FLC-solubility by using side-groups whose molecular structures are known to be compatible with a desired FLC host (here, side groups based on phenylbenzoates and phenylpyrimidines which are known to be miscible with phenylpyrimidine-based FLCs such as those in Table 2.1). This gives us great latitude in the optimization of this new class of materials.

2.4.3 Optical Microscopy

Hot stage polarized light microscopy examination of FLC cells was unable to discern shifts in transition tempereatures. Although SGCLPs frequently induce biphasic temparature ranges, none was obersved in any of the solutions tested. Polarized optical microscopy shows that addition of 1.0%-1.5% of the soluble polymers does not affect the FLC host LC transition temperatures, at least within the margin of error for this type of measurement. This is additional evidence that the polymers at these concentrations are soluble across the whole temperature range of interest (from room temperature acrros SmC* - SmA - N - I transition (Table 2.1).

Polarized optical microcopy also shows the zigzag defects that are prevalent in the pure FLC host are absent when 1.0%-1.5% side-on polymers are added (Figure 2.9f *vs.* 2.9g, for example). No special thermal history was used: the samples were simply allowed to cool to ambient conditions without any temperature control. This suppression of zigzag defects appears to be conferred by the additive itself. This additive thus eliminates the need for perfect thermal uniformity during cooling (a factor that has limited FLC displays to very small sizes and necessitated batch processing); they also eliminate the need for slow cooling (which has added to the cost of FLC displays due to long cycle times in batch processing).

Polarized optical microcopy also shows that 1.5% of Polymer 5, an end-on SGLCP suppresses zigzag defects in FLC-A, while 1.5% of Polymer **6** and Polymer **7** do not (Figure 2.10). However, it should be noted that other concentrations (0.75% and 1.0%) of Polymer **7** do, indeed, suppress zigzag defects in FLC-A. Factors that could affect the reduction of zigzags inclue host compostition, polymer structure, polymer concentration. Although they were not studied, surface anchoring and cell thickness may also play a role.

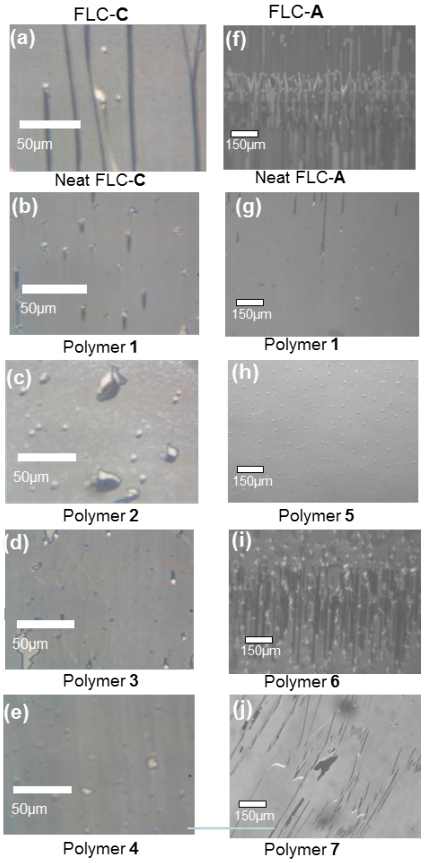

Figure 2.8. Polarized optical micrographs of 1.0% polymer-dopants in FLC-C (see Table 2.1) and and 1.5% polymer dopants in FLC-A (Table 2.1). (a),(f) Neat FLCs after uncontrolled cooling (zigzag defects), (b)-(e) Side-on polymers (1, 2, 3 and 4, see Figure 2.7) suppress zigzag defetcts in FLC-C. (g) Polymer 1 also suppresses zigzag defects in FLC-A. (h) End-on Polymer 2 (Figure 2.7) was also successful at suppressing zigzag defects. (i) End-on Polymer 6 (see Figure 2.8) was visibly insoluble in FLC-A, and (j) end-on Polymer 4 (see Figure 2.8), while soluble, was did not suppress zigzag defects at this concentration. Bright circles in some images correspond to glass spacer beads, while darker and lighter domains correspond to regions with different polarization directions (a distinction that vanishes when electric field is applied.

2.4.4 Electro-optic Measurements

Optical tests suggest that the absence of zigzag defects in the FLC-A/Polymer 1 mixture is not merely due to having a single chevron direction throughout the cell. A simple optical test for the presence of chevron defects is to test for bistable switching: FLCs that are not in bookshelf geometry are not bistable. Indeed, the cells we prepared with the neat FLC (FLC-A) itself were not significantly bistable: after a pulse aligned all the dipoles in one direction and was then turned off, an average of more than

60% of the transmission was lost within milliseconds (Figure 2.10a), which is typical of monostable switching . In contrast, cells prepared using the same thermal history, the same testing process, and the same FLC, but simply with the addition of 1.5% of the side-on SGLCP, Polymer **1**, clearly show bistable switching (Figure 2.10b). Indeed, at all frequencies tested, including 60 Hz – the typical video driving-frequency – the polymer-doped FLC retains at least 80% of the light transmitted after the field used to change the director orientation is removed. On the other hand, the response of FLC-A doped with end-on polymers look very similar to the response of the FLC itself: no significant bistability is seen.

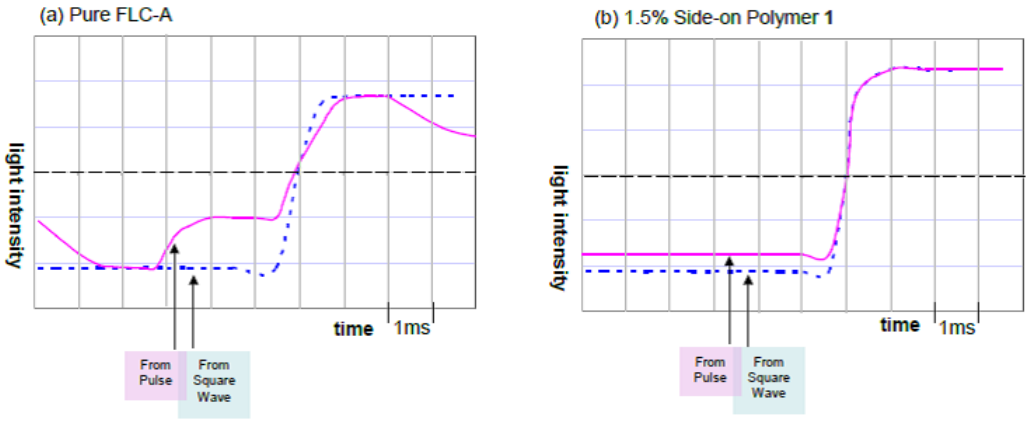

Figure 2.9. Transmitted light intensity through FLC cells for two different modes of switching: square-wave (dotted lines, blue) and bipolar pulse (solid lines, pink) for (a) Neat FLC host and (b) Polymer-doped FLC with 1.5% of Polymer 1. The change in light transmission under a DC balanced bipolar pulse (pink) shows the performance in the desired bistable operating mode for an FLC device – which is very poor for the FLC alone (low change in transmission relative to that under square wave applied voltage, blue trace). In contrast, this same FLC doped with polymer exhibits bistable behaviorthe signature of bookshelf alignment, without any complex alignment layers or annealing.

A well-known phenomenon occurs when a chevron SSFLC cell is observed under a polarized light microscope while an increasing voltage is applied slowly: “speed boats” with a triangular “bow” and a square “stern” are observed [1]. Reversing the polarity of the field reverses the direction of the speed boat, the triangular bow, becoming square and the stern becoming triangular. A cell in bookshelf geometry does not show speed boats. In collaboration with Professor Noel Clark, at the University of

Colorado at Boulder, we exmined our polymer-doped FLC cells under a polarized optical microscope while manually applying an increasing voltage (from 0 to $\sim$8V). Speed boats were clearly visible in the neat FLC-A host and a zigzag-free cell with 1.5% end-on Polymer **5** in FLC-A. On the other hand, when the voltage was applied to a cell with 1.5% Polymer **1** in FLC-A, we did not see any "speed boats". Rather, we saw an analog change in the grayscale while the voltage gradient was applied and the cell switched from dark to bright state. This effect was symmetrical: Professor Noel Clark was abule to show us that hthe graded responce to increasing boltage appeared identical when the cell was tilted in and out of the plane (approximate range $\pm 10^{\circ}$).

It is important to note that, in general, being soluble in the FLC, and being able to suppress zigzags in the bulk appear to be necessary but not sufficient criteria for enhanced bistability. Lower concentrations of (side-on) Polymer **1** and (end-on) Polymer **7**, were both soluble and suppressed zigzags, but showed no improvement in bistability over neat FLC-A.

Furthermore bistable switching was only seen in one FLC host, FLC-A, despite the fact that the three FLC hosts were designed to be very similar. the only salient different we noted was in their pitch. The pitch of FLC-A was 11 μm, while the pitch of the othe hosts were approximately half that. Therefore, the current working hypothesis is that the ability of side-on polymers to facilitate bookshelf alignment is quite sensitive to FLC helical pitch. A longer pitch indicates a weater dirving force for chiral order. Perhapys longer pitch SmC* phases allow more time for the SGLCP to facilitate layer equilibration prior to chevron formation after the transition from SmA to SmC*

The reduction of zigzag defects (and the bistability, in the case of Polymer **1**) is conferred by the polymer without loss of switching speed or tilt angle. Optical rise times (the time for transmittance to transition from 10% to 90%) of the FLC hosts were not significantly altered by the presence of the polymer dopants (Table 2.2).

Table 2.2. Rise times of 1% polymer concentration in all three FLC hosts. Rise time in FLC-A were measured optically, while those in FLC-B and FLC-C were measured electronically (error bars are shown for FLC-C measurements to give an indication of the precision of electronic measurements).

Material	Rise Time in FLC-A (μs)	Rise Time in FLC-B (μs)	Rise Time in FLC-C (μs)
Neat FLC	1180	115	173.8 ± 0.3
1% Polymer 1	1160	115	173.4 ± 0.3
1% Polymer 2	-	120	159.9 ± 1.2
1% Polymer 3	-	112	169.7 ± 1.0
1% Polymer 4	-	127	174.1 ± 1.2
1% Polymer 5	1160	-	-
1% Polymer 6	1220	-	-
1% Polymer 7	860	-	-

The electro-optic measurements also yeild an approximatevalue of the contrast ratio (the ratio of the transmittance in the bright state relative to that of the dark state). In general, addition of up to $\sim$1.5% of the soluble polymer dopants does not adversely affect contrast. Indeed, suprression of zigzags increases contrast ratio (for example the contrast ratio rises from 11:1 for FLC-A to 16.7:1 for 1.5% Polymer 1 and 12.3:1 for the same amount of Polymer 5, the end-on siloxane-linked SGLCP), another indication of a well-aligned system.

Other important FLC material properties also remain ralatively unchanged by doping with a small concentration of polymer. Specifically, polymer-dopants had little effect on the polarization, dielectric constant, and viscosity of the FLC host (Table 2.3).

Table 2.3. Polymers have little effect on FLC host polarization, dielectric constant and viscosity.

FLC Host	Polarization (nC/cm^2)	$\Delta\epsilon$	Viscocity (mpas)
FLC-C	19.7 ± 0.2	3.9	80
1% Polymer 1	19.6 ± 0.2	3.7	90
1% Polymer 2	20.2 ± 1.2	3.8	90
1% Polymer 3	20.4 ± 0.4	3.7	80
1% Polymer 4	19.4 ± 0.2	3.8	70

2.4.5 Small Angle X-Ray Scattering of Polydomain Samples: Tilt Angle

Capillary x-ray experiments, performed in collaboration with Torsten Hegmann's lab at the University of Manitoba, measure the average layer spacing of FLCs in the bulk. The temperature dependence of the layer spacing reveals the effect of polymer dopants on the the Smectic C* tilt angle (Figure 2.11). Like prior literature on *in situ* polymerized end-on SGLCP networks in FLC hosts which show that $\sim$1% typically changes the tilt angle of the FLC by 10-15%, the present end-on SGLCP solutions also show a 5-15% and the molecules start to tilt immediately after the Smectic A-to-C* phase transition [18]. In our case effects on tilt angle at concentrations of 0.75% and 1.5% (Figuree 2.11, near ambient temperature).The situation becomes more interesting with side-on polymers, particularly at 1.5% concentrations: althought the transition temperature is unchanged, no tilt occurs until the temperature is cooled to T_{AC} - 16°C (Figure 2.11). This indicatation of strong coupling of the side-on side-groups to the small molecule FLC correlates with the ability to stabilize boockshelf alignment. This "tilt delay," a window of termperature in which the neat FLC and the other solutions would be in the SmC* phase, yet the 1.5

On the other hand, SGLCPs that suppress zigzags but do not display bistability in FLC-A (i.e. do not eliminate chevron formation, for example 1.5% Polymer **5**, 1.0% Polymer **7**, and 0.75% of Polymer **1** in FLC-A, did not appear to "delay" the tilting of the small molecules (Figure 2.11). In FLC-B, tilt angles are decreased by $\sim$4% for the side-on polymer and $\sim$0.5% for the end-on polymers (not shown). Small changes in the tilt angle, without any "delay" in tilting, suggest that two separate mechansims exist for in zigzag suppression, depending on the polymers and concentrations involved. One permits adjustment of the number of layes while maintaining bookshelf orientation during the SmA to SmC* transitions; the other inhbits the nucleation of chevrons so that a chevron defect can grow to the scale of the entire sample.

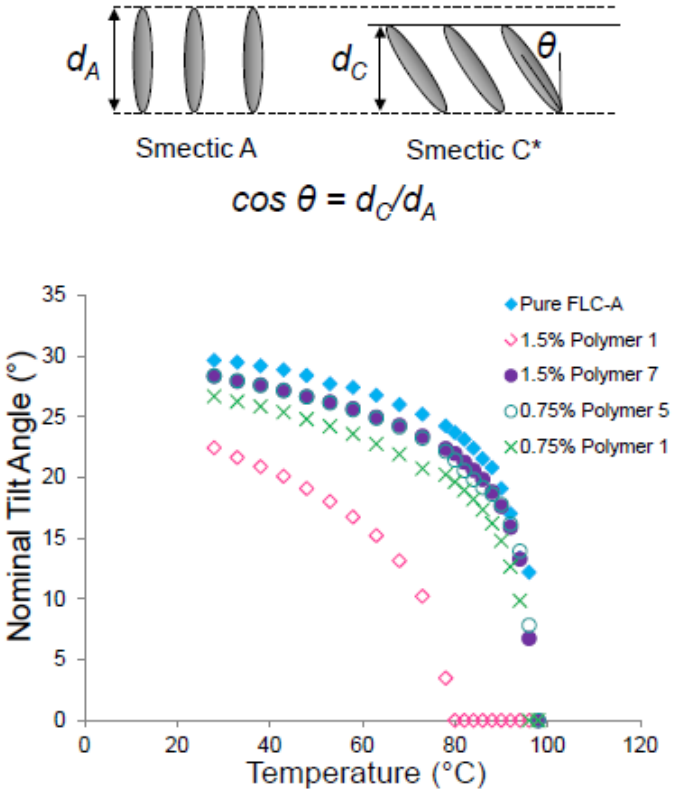

Figure 2.10. Small angle x-ray scattering of unaligned samples gives average layer spacings at both Smectic A and Smectic C* temperatures. These layer spacings can be used to determine the effect of both side-on and end-on polymers on tilt angle of the FLC molecules over a wide temperature range.

2.4.6 Small Angle X-Ray Scattering of Aligned Samples

In addition to x-ray scattering on polydomain samples, we measured the scattering of *aligned* samples in cells that are penetrable by x-rays (in this case using sapphire windows), enabling us to access information beyond the average layer spacing. Using aligned samples, x-ray diffactions can discriminate between bookshelf geometry and "single chevron" structures, and can reveal the effect of polymers on the chevron angle and layer spacing over the full range of smectic temperatures. In particular, rocking curves, the intensity at one particular q chosen based on the strongest peak at normal incidence as a fucntion of the angle of the cell normal relative to the beam, can be generated (Figure 2.12). If a sample is in bookshelf geometry, the layers will be in the Bragg condition when the sample is oriented perpen-

dicular to the beam (bookshelf smectic layers are tangent to x-ray beam, Figure 2.12 top left), giving a rocking curve that has the highest intenstity at 0°, decreasing as the cell normal is rotated away from the beam direction (Figure 2.12, top right). On the other hand, chevron layers will be in the Bragg condition only when the layers are rotated to angles that correspond to the chevron angle, resulting in rocking curves that have their highest intensity points at non-zero angles (Figure 2.12 bottom).

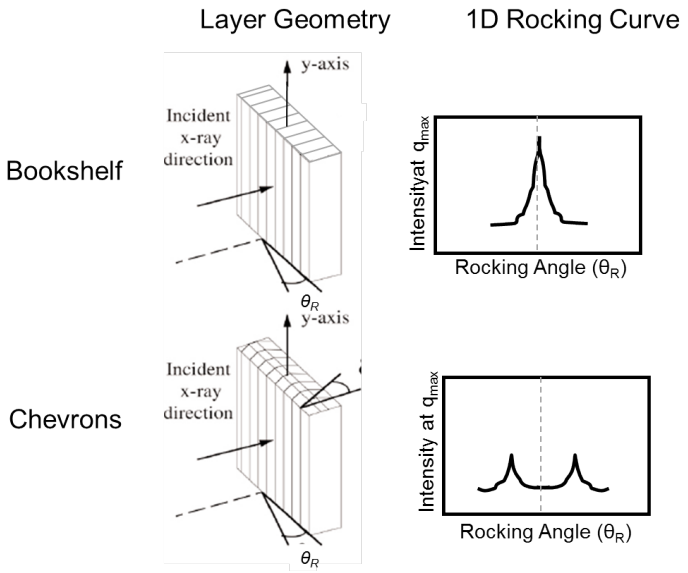

Figure 2.11. Small angle x-ray scattering of samples in bookshelf geometry (top) will result in rocking curves with the highest intensity at 0° rotation, when the bookshelf layers are in the Bragg Condition. On the other, hand, when samples are in chevron geometry (bottom), the layers are in the Bragg condition when the sample is rotated about the y-axis to angles corresponding to the chevron angles. The highest intensity points of the rocking curve generated by a chevron structure, are thus non-zero.

It should be noted here, that the following data were taken using polymer-doped FLC-C, a host that does not show bistability upon addition of side-on or end-on polymers. We therefore expect that the rocking curves of all polymer-doped FLC samples will indicate chevron architecture in the Smecitc C* phase.

In the Smectic A phase (95°C) bookshelf rocking curve, with high intensity at 0°, is seen for both neat FLC-C and FLC-C with 1.0% Polymer **1** (Figure 2.13). Rocking curves at 95°C of 1.0% end-on polymer (Polymer **7**) are also similar (not shown). Sharp rocking curves in the Smectic A phase also indicate that our sample cells contained well aligned FLC molecules. In addition, the x-ray data show that neither side-on or end-on SGLCPs change the Smectic A layer spacing (∼32.4-32.7Å) may indicate

that the polymers do not intercalate *between* the FLC layers, rather, they appear to thread *through* the layers, albeit without disrupting them.

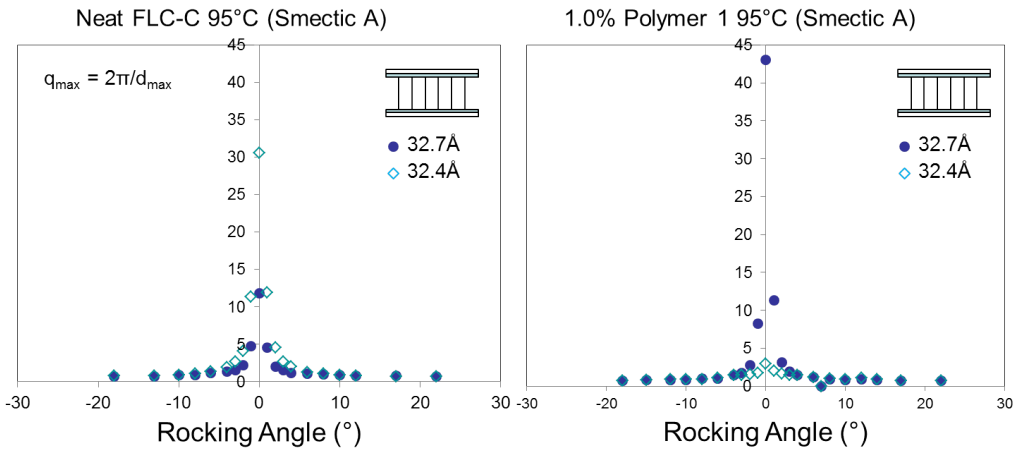

Figure 2.12. In the Smectic A phase, bookshelf alignement was manifested by a sharp single peak in the rocking curve: Rocking Curve of Neat FLC-C (left) and 1.0% Polymer 1 (right) at 95°C – in the Smectic A phase. 1.0% Polymer 1 does not affect the Smectic A layer spacing. High intensity at 0° indicates bookshelf alignment (inset).

At Smectic C* temperatures, chevron rocking curves were seen (Figure 2.14), as anticipated. At 40°C, neat FLC-C showed a very typical chevron rocking curve, with highest intensity peaks at 25-26° at a layer spacing of 29.3-29.5Å (Figure 2.14, left). Very similar rocking curves were seen upon the addition of 1.0% end-on polymer (Polymer **7**, not shown). In contrast to end-on SGLCP, addition of 1% of side-on SGLCPs (Polymers **1**, **2**,**3**, and **4** all showed similar effects) changed the rocking curve. Two strong peaks at +28 and -28 tilt from normal incidence remain with orientations similar to the neat host; however, a new peak is observed at normal incidence. We return to this surprising result in the Discussion.

One sample of 1.0% Polymer 1 in FLC-C showed an interesting asymmetric deviation from both the chevron and the aforementioned geometry (Figure 2.15). The intensity in these rocking curves in the positive rotation direction is much higher than that in the negative rotation direction, indicating that there may be an asyymetric chevron (Figure 2.14) or even, perpaps a tilted structure (Figure 2.14, right). Assymetric chevrons cannot satisfy both surface boundary conditions, a possible indication that the

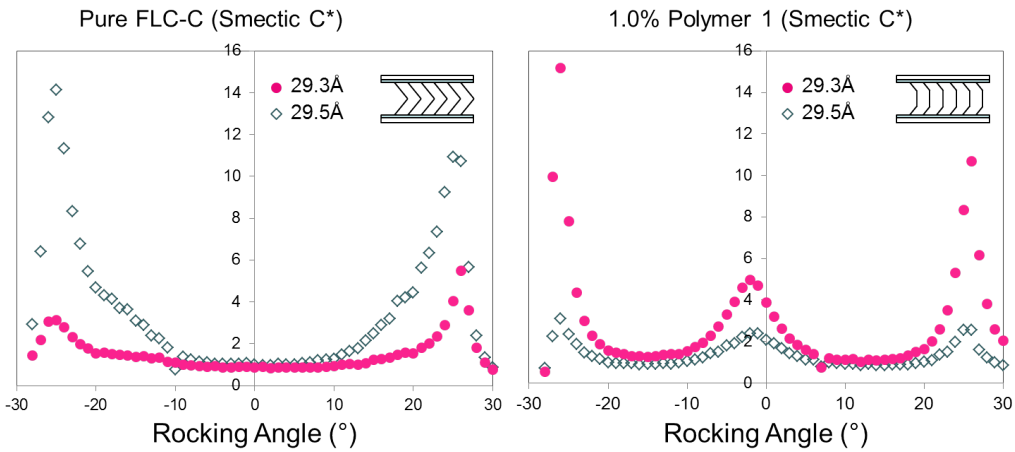

Figure 2.13. Rocking Curve of Neat FLC-C (left) and 1.0% Polymer 1 (right) at 40°C – in the Smectic C* phase. Although the neat FLC rocking curve indicates a typical chevron alignement (inset, left), addition of 1.0% Polymer 1 appears to distort the chevron structure (inset, right).

polymer is acting on the surface of this cell (and overcoming the boundary condition). Heating the sample to isotropic temperatures and quenching in the SmA phase reveals a typical bookshelf geometry. Heating it from SmA to isotropic and quenching it 7.5 °C below the SmA-SmC* transition leads to a symmetric chevron. However, further heating and quenching to lower temperatures (11.5°C and 15°C below the SmA-SmC* transition temperature) reveals the asymmetric chevron again. At room tempertature, even after a complicated thermal history, this sample of 1.0% Polymer 1 appears to be an asymmetric chevron structure (Figure 2.14, left). Indeed, this asymmetry persisted for two separate x-ray scattering trips. It should be noted that the same protocol for spin coating nylon onto the sapphire windows and for brushing to induce alignement was used for all of the cells for the synchotron (capillary action flow at 110°C was used for all of the cells.

2.4.7 Block Coplymers in FLC hosts

Based on our group's prior work on reversible gels in nematics, which provide optically uniform gels with rapid response times [13] [19] [14], we examine coil-SGCLP diblocks and coil-SGCLP-coil triblocks in FLC hosts. In particular, based on the solubility of the SGLCPs with the side-on groups "BB,"

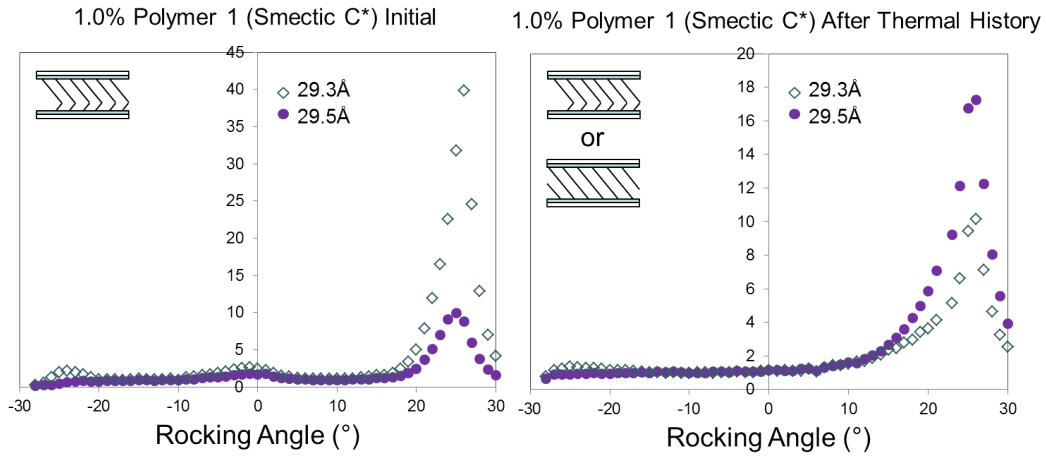

Figure 2.14. Rocking Curve of 1.0% Polymer 1 in FLC-C at 40°C – in the Smectic C* phase. Even after multiple heating and cooling events (specifically, the sample was heated to 110°C, quenched to the SmA phase, (95°C, 92°C), quenched to multiple points in the SmC* phase (90°C, 88°C and 86°C and 40°C), this sample of 1.0% Polymer 1 appears to promote an asymmetric chevron structure for most of the SmC* (inset, left). (It should be noted that at the 90°C quench, this sample showed a symmetric chevron

we hypothesized that PS-SiBB-PS would dissolve in the isotropic phase of FLC-A and form a gell upon cooling into the smectic phase. The polymers available for this studey were derived from a polymer having 57kg/mol PS – 140k 1,2 PB – 67k PS (as described in Kempe 2004), in which 66% of the repeat units in the midblock were converted to SiBB (2, Scheme 2.2). Unfortunately, the FLC was unable to dissolve the PS end blocks in its isotropic phase (tested at 1.5% w/w), perhaps due to the polarity of phenylpyrimidine. Future work might examine triblocks in which the coil domain is a phenylpyrimidine or a methyacrylate. Homopolymers of canditate coil domains can be use to identifty coild domains that dissolve in the isotropic phase of the FLC of interest. Once an appropriate coil domain is identified, a series of polymers with systematically varied coil domain length starting from a relatively short length to favor stability (10 kg/mol) could be used to vary the temperature of the sol-gel transition relative to the LC phase transition temperatures [11] [10] [12] [20].

2.5 Discussion

The key issues that we addressed in this work are: (1) identify polymer dopants that dissolve homogeneously in FLC hosts A-C, (2) establish that elastic, viscous constants and polarization of the FLC are not detrimentally affected by the dopant (up to the solubility limit of SiBB, 1.5% w/w and to the shighes concentration tested for SiC8PPC10, 3%). (3) examine the effect of the polymers on the inhibition of zigzag defects, (4) demonstrate that polymer dopants do not adversely affect switching speed (in view of (2), this indicates the polymers do not interfere with anchoring at the FLC-substrate interface), and (5) elucidate the mechanism of polymer-stabilization by examining bistability and x-ray layer spacing.

The very solubility of side-on Polymers **1** and **2** in FLC hosts is promising for the broad usefulness of polymer dopants, since they were not specifically designed for the FLC system and they possess no dipole to encourage strong side group/solvent coupling (Figure 2.8). Increasing the alkyl tail of the side-on side-group from four methylene groups in Polymers **1** and **2** to six methylene units in Polymer **3** did not appear to affect the solubility of the side-on polymers.

Of the molecularly designed siloxane-coupled phenylpyrimidine polymers, the 7-carbon spacer phenylpyrimidne, **5**, was soluble, while the 8-carbon spacer phenylpyrimidne, **6**, was not. These polymers differ by only one carbon in their spacers, their molecular weight, percent conversion and mesogenic cores were very similar, so it appears that the large impact on the solubility of the polymer may be a manifestation of an odd-even effect [21] [22]. It should be noted, however, that there is a risk that the polymer might have become slightly crosslinked over time; future work should compare freshly prepared SGCLPs of **6** in FLC can be achievable. The thiol coupled phenylpyrimidine end-on polymer, Polymer **7**, was broadly soluble at all concentrations tested (3% and lower) even though thiol-linked polymers inherently have a much lower conversion of polybutadiene to mesogenic side group than siloxane linked polymers [23].

Based on polarized optical microscopy and electro-optic effects, our hypothesis, supported by x-ray tilt angle measurements, is that an embedded polymer can capture a bookshelf-like geometry as the FLC cools from the SmA to SmC* phase: the coupling of mesogenic side groups on the polymer with the FLC molecules may delay chevron formation long enough that the more thermodynamically favored bookshelf alignment can form. The polymer may resist the shearing deformation that occurs as chevrons form, kinetically hindering chevron formation and consequently allowing time for the nucleation of new layers, a generally slower process. Given that free energy of the chevron state is greater than that of the bookshelf state due to the tilt wall penalty of the chevron, kinetically favoring layer nucleation will lead to a permanent reorientation into bookshelf geometry. The polymers' resistance to deformation is also expected to stabilize of the desired orientation against mechanical shocks (another technical challenge in SSFLCs).

On the other hand, although the end-on polymers (Polymers 5 and 7) also suppress zigzag defects, they show much reduced bistability enhancement. End-on polymers promoting the FLC to relax into a single chevron direction upon cooling would account for the general lack of both zigzags and bistability.

Addition of both types of polymer-dopants had little negative effect on the polarization, dielectric constant, and viscosity of the FLC host, indicating that the polymer is likely threading through the layers, without disrupting them (Figure 2.16). This is corraborated by small angle x-ray studies at both Smectic A and Smectic C* temperatures: the polymers have little effect on layer spacings.

From our work with similar polymers in aligned nematic solvents (Chapter 4), we know that the side-on SGLCPS are more extended than end-on SGLCPs, so its likely that side-on SGLCPs penetrate more smectic layers than the end-on polymers (Figure 2.16). It's possible that this enables the coupling with more small molecules than the more compact end-on SGLCPs. Small angle x-ray scattering of aligned samples also indicates that the coupling between the side-on side groups and the FLC molecules is

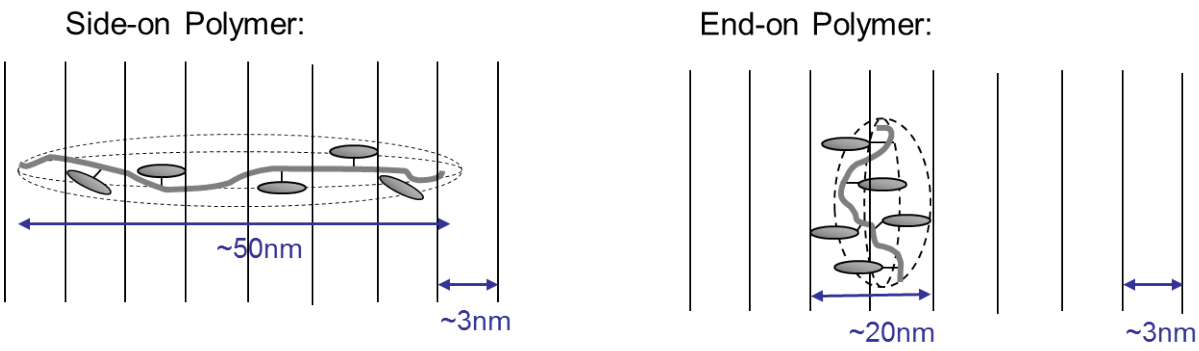

Figure 2.15. A molecule's eye view: based on size information extracted from small angle neutron scattering in aligned nematic solvents (Chapter 4), side-on polymers would span more layers than end-on polymers.

stronger than that between end-on side groups and the FLC molecules – distortions of chevron tilt angle at 1.5% w/w concentration is much greater than for Polymer **1** thane for Polymer **7** (Figure 2.11).

The surprising feature seen in the aligned SAXS patterns of FLC-C+ Polymer **1** (Figure 2.14) could indicate the coexistance of chevron domains and bookshelf domains. However, that is inconsitent with the absense of a "speed boat." Instead, the analog change in grayscale with increasing voltage suggests the coexistence of chevron and bookshelf orientation throught the cell (inset, Figure 2.14, right). (Though it should be noted that electro-optics weren't preformed on this particular cell).

2.6 Conclusions

We have developed a family of polymer dopants that confer alignment-stabilizing properties to FLC host. These polymer-doped FLCs can suppress zigzag defects, and retain the fast electro-optic responses, good contrast and appropriate tilt angle required for SSFLC display devices. Side-on SGLCPs were also demonstrated to robustly and rapidly (without controlled cooling or annealing) adopt an alignment that enables bistable switching. End-on SGLCPs appear to stabilize a single chevron direction in the host. Further physical experiments, particularly time resolved x-ray scattering, could test the hypoth-

esis that the mechanisms of bookshelf alignmen is due to delayng the formation of a chevron defect.

To the best of our knowledge, we are the first to develop a dilute additive that can transform an FLC into a material that enables rapid, high yield production of FLC cells without zigzag defects. Unlike prior approaches, the additive could potentially be applied equally well to large area displays, opening the way to applications ranging from camera viewfinders to home theater displays.

Bibliography

[1] Sven T. Lagerwall. *Ferroelectric and Antiferroelectric Liquid Crystals*. Wiley-VCH, Weinheim, 1999.

[2] Peter J. Collings and Michael Hird. *Introduction to Liquid Crystals: Chemistry and Physics*. Taylor & Francis, London, 2001.

[3] Noel A. Clark and Sven T. Lagerwall. Submicrosecond bistable electro-optic switching in liquid crystals. *Applied Physics Letters*, 36(11):899, 1980.

[4] Jan P. F. Lagerwall and Frank Giesselmann. Current topics in smectic liquid crystal research. *Chemphyschem: A European Journal of Chemical Physics and Physical Chemistry*, 7(1):20–45, January 2006.

[5] T. P. Rieker, N. A. Clark, G. S. Smith, D. S. Parmar, E. B. Sirota, and C. R. Safinya. "Chevron" local layer structure in surface-stabilized ferroelectric smectic-c cells. *Physical Review E*, 59(23):2658–2661, 1987.

[6] C. Ajlun. Stamp-Sized Ferrolectric LCD Can Power 50-In. TV Screens. *Electronic Design*, page 26, 2000.

[7] Yukio Ouchi, Ji Lee, Hideo Takezoe, Atsuo Fukuda, Katsumi Kondo, Teruo Kitamura, and Akio Mukoh. Smectic C* chevron layer structure studied by x-ray diffraction. *Japanese Journal of Applied Physics*, 27(5):L725–L728, 1988.

[8] Yukio Ouchi, Hideo Takano, Hideo Takezoe, and Atsuo Fukuda. Zig-zag defects and disclinations in surface-stabilized ferroelectric liquid crystals. *Japanese Journal of Applied Physics*, 27(1):1–7, 1988.

[9] Yuzuru Sato, Taka-aki Tanaka, Hidekazu Kobayashi, Aokim Kazuo, Hiroshi Watanabe, Hiroshi Takeshita, Yukio Ouchi, Hideo Takezoe, and Atsuo Fukuda. High quality ferroelectric liquid crystal display with quasi-bookshelf layers. *Japanese Journal of Applied Physics*, 28(3):L483–L486, 1989.

[10] Kyehun Lee and Sin-Do Lee. Fast linear electro-optical switching ferroelectric liquid crystals properties of polymer-dispersed. *Applied Physics Letters*, 64(6):718–720, 1994.

[11] Takeshi Murashige, Hideo Fujikake, Hiroto Sato, Hiroshi Kikuchi, Taiichiro Kurita, and Fumio Sato. Polymer alignment behavior with molecular switching of ferroelectric liquid crystal. *Japanese Journal of Applied Physics*, 46(2):L37–L39, January 2007.

[12] Hideo Fujikake, Tahito Aida, Jun Yonai, Hiroshi Kikuchi, Masahiro Kawakita, and Kuniharu Takizawa. Rigid formation of aligned polymer fiber network in ferroelectric liquid crystal. *Japanese Journal of Applied Physics*, 38(9):5212–5213, 1999.

[13] Michael D. Kempe, Neal R. Scruggs, Rafael Verduzco, Jyotsana Lal, and Julia A. Kornfield. Self-assembled liquid-crystalline gels designed from the bottom up. *Nature Materials*, 3(3):177–82, March 2004.

[14] Rafael Verduzco. *Self-assembled liquid crystal polymer gels*. Phd thesis, California Institute of Technology, 2007.

[15] S. Umadevi, Xiang Feng, and Torsten Hegmann. Large area self-assembly of nematic liquid-crystal-functionalized gold nanorods. *Advanced Functional Materials*, pages 1393–1403, October 2012.

[16] Harry Road, San Jose, Analytical Technology Division, Eastman Kodak Company, and Kodak Park. X-ray powder diffraction analysis of silver behenate, a possible low-angle diffraction standard. *J. Appl. Cryst.*, 3:180–184, 1993.

[17] Jan Illavsky. Nika - software for 2D data reduction. *J. Appl. Cryst.*, 45:324–328, 2012.

[18] Upindranath Singh. Effect of polymer networks on the smectic-C^{*} phase of a ferroelectric liquid crystal: High-resolution x-ray studies. *Physical Review E*, 83(6):061707, June 2011.

[19] Neal R. Scruggs. *Coupling polymer thermodynamics and viscoelasticity to liquid crystalline order: self-assembly and relaxation dynamics of block copolymers in a nematic solvent*. Phd thesis, California Institute of Technology, 2007.

[20] Hiroto Sato, Hideo Fujikake, Yoshiki Iino, Masahiro Kawakita, and Hiroshi Kikuchi. Flexible grayscale ferroelectric liquid crystal device containing polymer walls and networks. *Japanese Journal of Applied Physics*, 41(8):5302–5306, August 2002.

[21] S Marčelja. Chain ordering in liquid crystals. I. Even-odd effect. *Journal of Chemical Physics*, 60:3599, 1974.

[22] S. K. Lee, S. Heo, J. G. Lee, K-H. Kang, K. Kumazawa, K. Nishida, Y. Shimbo, Y. Takanishi, J. Watanabe, T. Doi, T. Takahashi, and H Takezoe.

[23] R. L. Ameri David and Julia A. Kornfield. Facile, Efficient Routes to Diverse Protected Thiols and to Their Deprotection and Addition to Create Functional Polymers by ThiolEne Coupling. *Macromolecules*, 41(4):1151–1161, February 2008.

Chapter 3

Polymer-Doped Vertically Aligned Nematic Liquid Crystals

The experiments discussed in this chapter were done in collaboration with Michael D. Wand of LC Vision. He, along with his postdocs, Dr. Mikhail Nishinov and Dr. Jacob Clary, synthesized most of the liquid crystal side groups, which I then added to polymer backbones. Were also grateful to Phillip Chen, from National Chiao Tung University in Taiwan and his students for conoscopic electro-optic analysis.

3.1 Abstract

We demonstrate a new class of polymer additives that enhance the viewing characteristics of a vertically aligned (VA) display in multiple critical areas: addition of a little as 0.1% of both negative and positive $\Delta\epsilon$ homopolymer dopants improve VA cell contrast while decreasing rise time – without any detrimental effects on the cells threshold voltage or saturation voltage. Two polymer dopants also appear to decrease the fall time of a VA host. The polymer dopants appear to be acting at the surface of the electro-optic cell, demonstrating cooperative ordering with the rubbed alignment layer.

3.2 Introduction

3.2.1 Background

Molecules in a vertically aligned (VA) nematic liquid crystal display (LCD) have a negative dielectric anisotropy ($\Delta\epsilon$), where the dielectric constant along the short axis of the LC molecule is larger than along the long axis (also called a "transverse dipole," Figure 3.1a). When a "vertical" electric field is applied to a VA cell, the LC molecules reorient from the homeotropically aligned "dark state," to the homogeneously aligned "bright state" as their dipoles align in the direction of the field (Figure 3.1a). Perfectly vertically aligned molecules give rise to the very dark, "dark" state responsible for the VA nematric displays excellent inherent contrast ratios (Figure 3.1a, left). Unfortunately, however, this state presents a challenge to the molecular reorientation upon application of a vertical electric field: perfectly vertically aligned molecules have no preferred azimuthal direction and experience no torque, because their symmetry axis is parallel to the field. Thus the time it takes for the molecules to reorient is long (switching is slow) (Figure 3.l1a, top). When the molecules are biased with a slight pretilt, they experience torque as soon as the electric field is applied and cooperatively rotate in the same direction, consequently, the switching speed improves (Figure 3.1b). [1] This pretilt bias must be kept small, in order to ensure that the VA nematic displays dark state, and hence contrast ratio, is retained.

The LCD industry currently uses two main modifications of the VAN cells described above in order to increase switching speed: multidomain vertical alignment (MVA) and patterned vertical alignment (PVA). In MVA cells, polymer protrusions are patterned on the glass substrate surface to encourage a pretilt in the LC molecules. The pretilt generated by the surface protrusions does speed up the LC reorientation, however, because this is a surface effect, it takes a nontrivial amount of time for the effect to extend over the entire pixel area [1]. In addition to the extra manufacturing cost of the protrusions, MVA cells also suffer from reduced contrast, because of the pretilt inherent in their design. A PVA

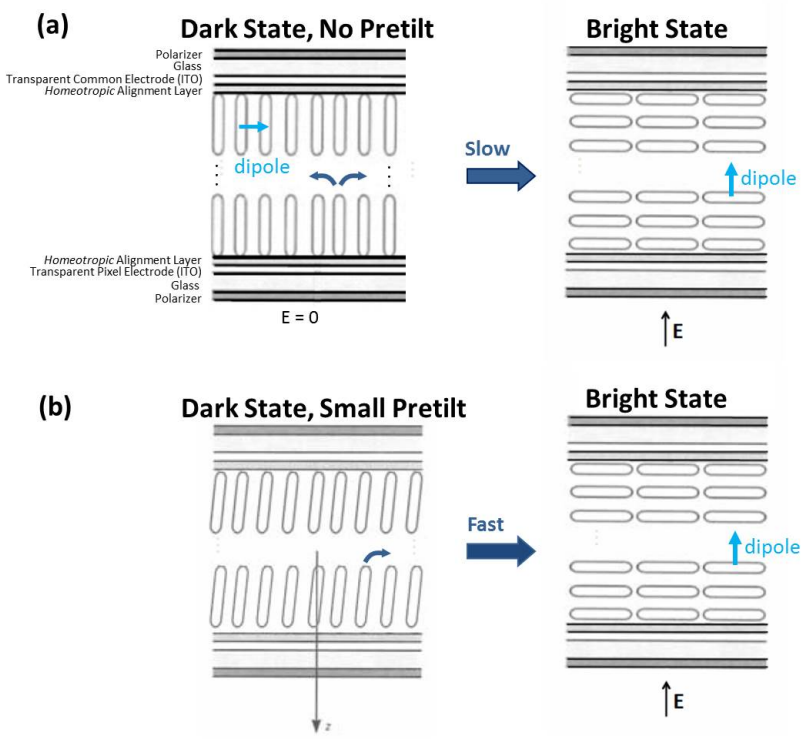

Figure 3.1. Because VA nematic molecules have a transverse dipole (light blue arrow) and hence a negative dielectric anisotropy ($\Delta\epsilon$), when a vertical electric field is applied to the homeotropically aligned VA LCs, in the "dark state," their (transverse) dipole will align with the field, causing the molecules to rotate into parallel alignment, the "bright state. When VA molecules have zero pretilt (a), the LCs can rotate in any azimuthal direction, significantly lengthening the rise time. A slight pretilt (b) can dramatically improve the rise time.

device, on the other hand, uses micro- or nanopatterned electrodes (both front and the back electrodes, called the common and the pixel electrodes, respectively) to induce faster reorientation when a field is applied. Because the reorientation in a PVA device is electronically enhanced, PVA devices do not show a decrease in contrast. However, instead of traditional spun-coated transparent electrodes, these devices require the additional, expensive step, of lithographic patterning of the electrode layer. Assembling PVA devices also requires highly accurate registration and alignment of the top and bottom panels, again increasing the difficulty and hence the manufacturing cost [1]. Both MVA and PVA devices have been successfully commercialized, although it is widely acknowledged that there is significant room for improvement in performance and cost in both MVA and PVA LCDs [1] [2].

3.2.2 Polymer-Stabilzed VA Nematic Cells

Many groups have used UV-cured in situ polymer networks to further stabilize and lock-in the pretilt in both MVA and PVA type devices, accessing the potential for switching speed improvement available with a *nonsurface* effect. The polymerization is performed *inside* the LC cell: monomers are introduced into the active medium of the display, aligned with an electric field greater than the threshold voltage of the VA LC, and polymerized *in situ* throughout the bulk by exposing the cell to ultraviolet (UV) light for a specific duration creating an aligned polymer network [2]. When the polymer content is less than 3% by weight of the total mixture, these systems are called "polymer-stabilized" vertically aligned (PS-VA) LCs [3]. PS-VA cells that sustain a pretilt angle at the substrate surface have also been demonstrated to reduce the rise time of the VA-type LC displays, but the presence of a 3-D polymer network typically leads to a somewhat long fall time. Polymer networks formed this way are generally insoluble in the host LCs, leading to phase separation between the polymer and the host [4]. Unless carefully controlled, the difference in refractive index between the crosslinked polymer network and the VA host can cause light scattering and reduce light transmission. Degradation of optical properties has been seen for PS-VA systems with 2-3% by weight polymer [4] [5], hence the need for very low concentrations of polymer.

Although polymer-stabilized vertical-alignment (PS-VA) technology can significantly improve the speed in VA-LCDs, it suffers from four significant drawbacks. First, as mentioned above, the phase separated polymer networks can disturb the homeotropic alignment of the dark state, causing light leakage – sacrificing the high contrast that motivates VA neamtic LCDs. Phase separation also often results in a higher threshold voltage [6]. Second, it introduces a difficult (10 min to 2 hrs) irradiation step during processing to polymerize the monomer that requires precise control of the uniformity and the duration of UV irradiation. Third, the free-radical species created during UV irradiation have long-term deleterious effects on the LCD (such as increasing the power consumption and reducing the display lifetime). Fourth, it excludes an entire class of small molecule components that are widely used to reduce the viscosity

(and hence increase the speed) of nematic displays (specifically, molecules with vinyl groups that would react with radicals generated in the polymerization process) [7].

3.2.3 Polymer-Doped Nematics

Rather than performing the radical step polymerization inside the display, our approach uses side group liquid crystal polymers (SGLCPs) synthesized and purified *outside* of the display that are then added at a low concentration to the VA nematic LC host before it is loaded into the LCD. The Kornfield group has shown that SGLCPs can dissolve homogeneously in (non-vertically aligned) nematic LCs, resulting in materials with exceptional optical uniformity, [8] and, when the concentration of polymer is kept low, rapid switching speed [9]. Our previous success with the optical and electro-optic properties of SGCLP networks at concentrations above 5% has served as a starting point for us to develop SGLCPs as polymer dopants (homogenously dissolved homopolymers at even lower concentrations).

Negative $\Delta\epsilon$ SGLCPs were designed with the 2,3-difluorophenyl moiety to include a transverse dipole in the side group (Figure 3.2, blue). This moiety was chosen because of its widespread use in small molecule VAN LCs [10] [11]. The chemical similarities of the side group to the nematic solvent is important to ensure that the polymers dissolve homogenously without phase separation [12]. By varying the side group core, and the linking group, while keeping the molecular weight and degree of polymerization constant, we are able to better target the effect of polymer molecular structure on the electro-optic properties of the polymer-VA solutions.

This chapter explores the possibility of using a small concentration of SGLCPs to stabilize VA nematic LCs. We show that our polymer dopants can dramatically improve switching speed (without introducing radical impurities produced during UV irradiation). Above and beyond eliminating the problem of light leakage that plagues PS-VA technology, we observed that our polymer dopant can increase contrast. By

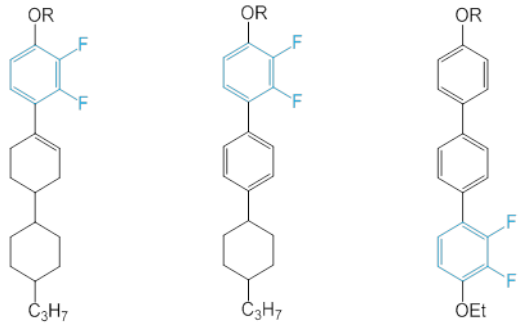

Figure 3.2. Negative $\Delta\epsilon$ SGLCPs with the 2,3-difluorophenyl moiety (blue), in three slightly different cores (above) were synthesized to determine the effect of transverse dipole, dipole placement and side group rigidity on the electro-optic properties of VAN hosts.

using polymers that dissolve uniformly in the active medium of the display, this approach maintains the optical uniformity of the LC and avoids the polymerization-induced phase-separation that occurs during the *in situ* UV photopolymerization of monomers in LCs.

3.3 Experimental

3.3.1 Materials and Instrumentation

Negative $\Delta\epsilon$ liquid crystal hosts MLC6608 (T_{NI} = 90°C $\Delta\epsilon$ = -4.2), a commercially available host and MX40424 (T_{NI} = 91°C; $\Delta\epsilon$ = -6.6), an LC Vision in-house VA host were obtained from LC Vision in Boulder, CO, while host LC MLC6886 (T_{NI} = 75°C; Δn= 0.0899; $\Delta\epsilon$ = -3.8, γ = 146 mPa s) was obtained by Phillip Chen's laboratory at National Chiao Tung University. The cyanobiphenyl homopolymers along with Polymer 1 and Polymer 2, phenylpyrimidine-based homopolymers (Figure 3.3) were previously synthesized according to methods devised by the Kornfield group [9] [13]. The synthesis of the cyanobiphenyl polymer is recorded in Chapter 4, while the syntheses of Polymers 1 and 2 are recorded in Chapter 2. Vinyl terminated side groups with cyclohexycyclohexenyl-2,3-difluorophenyl, cyclohexyl-2,3-difluorbiphenyl and 2-3-dfluoroterphenyl cores, were synthesized by LC Vision. Polybutadiene (98% 1,2 content) of size 1.07x10^3 g/mol and narrow molecular weight distribu-

tion (polydispersity index: 1.07) was synthesized by Dr. Steven Smith of Procter and Gamble Co. Polymer 5 (Figure 3.3) was synthesized by LC Vision using the cyclohexyl-2,3-difluorbiphenyl side group and the aforementioned polybutadiene prepolymer using methods devised by the Kornfield group [14]. Platinum catalysts were obtained from United Chemical Technologies in Bristol, PA and used as received. Homeotropic cells (3 μm) for elastic and viscous constant measurements were obtained from LC Vision. Other test electro-optic cells with either rubbed or unrubbed homeotropic alignment layers were manufactured by EHC, Japan, and obtained by Phillip Chen's laboratory at National Chiao Tung University. All other reagents were obtained at 99% purity from Sigma Aldrich and used as received, unless stated otherwise.

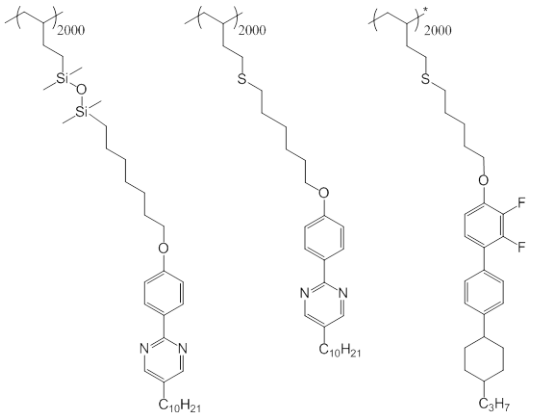

(1) **(2)** **(5)**

Figure 3.3. The synthesis of Polymers 1 and 2, the positive $\Delta\epsilon$ control SGLCPs is reported in Chapter 2. Polymer 5 was synthesized by LC Vision, according to methods also described in Chapter 1.

Reaction temperatures were controlled by an IKAmag RET basic temperature modulator. Thin-layer chromatography (TLC) was performed using J. T. Baker silica gel IB and visualized by short wave UV (254 nm). EMD Silica gel (particle size 0.040-0.063 mm) was used for flash column chromatography.

^{1}H NMR spectra were obtained using an Inova 500 MHz NMR spectrometer, recorded in $CDCl_3$ and referenced to tetramethylsilane. In some cases, a 300 MHz Varian NMR spectrometer was used to collect ^{13}F NMR spectra to characterize the fluorination of the side groups provided by LC Vision.

Polymer molecular weight measurements were obtained by gel permeation chromatography in tetrahydrofuran (THF) at 25°C eluting at 0.9 mL/min through four PLgel 10μm analytical columns (Polymer Labs, 10^6 to 10^3 Å in pore size) connected to a Waters 410 differential refractometer detector (λ = 930 nm). The molecular weight measurements were analyzed based on calibrations using polystyrene standards.

Elastic and viscous constants were measured using the Liquid Crystal Analysis System, LCAS-3, an automated capacitance-based device developed by LC Vision to measure nematic and ferroelectric LC properties. Conoscopic measurements were conducted using an Autronic-MELCHERS Conocontrol Conoscope with a two-dimensional CCD-detector in Phillip Chen's laboratory.

3.3.2 Methods

3.3.2.1 Synthesis of Negative $\Delta\epsilon$ End-on SGLCP Homopolymers

Siloxane-linked end-on SGLCPs with negative $\Delta\epsilon$ side groups were prepared by two sequential platinum-catalyzed hydrosilation steps, first of the vinyl-terminated side group and tetramethyldisiloxane and finally of the product of the first reaction with the pendant vinyl groups of 107 kg/mol polybutadiene prepolymer. Thioether-linked end-on SGLCPs with negative $\Delta\epsilon$ side groups were synthesized in one step by thiol-ene coupling to the same 107 kg/mol 1,2-polybutadiene. Silane-linked end-on SGLCPs with negative $\Delta\epsilon$ side groups were synthesized by LC Vision) followed by platinum catalyzed hydrosilation. Polymer analogous chemistry is used to unambiguously determine the effect of the polymer on the VA host, by holding the polymer backbone molecular weight and degree of polymerization fixed while being able to change the side group and linking chemistry. Detailed descriptions of the individual syntheses of siloxane linked, end-on SGLCPs with the 2,3-difluorophenyl moiety (Polymers 3 and 6) and a silane-linked, end-on SGLCP, also containing the 2,3-difluorophenyl moiety (Polymer 4) follow.

Synthesis of Polymer 3. The silane-terminated, 2,3-difluoroterphenyl mesogen (with 4-carbon spacer), (4-((2,3-difluoro-4'-(4-propylcyclohexyl)-[1,1'-The vinyl-terminated, 2,3-difluorophenylcylohexenyl mesogen (with 8-carbon spacer), 4-(2,3-difluoro-4-(oct-7-en-1-yloxy)phenyl)-4'-propyl-[1,1'-bi(cyclohexan)]-3-ene, was synthesized by LC Vision. This side group (0.2441 g, 0.582 mmol) was dissolved in 20 mL anhydrous toluene along with an eightfold excess of 1,1,3,3-tetramethyldisiloxane (TMDS) (0.8 mL, 4.5 mmol) and one drop of platinum catalyst (PC072, platinum divinyl complex in xylene) (Scheme 3.1). This mixture was stirred at 50°C for 4 days, and when completed (as monitored by thin layer chromatography), the solvent and excess TMDS are evaporated at 80°C under vacuum and the product was purified by anhydrous column chromatography using anhydrous 10% ethyl acetate in hexanes as the mobile phase (0.261 g, 81% yield).

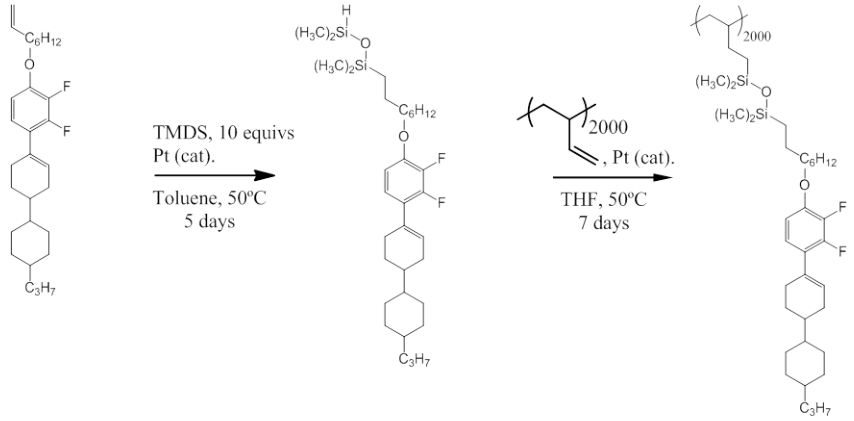

(**3**)

Scheme 3.1. The synthesis of siloxane-linked SGLCP homopolymer with cyclohexylcyclohexenyl-2,3-difluorophenyl transverse-dipole side-group.

The siloxane-linked mesogen was then attached to the pendant vinyl groups of 1,2-polybutadiene, also by platinum catalyzed hydrosilation (Scheme 3.1). Polybutadiene (0.0086 g, 0.159 mmols) was dissolved in 10 mL of anhydrous tetrahydrofuran (THF) under inert atmosphere with a threefold excess of freshly purified siloxane-terminated side group and one drop of platinum catalyst (PC085, platinum cyclovinyl complex in vinylmethylsiloxanes) and the heated at 50°C for five days. Reaction progress was monitored by ^{1}H NMR and when completed, the reaction was quenched with excess styrene and

heated at 50°C overnight.

The polymer (3) was purified by repeated precipitation in methanol (containing 10 ppm BHT), filtration through at 0.45 μm PTFE syringe filter followed by solvent fractionations using a tetrahydrofuran-methanol mixture as the good solvent and methanol (containing 10 ppm BHT) as the poor solvent. The methanol was added at room temperature to a solution (approximately 0.5% polymer) of the polymer in the good solvent until the cloud point was reached (typically the same amount of methanol as good solvent was needed to reach the cloud point). 5-15 mL of methanol was added to the cloudy solution which was then heated to 70°C until it became clear, whereupon it was poured into an oven-hot, insulated separatory funnel and allowed to separate slowly, overnight, protected from air currents. The next day, a viscous syrup (composed largely of high molecular weight polymer) sat at the bottom of the separatory funnel, and was drained off, precipitated with methanol, and dried in vacuum. The low molecular weight polymer remained in the dilute solution (above the high molecular weight fraction in the separatory funnel after cooling) and was recovered by evaporating the solvent, precipitating with methanol then drying in vacuum overnight. In the case of this polymer, two sequential fractionations were needed to obtain suitable, un-crosslinked fractions.

Synthesis of Polymer 4. The silane-terminated, 2,3-difluoroterphenyl mesogen (with 4-carbon spacer), (4-((2,3-difluoro-4'-(4-propylcyclohexyl)-[1,1'-biphenyl]-4-yl)oxy)butyl)(2-(dimethylsilyl)ethyl)dimethylsilane, was synthesized by LC Vision. The SGLCP homopolymer containing this side group was prepared by platinum-catalyzed hydrosilation with the pendant vinyl groups of the polybutadiene backbone (Scheme 3.2). The silane mesogen was first purified by anhydrous column chromatography using a solvent gradient (1%-10% anhydrous ethyl acetate in hexanes). The purified silane-terminated mesogen (0.600 g, 1.13 mmol) was then attached to the pendant vinyl groups of 1,2-polybutadiene, by platinum catalyzed hydrosilation (Scheme 3.2). Polybutadiene (0.0215 g, 0.397 mmols) was dissolved in 10 mL of anhy-

drous tetrahydrofuran (THF) under inert atmosphere with a three-fold excess of freshly purified (4-((2,3-difluoro-4'-(4-propylcyclohexyl)-[1,1'-biphenyl]-4-yl)oxy)butyl)(2-(dimethylsilyl)ethyl)dimethylsilane and one drop of platinum catalyst (PC085, platinum cyclovinyl complex in vinylmethylsiloxanes) and the heated at 50° for five days. Reaction progress was monitored by ^{1}H NMR and when the polybutadiene peak at 4.9 ppm remained the same for two days, the reaction was quenched with excess styrene and heated at 50°C overnight. The resulting polymer was purified by repeated precipitation with methanol followed by drying in vacuum overnight. In this case, no fractionation was needed to obtain suitable, un-crosslinked material.

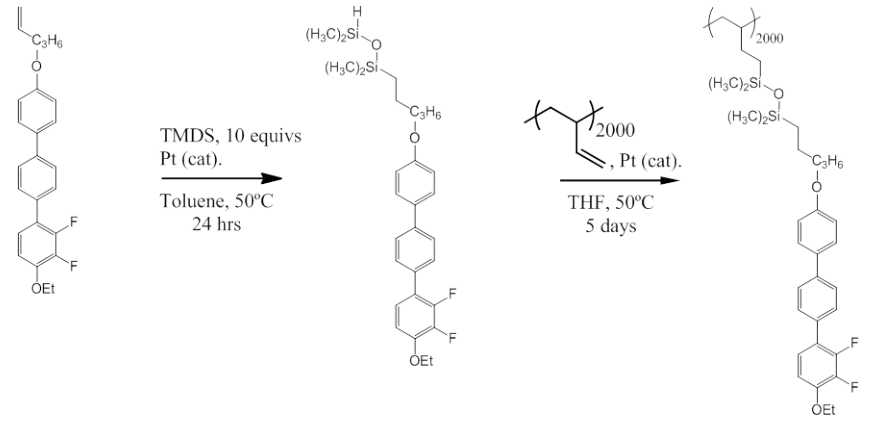

(**6**)

Scheme 3.2. The synthesis of silane-linked SGLCP homopolymer with transverse-dipole biphenylcyclohexyl side groups.

Synthesis of Polymer 6. The vinyl-terminated, 2,3-difluoroterphenyl mesogen (with 5-carbon spacer), 4-ethoxy-2,3-difluoro-4"-(pent-4-en-1-yloxy)-1,1':4',1"-terphenyl, was synthesized by LC Vision. The SGLCP homopolymer was prepared by platinum-catalyzed hydrosilation, first of the vinyl-terminated side group, with tetramethyldisiloxane and then another hydrosilation of the product of the first reaction with the pendant vinyl groups of the polybutadiene backbone (Scheme 3.3).

4-ethoxy-2,3-difluoro-4"-(pent-4-en-1-yloxy)-1,1':4',1"-terphenyl (0.2465 g, 0.625 mmol) was dissolved in 20mL anhydrous toluene along with an tenfold excess of 1,1,3,3-tetramethyldisiloxane (TMDS) (1.5

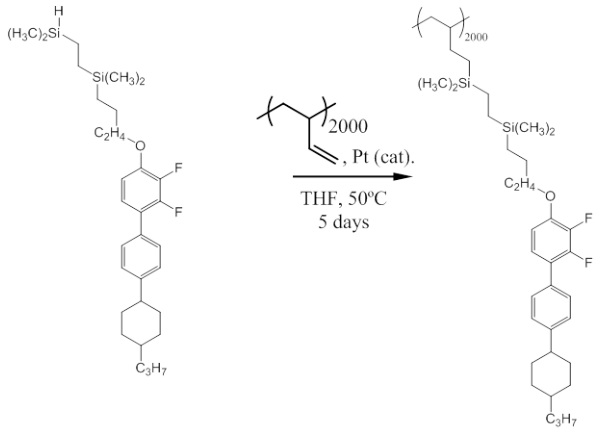

(**4**)

Scheme 3.3. The synthesis of siloxane-linked SGLCP homopolymer with transverse-dipole terphenyl side groups.

mL, 8.4 mmol) and one drop of platinum catalyst (PC072, platinum divinyl complex in xylene). This mixture was stirred at 50°C overnight, and when completed (as monitored by thin layer chromatography), the solvent and excess TMDS are evaporated at 80°C under vacuum and the product was purified by anhydrous column chromatography using anhydrous 10% ethyl acetate in hexanes as the mobile phase.

The siloxane-linked mesogen was then attached to the pendant vinyl groups of 1,2-polybutadiene, also by platinum catalyzed hydrosilation (Scheme 3). Polybutadiene (0.0438 g, 0.809 mmols) was dissolved in 20mL of anhydrous tetrahydrofuran (THF) under inert atmosphere with freshly purified 1-(5-((4"-ethoxy-2",3"-difluoro-[1,1':4',1"-terphenyl]-4-yl)oxy)pentyl)-1,1,3,3-tetramethyldisiloxane and one drop of platinum catalyst (PC085, platinum cyclovinyl complex in vinylmethylsiloxanes) and the heated at 50°C for five days (Scheme 3.3). Reaction progress was monitored by ^{1}H NMR and when completed, the reaction was quenched with excess styrene and heated at 50°C overnight. The polymer (6) was purified by repeated precipitation in methanol (containing 10 ppm BHT), filtration through at 0.45 μm PTFE syringe filter. In this case, no fractionation was needed to obtain suitable, un-crosslinked material.

3.3.2.2 Polymer Characterization

Proton nuclear magnetic resonance spectroscopy (^{1}H NMR). ^{1}H spectra (16 or 32 scans) of solutions of polymer (with concentrations of approximately 10 to 20 mg/mL) in $CDCl_3$ were recorded at room temperature on an Inova 500 MHz NMR spectrometer. The percent conversion of the pendent vinyl groups was determined by comparing the integrated area for the peaks corresponding to both the 1,2-polybutadiene and mesogen at 4.7-4.9 ppm, with peaks corresponding to the alkyl spacers on the mesogen.

Gel Permeation Chromatography (GPC). The side group liquid crystal polymers relative molecular weight and molecular weight distributions (PDI = M_w/M_n), were measured using gel permeation chromatography (GPC) calibrated with monodisperse PS standards.

2-7 mg polymer was dissolved $\sim$1 mL of tetrahydrofuran (THF) and shaken for at least 30 min with a mechanical shaker. These solutions were filtered with a 0.45 μm syringe filter prior to being injected into the GPC. The total time to traverse all four columns was approximately 45 minutes.

Polymer-VAN Solutions. Solutions of 0.1%, 0.25%, and 0.5% by weight of SGLCP homopolymers in negative $\Delta\epsilon$ nematic liquid crystal solvents were prepared by adding known masses of the polymers to known masses of the liquid crystal (either MLC6608, MLC6886, or LC Vision's in-house VA host: "MX40424"). The polymers were dissolved into the host materials by repeated iterated heating to the isotropic phase followed by centrifugation and vortex mixing.

The polymer-VAN solutions were loaded into test cells with an active area of 2 x 2.5 cm and an approximate thickness of 4 μm for electro-optic measurements. (The exact thickness of each cell is measured electro-optically prior to filling and this information is used to normalize the electro-optic data).

Polymer-doped VAN cells were then cooled from the isotropic phase (80°C, T_{NI} + 5°C) to room temperature (nematic phase) under an applied AC voltages of 0, 1.5, 2.0, or 3.0V/μm at cooling rates of 5 °C/min or, in the case of "fast cooling," 10 °C/min.

3.3.2.3 Elastic and Viscous Constants

We evaluated elastic and viscous properties of appropriate concentrations of polymer dopant in commercial VA nematic host MLC6608, and LC Visions in house very neagative $\Delta\epsilon$ LC with low threshold voltage (MX40424) using the LCAS-3 instrument provided by LC Vision. First the system measures and nulls any parasitic capacitance of the cables and LCAS system without a cell in it. The cells resistance and capacitance are then measured and nulled. Threshold voltage, dielectric anisotropy ($\Delta\epsilon$), splay elastic constant (K_{11}), bend elastic constant (K_{22}) and rotational viscosity (γ) are determined using known relationships to the measured capacitance. Finally, the data is normalized by previously measured cell thickness information.

3.3.2.4 Voltage-Transmission Curves

Voltage-dependent transmission curves were obtained using cells with both unrubbed and rubbed alignment layers. The transmittance was recorded at 0.2V intervals as the voltage increased from 0 to 8 V (or 15 V) and normalized by cell thickness.

3.3.2.5 Switching Speed Measurements

Cells with both unrubbed and rubbed alignment layers were used for electro-optic switching speed measurements. The LC response time consists of rise time, the time it takes for the LC to switch on and fall time, the time it takes for the LC to switch off. Rise time was calculated as the time it took for the

light transmission to go from 10% to 90% of the transmission generated when a 10 V square wave is applied, and the fall time was determined by the time it took for the light transmission to fall from 90% to 10% after a 10 V pulse was released.

3.3.2.6 Viewing Angle and Contrast

The effect of the polymer on the optical uniformity of the VAN cell was characterized using conoscopic measurements by Philip Chens group at the National Chiao Tung University in Taiwan. The sample is located of the optical system. Convergent polarized light is passed through a sample placed in front focal plane while the resulting two dimensional interference is generated in the rear focal plane of the optical system. This 3-D viewing angles are represented as a polar diagram where hemispheric ("horizontal") viewing angles (θ) appear as concentric circles around the center, while azimuthal viewing angles (ϕ) appear as spokes around the circle. Each location in the conoscopic figure, then corresponds to exactly one direction of light propagation (θ, ϕ). Luminance, and hence the contrast ratio (defined as ratio of the luminance of the device in the on-state to the luminance in the off-state), for every viewing angle can thus be measured and portrayed on a single figure.

3.4 Results

We synthesized a series of SGLCP homopolymers with the 2,3-difluorophenyl moiety (Polymers 3 to 6 in Figure 3.4), in order to isolate the effects of dipole placement (Polymers 3 to 5 vs Polymer 6), dipole strength (Polymer 3 vs Polymers 4 and 5), and linking group type (*i.e.* siloxane (Polymer 3), alkylsilane (Polymer 4) or thioether (Polymer 5)) on the stabilization of VAN LCs. We also synthesized two polymers with phenylpyrimidine side groups ($\Delta\epsilon \approx +1$ to 2) as positive $\Delta\epsilon$ controls (Polymers 1 and 2, Figure 4). Other positive $\Delta\epsilon$ controls, polymers with cyanobiphenyl side groups ($\Delta\epsilon \approx +13$),

were insoluble in both commercially available -$\Delta\epsilon$ LC hosts, MLC6608 and MLC6886.

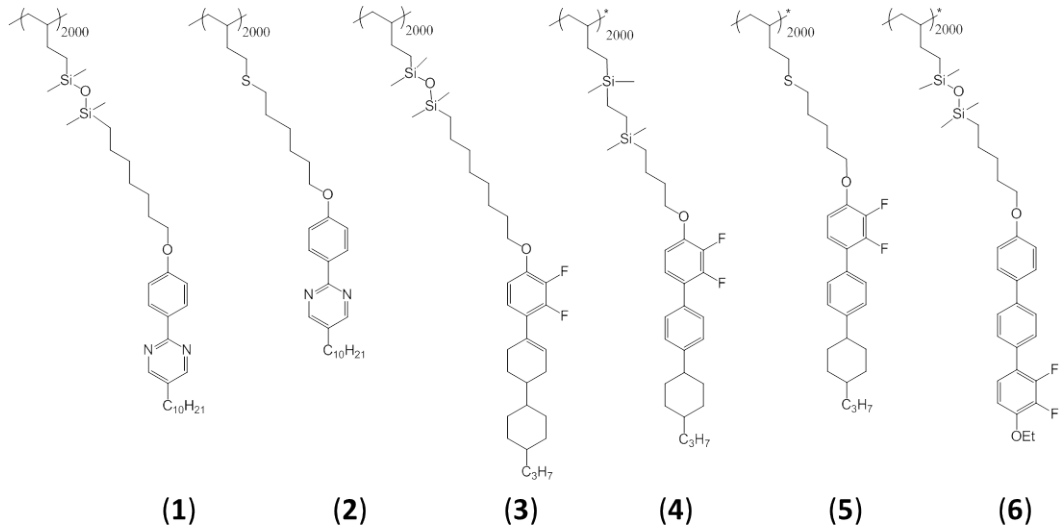

Figure 3.4. The synthesis of Polymers 1 and 2, the positive $\Delta\epsilon$ control SGLCPs is reported in Chapter 2. Polymer 5 was synthesized by LC Vision, according to methods also described in Chapter 2.

We first measured the relationship between molecular design of the side-groups and important material properties, including solubility, dielectric anisotropy, LC elastic and viscous constants. We then determined the effect of SGLCPs on several VAN cell performance criteria: threshold voltage, brightness, switching speed, and contrast.

3.4.1 Solubility

Polymer 3, with a side group containing the cyclohexylcyclohexenyl-2,3-difluorophenyl core, and Polymers 4 and 5, both with side groups made up of the cyclohexyl-2,3-difluorbiphenyl core, were readily soluble in the negative $\Delta\epsilon$ host, MLC6886 at all concentrations tested, confirming the molecular compatibility of these three side groups and the host. However, Polymer 6, which contains a 2,3-difluoroterphenyl core, was only soluble at 0.1% by weight in MLC6886, likely due to the rigid, all-aromatic 3-ring core as well as the presence of the two oxygens on either side of the terphenyl core. The percent conversion of Polymer 6 was also low, another factor that may have led to poor solubil-

ity. The positive $\Delta\epsilon$ controls, containing phenylpyrimidine side groups were soluble up to 0.5% and lower concentrations, thus easily soluble at the concentrations or interest ($\leq$ 0.25% by weight); again, cyanobiphenyl side group polymers could not be used as positive $\Delta\epsilon$ controls because they did not dissolve in MLC6608 or MLC6886.

3.4.2 Elastic and Viscous Constants

A good probe into polymer-host interactions is the evaluation of the polymer dopants in negative $\Delta\epsilon$ nematic host for their effect on dielectric anisotropy and LC elastic constants.We evaluated these properties in both a commercial VA nematic host, MLC6608, and LC Visions in-house very negative $\Delta\epsilon$, low-threshold voltage VA LC (MX40424). First 0.25% of Polymer 1 (positive $\Delta\epsilon$ control) along with representative siloxane and silane linked negative $\Delta\epsilon$ SGLCPs, Polymers 3 and 4, respectively, were examined in MX40424 (Table 3.1). The polymer has no adverse effect on the threshold voltage, even for a host with a very low intrinsic threshold voltage. Addition of the SGLCP dopants also does not significantly change the dielectric anisotropy ($\Delta\epsilon$) or the elastic constants. Similar results were obtained for 0.25% polymers in MLC6608.

Table 3.1. Electric spectroscopy results for 0.25% by weight of Polymers 1, 3 and 4 in pure VA host (MX40424)

Property	Pure VA host	0.25% Polymer 1	0.25% Polymer 3	0.25% Polymer 4
V_{th}	1.4	1.4	1.5	1.5
$\Delta\epsilon$	-6.6	-6.7	-6.7	-6.7
K_{11}	12.2	12.3	14	13
K_{22}	22	18	18	22
Viscosity	390	370	350	400

The above measurements showed the effects of the polymer-dopants on the VA LCs material properties; what follows is how these materials affect the *performance* of VA cells. The first performance criterion is voltage-transmission curves, which provide direct information about both the threshold voltage and overall transmittance. Measurements were first taken in unrubbed, homeotropic cells, where the

molecules feel no net torque. We limited electro-optic measurements in unrubbed cells for reasons that will become obvious in section 3.4: the rise time of the LC in unrubbed cells was on the order of seconds, rather than miliseconds required in VA LCDs. Rubbed cells provide some pretilt (though, again, it must be kept small to avoid reducing the cells contrast), giving the molecules slight coherent tilt. The surface anchoring in rubbed cells is stronger than unrubbed cells typically, leading to a better-aligned bright state (higher transmittance). Before electro-optic measurements were taken, the cells were cooled to room temperature from the isotropic phase while a voltage (1.5, 2 or 3 V/μm) was applied. We term this "annealing." The magnitude of the annealing voltage turns out to be an important parameter in cell performance.

3.4.3 Voltage-Transmission Curves in Cells with Zero Pretilt

The normalized voltage-dependent transmittance of VAN cells between crossed polars was first measured in unrubbed cells. Solutions of a positive $\Delta\epsilon$ control, Polymer 2, and Polymer 3, which contains a negative $\Delta\epsilon$ side group, were loaded into test cells and annealed at 3 V/μm, and V-T curves were taken. Polymer 2 and Polymer 3 have identical backbones and siloxane linkers as well as similar alkyl-spacer lengths, differing mainly in mesogenic side group, in particular, the sign the $\Delta\epsilon$ of the side groups. The threshold voltage of MLC6886 was unaffected by the addition of 0.25% of both polymers (Figure 3.5). However, while the transmittance of the VA host was unaffected by 0.25% of Polymer 2, addition of 0.25% of Polymer 3, the SGLCP with the transverse dipole side-group, to the VA host displayed higher transmittance, implying brighter bright state than the host alone.

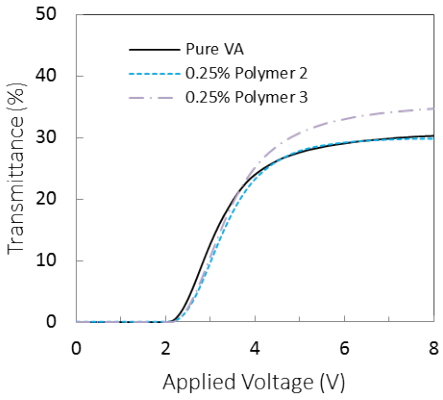

Figure 3.5. The voltage-dependent transmittance of 0.25% polymers in MLC6886 in unrubbed (zero pretilt) VA cells, previously annealed at 3 V/μm. Neither 0.25% Polymer 1 (positive$\Delta\epsilon$ control), nor 0.25% Polymer 3 (negative $\Delta\epsilon$ SGLCP) adversely affect the threshold voltage of the VA host. The transmission of the VAN cell at higher voltage is increased upon addition of Polymer 3.

3.4.3.1 Voltage-Transmission Curve in Rubbed Cells

Voltage-dependent transmission measurements were also taken under conditions closer to those used in industry: in cells that were rubbed to create a small amount of pretilt (Figure 3.6). Solutions of the negative $\Delta\epsilon$ polymers (Polymer 3, Polymer 4, Polymer 5 and Polymer 6) were loaded into test cells and annealed at 3 V/μm, and V-T curves were taken. Although they are all negative $\Delta\epsilon$ SGLCPs, the side groups of these polymers differ in rigidity: Polymer 3 contains only one phenyl ring in its three ring core, Polymers 4 and 5 have 2 phenyl groups, but differ in their linking groups, while all three rings in the core of Polymer 6 are phenyl rings.

As expected, all polymer-VAN solutions in the rubbed cells showed higher transmittance than in unrubbed ones ($\sim$1.5-fold increase). Polymers 3, 5, and 6, annealed at 3 V/μm, showed no change in threshold voltage at 0.1% by weight (Figure 3.5c, and d), and it appears that Polymer 4 decreases the threshold voltage slightly (Figure 3.5b). At all three annealing voltages, 1.5, 2, and 3 V/μm, 0.1% Polymer 3 in MLC6886 showed no change in the threshold voltage. However the transmittance was

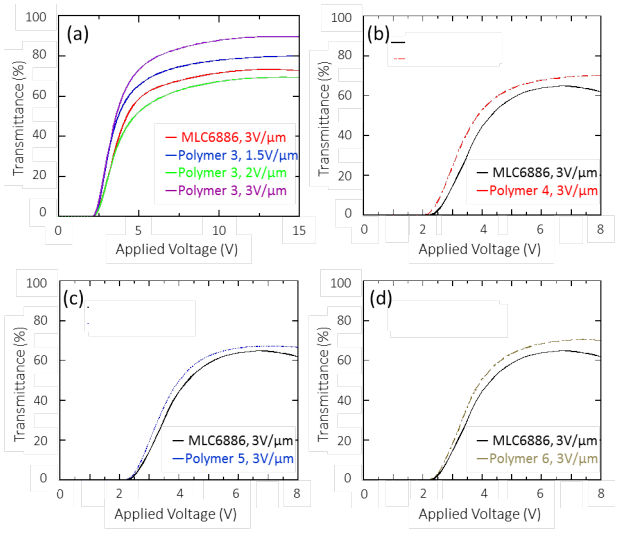

Figure 3.6. Voltage-dependent transmission curves of 0.1% polymers in VA host, MLC6886 in rubbed cells (pure VA annealed at 3 V/μm). (a) 0.1% Polymer at a variety of annealing conditions, (b) 0.1% Polymer 4, annealed at 3 V/μm, (c) 0.1% Polymer 5, annealed at 3 V/μm and (d) 0.1% Polymer 6, annealed at 3 V/μm. The threshold voltage of the VAN host is not negatively affected by the addition of 0.1% of these polymers. It appears that Polymer 4 slightly decreases the threshold voltage of the VAN host.

more affected by annealing voltage: annealing at both 1.5 and 3 V/μm increased transmittance, while annealing at 2 V/μm resulted in transmittance levels lower than the VAN host across most voltages.

To help elucidate polymer-host interactions, the transmittance of VA cells were also measured relative to rotation angle of the cell (Figure 3.7). The polymer dopant increases the anisotropy of this transmittance (red ellipse), indicating an enhancement of the LC orientation on the cell surface. The dopant appears to be providing a pretilt bias to the LC, aligning more strongly in the rubbing direction.

3.4.4 Switching Speed

3.4.4.1 Switching Speed Measured in Cell with Zero Pretilt

The rise and fall times of polymer-doped cells reveal the effects of the dopant on the pretilt angle and the surface anchoring strength of the VAN LC. Measurements of the optical rise time of the pure VA

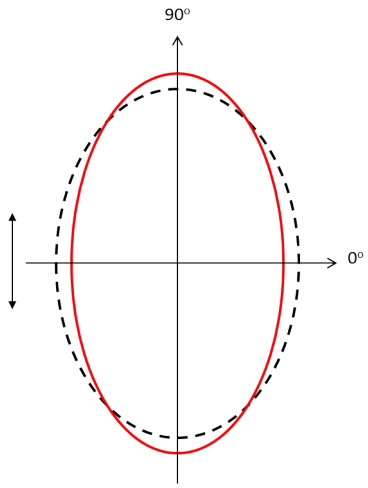

Figure 3.7. The transmittance versus rotation angle of the cell was measured by rotating the cell 360° under polarized light and recording the resulting transmittance intensity. Rubbed cells annealed at 3 V/μm we used in these measurements. The black dotted line is the polarization intensity of the pure VA host, while the red solid line is the polarization intensity of the host with 0.1% polymer dopant. The double headed arrow indicates the direction of rubbing and filling. The presence of the dopant increased the intensity of the transmittance in the rubbing direction, indicating an enhanced orientation of the VA nematic LC on the cell surface.

nematic LC host relative to the same host doped with 0.25% of Polymers 1 and 3 (Table 3.2) show that the rise time improves with the addition of both polymers. Polymer 1 (the positive $\Delta\epsilon$ control) decreases the rise time by more than four and half fold, while Polymer 3 (a negative $\Delta\epsilon$ SGLCP) decreases the rise time by more than 8-fold. The fall times appear to be less affected, both doped and undoped falling within the uncertainty of the measurement.

Table 3.2. Response time of pure VAN host (MLC6886) and 0.25% polymer-doped VAN mixtures in 4 μm unrubbed cells, annealed at 3 V/μm.

Material	Rise Time (s)	Fall time (ms)
Pure VA	20.3	8
0.25% Polymer 1	4.32	7.6
0.25% Polymer 3	2.5	8.8

It should be noted here that in this test, the reported rise times are much longer than would be used in commercial VA displays. MLC6686 is known to have a long rise time, but, more significantly, we used a simple 1 KHz 5V AC driving voltage to measure these rise times. In commercial VA displays, many other techniques (*e.g.*,overdrive schemes coupled with lookup tables), are used to achieve more rapid

rise time (*i.e.* reported in miliseconds rather than seconds).

Table 3.3 shows the effect of 0.1% polymer dopants on the response time of VA cells. At 0.1% by weight, the polymers have a smaller, but still significant, effect on the rise time than at 0.25%. Polymer 1, the siloxane-linked positive $\Delta\epsilon$ control SGLCP decreases the rise time from 20.3 to 7.0 s (35% of original value), while Polymer 2, the thiol-linked positive control slows the rise time to 31.8 s (156% of original value). The siloxane-linked negative $\Delta\epsilon$ SGLCPs 3 and 5 both improve the rise time (to 8.2 and 7.7 s, respectively). The fall time appeared to be unaffected by 2, 3, and 5, within the margin of error of these measurements. Polymer 1 appears to slightly improve the fall time of the VA host (this decrease is above the margin of error for these experiments, about $\pm$1.5ms for the fall time measurements).

Table 3.3. Response time of pure VA host (MLC6886) and 0.1% polymer-doped VA mixtures in 4 μm unrubbed cells, annealed at 3 V/μm.

Material	Rise Time (s)	Fall time (ms)
Pure VA	20.3	8
0.1% Polymer 1	7.0	5.2
0.1% Polymer 2	31.8	6.8
0.1% Polymer 3	8.2	8.0
0.1% Polymer 5	7.7	8.2

3.4.4.2 Switching Speed Measured in Cell with Small Pretilt (Rubbed Cells)

In a rubbed cell, under conditions more similar to those used in industry, the optical rise time of the pure VA nematic LC is almost two orders of magnitude lower, (232 ms *vs.* 20.3 s), a more industrially relevant speed. This faster rise time is still improved by the addition of 0.25% by weight of 3 and 5 (Table 3.4), decreasing from 232 to 130 and 144 ms, respectively, 56% and 62% of the original value. Unlike what was observed in unrubbed cells, where the negative $\Delta\epsilon$ SGLCPs did not appear to affect the fall time, the fall time decreases from 8.0 to 4.5 ms upon addition of Polymer 3, while it remained unchanged, or slightly increased upon doping with Polymer 5.

Table 3.4. Response time of pure VA host (MLC6886) and 0.25% and 0.1% polymer-doped VA mixtures in 4 μm rubbed cells, annealed at 3 V/μm.

Material	Rise Time (s)	Fall time (ms)
Pure VA	232	8.0
0.1% Polymer 2	130	4.5
0.1% Polymer 3	144	8.0
0.1% Polymer 5	85.6	10

At 0.1% by weight, Polymer 3 has an even more significant effect on the rise time of the VA host in rubbed cells, decreasing it from 232 to 85 ms (37% of original value) while the fall time falls within the margin of error of these measurements. Other measurements of 0.1% polymers in VA host were taken in more weakly rubbed cells. Although the reported switching speed was different, changes in rise time were evident. Polymer 4 decreased the initial value (4.0 s) to 30% of its original value, while Polymers 5 and 6 decreased the rise time of the host to 65% and 60% of its original value. The fall time was unaffected or slightly raised (though this was hard to tell with the margin of error in these experiments).

The decrease in rise time cannot be attributed to the polymers effect on viscosity or $\Delta\epsilon$, as data gathered in section 3.2 show that the polymer dopants have a negligible effect on both the viscosity and $\Delta\epsilon$ of the overall mixture. This suggests that the polymer dopants increase the pretilt of the LC. The decrease in the fall time upon addition of Polymer 1 in the unrubbed cell and Polymer 3 in the rubbed cell cannot be attributed to any effect the polymer has on K_{11} or K_{22}, again because measurements in section 3.4.2 show the polymer has little to no effect on the elastic properties of the VA LC. This suggests that the polymer is providing an anchoring condition that can induce the molecules to relax back faster.

3.4.5 Viewing Angle and Contrast

The contrast ratio (the ratio of the transmittance in the bright state vs. the dark state) was measured as a function of viewing angle for both rubbed and unrubbed cells (Figure 3.8). As expected, the VA cells show the most contrast in the direction of the polarizers (Figure 8, red arrows) where the dark state is

expected to be the darkest, and the contrast off axis from these (at 0° and 90°) is the least. This is typical of VAN cells [15]. At both concentrations, 0.25% and 0.1%, in both rubbed and unrubbed cells, Polymer 3 improved the contrast of MLC6886, especially at low angles. The effect of the polymer is stronger in rubbed cells, relative to unrubbed cells. In unrubbed cells, 0.1% Polymer 3 has nearly as strong an effect as 0.25% Polymer 3, while in rubbed cells the significant increase in contrast occurs at 0.1%, with very little change upon increasing the concentration of polymer. It should be also noted that while rubbing appears to make very little difference to the pure VA host, it does affect the polymer-doped VAN solutions.

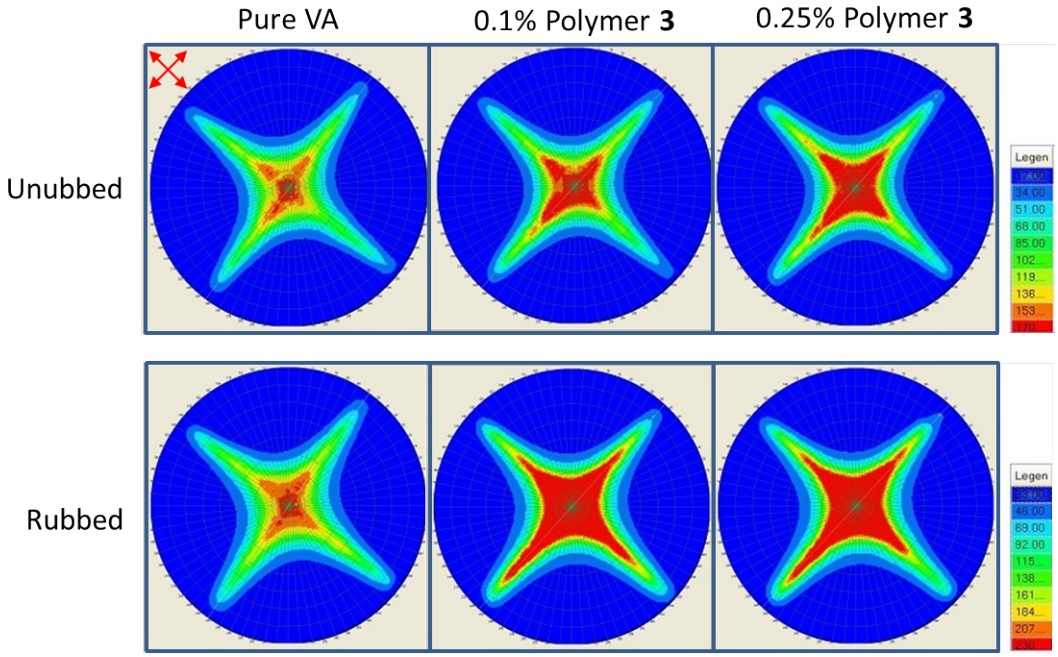

Figure 3.8. Iso-contrast plot of two concentrations of Polymer 3 (0.1% and 0.25% by weight) in VAN host in both unrubbed (top) and rubbed (bottom) cells. Red arrows show the direction of the polarizers. In all cases the cells were annealed at 3 V/μm.

The effect of the polymer on the contrast of the VAN cell was also characterized using conoscopic measurements as a function of the applied annealing voltage on a rubbed cell using 0.1% Polymer 3 (Figure 3.9) in MLC6686 host. The effect of the magnitude of the imposed AC voltage during cooling showed that the optical quality improved when an AC voltage as low as 1.5 V/μm (in this case 6V) was applied (relative to a control processed with a 3 V/μm field) and that the benefit increased only slightly

as the annealing voltage increased to 2 and 3 V/μm. Polymer 1, the siloxane-linked positive $\Delta\epsilon$ control, also increases contrast, but by a smaller amount (not shown). Addition of this polymer gave a more optically uniform bright state than the pure VA host alone, at all annealing conditions.

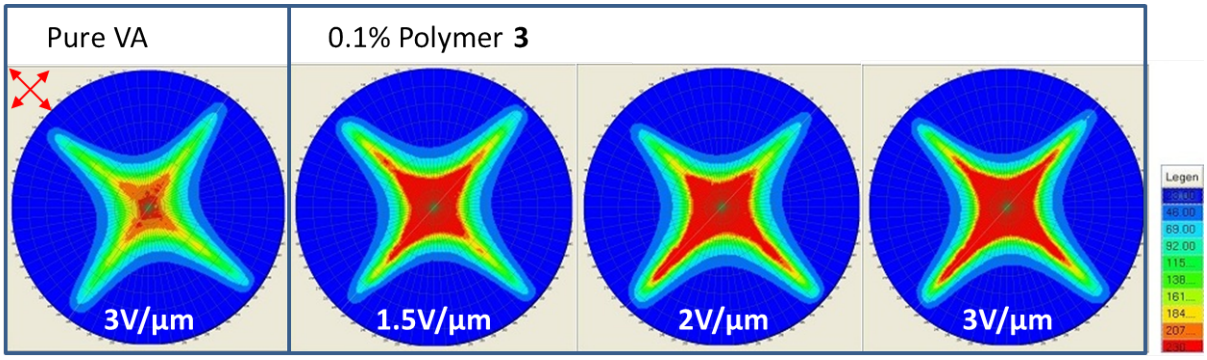

Figure 3.9. Iso-contrast plot of 0.1% Polymer 3 in VAN host in cell at annealing rates from 1.5 to 3 V/μm. Red arrows show the direction of the polarizers

3.4.6 Considerations for Industrial Applicability

To judge the potential success this technology may have if used in the display industry, we took preliminary measurements on the effect of annealing rate (Figure 3.10) as well as how the VA cell performance changes with increasing temperature (Figure 3.11). The faster annealing rate we are able to achieve, the shorter the residency time an LCD of this type would have on the manufacturing line. VAN performance ideally should not degrade until temperatures are >80-90°C, both to ensure stability under any potential environmental conditions and as a simulated lifetime measurement (lower degradation temperatures correspond to shorter device lifetimes).

When the annealing rate is increased from 5 to 10 °C/min, the threshold voltage remains the same, but voltage-dependent transmittance decreases dramatically, becoming worse than that of the pure VA host (annealed at 5 °C/min).

Temperature-based lifetime tests of Polymer 5 in rubbed cells showed cell failure above 60°C (Figure 3.11). Similar measurements in unrubbed cells showed similar results, with failure seen above 50°C.

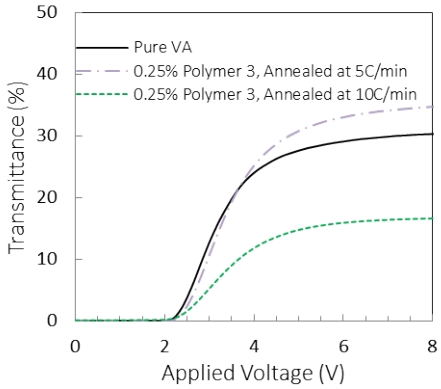

Figure 3.10. Voltage-dependent transmission curves of 0.1% Polymer 5 in VAN host MLC6886, in rubbed cells annealed at 3V/m at a variety of temperatures. Cell failure appears to begin between 60 and 70 °C.

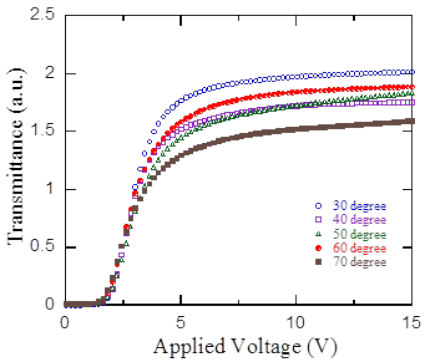

Figure 3.11. Voltage-dependent transmission curves of 0.1% Polymer 5 in VAN host MLC6886, in rubbed cells annealed at 3 V/μm at a variety of temperatures. Cell failure appears to begin between 60 and 70°C.

3.5 Discussion

Side groups containing a transverse dipole (specifically the 2,3-difluorophenyl moeity) were designed both to increase the solubility of the polymer in the VA nematic host and to have a dipole direction and magnitude commensurate with that of the solvent, while phenyl pyrimidine cores were used to make weakly positive $\Delta\epsilon$ control polymers. We first demonstrated that these SGLCPs can, by choice of their side group, be readily soluble in negative $\Delta\epsilon$ hosts. Polymer dopants with negative $\Delta\epsilon$ side groups were shown to dissolve homogeneously in negative $\Delta\epsilon$ nematic hosts, though the 1,2-difluoroterphenyl side group was less readily soluble, likely owning to the rigid terphenyl core. SGLCPS with phenylpyrim-

idine were also shown to dissolve homogeneously in negative $\Delta\epsilon$ nematic hosts below 0.5%. Polymer dopants with highly positive $\Delta\epsilon$ side groups were not soluble in the negative $\Delta\epsilon$ hosts tested.

Measurements of elastic and viscous constants show that both positive and negative $\Delta\epsilon$ SGLCPs have little effect on the bulk material properties of the VA host at all concentrations tested (0.1% to 0.5% by weight).

Both electronic and electro-optic measurements of the threshold voltage show that at low concentrations, neither the positive nor the negative $\Delta\epsilon$ SGCLPs increase the threshold voltage. Interestingly, 0.1% of Polymer 4, the silane linked SGLCP with the 2,4-difluorobiphenylcyclohexyl side group, appears to decrease the threshold voltage slightly. In practice, this could translate into lower power consumption in a commercial LCD. Polymer 4 was the only silane-linked polymer tested; it would thus be interesting to find out if other silane-linked SGLCPs were able to generalize this effect. Regardless, it should be noted that *in situ* PS-VA systems generally increase the threshold voltage of a VA host [3].

It should also be noted that the annealing step used to prepare the polymer-doped VAN cells is on par with the most competitive UV irradiation times: an AC voltage is applied as the cell is cooled into the nematic phase and down to ambient temperature over the course of a few minutes (cooling from 80 to 30°C, at 5 °C/min). The magnitude of the imposed AC voltage during cooling proved to be an important variable, which we call the annealing voltage. An AC annealing voltage as low as 1.5 V/μm improved the response time in polymer doped VAN (and had no effect on undoped controls); and the benefit increased as the annealing voltage was increased to 3 V/μm.

In industrially relevant rubbed-cells, the optical rise times of the virgin VA nematic LC doped with 0.25% of Polymer 3 show that the rise time is improved dramatically, from 232 to 130 ms, by addition of the polymer dopant (Table 4). Polymers 4, 5, and 6, the other negative $\Delta\epsilon$ SGLCPs, showed qualitatively similar, but not as large, improvements in rise time, Polymer 1, the siloxane linked positive $\Delta\epsilon$ control,

also gave improvements in the rise time. However Polymer 2 significantly increased the rise time of the VA-host in unrubbed cells. Because Polymer 2 was made through thiol-ene chemistry, the conversion of the polybutadiene pendant vinyl groups to mesogenic side groups is much lower (on average 50%, vs 80% to 100% in the siloxane and silane chemistries), indicating that side group density is likely a factor in these rise time improvements.

Because weve shown that the polymer dopants have little effect on the viscosity, $\Delta\epsilon$ and elastic constants, we know that the decreases in rise time cannot be attributed to changes in these properties. This suggests that the polymer dopants act by increasing the pretilt of the LC, an effect that could primarily act on the surface of the cell. Indeed measurements of transmittance versus rotation angle of the cell show that doped cells have an anisotropic increase of transmittance (primarily in the rubbing direction), indicating that the LC alignment at the surface is, in fact, changed.

The fact that a cells transmittance increases in the rubbing direction also seems to indicate some cooperative alignment of the polymer dopants and the rubbed layer. This is also seen in the contrast measurements: the contrast of the pure VA host changes only slightly in rubbed vs. unrubbed cells, while the contrast with 0.1% Polymer 3 increases significantly in rubbed cells. Though the contrast increased in both types of cells with addition of polymer dopants, this is another indication that the mechanism of polymer stabilization is at the surface.

It should be noted, however, that upon addition of 0.1% Polymer 3, the fall time of the VA host is improved by about the same factor as the rise time is, from 8 ms to 4.5 ms (Table 3.4). The fall time is also improved by the addition of Polymer 1, the positive $\Delta\epsilon$ control, though by a smaller amount. Addition of Polymers 4, 5 and 6 showed no change in fall time, within the margin of error of the experiments. Again, the decrease in the fall cannot be attributed to any effect the polymer has on K_{11} or K_{22}, because measurements in section 3.2 show the polymer has little to no effect on the elastic

properties of the VA LC. Unlike changes in rise time, changes in fall time argue for the presence of a polymer network throughout the cell, providing an anchoring condition in the bulk that can induce the molecules to return to its relaxed state faster than they would have otherwise. The fall time improvement effect was seen for one positive $\Delta\epsilon$ control SGLCP and one negative $\Delta\epsilon$ SGLCP, indicating that while the rise time effect was sensitive to the sign of the dipole, the fall time effect may not be. Polymers 1 and 3 were both siloxane-linked and had the largest spacer lengths of all the polymers tested, suggesting that while more investigations are needed to determine the exact mechanism of fall time improvement, spacer length may play an important role.

Unlike many types of in situ polymer stabilized VAN cells, our polymer dopants did not decrease the contrast or optical uniformity of the cells. Contrast in both rubbed and unrubbed cells was increased by adding as little as 0.1% polymer dopant to the host. Relative to a control cell prepared with pure VA, the doped-VA cells showed equally good dark states, indicating that this increase in contrast is due to the increased bright state. Indeed, voltage-transmittance curves of negative $\Delta\epsilon$ SGLCPs in VA host show higher transmittance than the undoped cell alone, also indicating a brighter bright state. This is a further argument that the polymer is acting on the surface of the cell.

3.6 Conclusions

The key issues that we addressed in this work are (1) prove that polymer dopants dissolve homogeneously in VA nematics, (2) establish that elastic and viscous constants of the LC are not detrimentally affected by the dopant, (3) demonstrate that polymer dopants do not adversely affect switching speed– indeed some polymers gave improvements in both rise and fall times, and (4) examine the effect of polymer dopant on viewing angle and contrast.

Polymer analogous chemistry using separately synthesized mesogens and identical polymer backbones

enable us to unambiguously determine the effect of side-group structure by holding the polymer backbone length fixed. Three different side groups (the 2,3 difluorophenyl bicyclohexyl group, the 2,3-difluorbiphenylcyclohexyl and the 2-3-dfluoroterphenyl) and three coupling chemistries (siloxane, thiol-ene, and silane coupling) were compared. By selecting the mesogenic side group (with different dipole strength and side group rigidity) and linking group structure (sterically large vs small and free to rotate), we are able to control the miscibility of the SGLCP and explore the influence that the side group structure has on the nematic-polymer-host matrix.

In collaboration with Dr. Michael Wand at LC Vision and Prof. Philip Chen, at National Chiao Tung University, we have shown that the polymer additives we have developed enhance the viewing characteristics of a vertically aligned (VA) display in multiple critical areas: addition of a little as 0.1% of our first generation of polymer dopants improved contrast and brightness, while cutting the rise time almost in half and without adversely affect the threshold voltage, saturation voltage, or viscosity.

Although we've shown that the VA host is broadly tolerable to many side groups, three linking chemistries and a variety of spacer lengths, the magnitudes of the electro-optic effects appear sensitive to all three variables. As we anticipated, the sign of the dielectric anisotropy of the mesogenic side groups appears to be important: polymer dopants bearing mesogens that have $\Delta\epsilon > 0$ are good and mesogens that have $\Delta\epsilon < 0$ are even better by all three display performance criteriabrightness, rise time, and contrast.

Of the three linking chemistries, thiol-ene coupling was the only one that provided a dopant that gave worse performance than the VA host; in addition Polymer 2, the thioether-linked positive $\Delta\epsilon$ control, increased the cells rise time. The only silane-linked SGLCP, Polymer 4, was also the only polymer that showed a decrease in threshold voltage. Using the two polymers with the largest spacer lengths (one positive $\Delta\epsilon$ siloxane-linked SGLCP, one negative $\Delta\epsilon$, siloxane-linked SGLCP), the fall time of the VA host was also decreased.

The decrease in rise time suggests that the polymer dopants, increase the pretilt of the LCs, while the decrease in the fall time suggests that some polymers are also providing an anchoring condition that induces the molecules to relax back faster.

Cooperative ordering with the rubbed alignment layer was also seen. In rubbed cells, polymer-dopants showed higher transmittance in the rubbing direction, better contrast, and faster switching speed. The difference in contrast, for example, of the doped-VA in rubbed cells relative to unrubbed was more significant than the difference between the undoped cell under these same conditions indicating, perhaps, a synergistic effect of the combination of the rubbed layer and the polymer dopant.

While these systems are not yet entirely industry-ready (temperature degradation of performance must first be dealt with), polymer dopants may, one day, provide a "drop-in solution" for introducing a small pretilt that confers fast response without causing light leakage. Complex infrastructure for UV irradiation is not needed and the electrodes that are already part of the LCD can be used to apply the "annealing voltage" during the cooling step after filling the cell. This approach eliminates formation of the undesired by-products of UV irradiation (radicals that increase power consumption and reduce the lifetime of a display). Using our newly synthesized negative SGLCPs as dopants, we have shown that addition of on the order of 0.1% dopant into the VA LC host can simultaneously confer three benefits: reduce the rise time, increase the contrast and improve viewing-angle symmetry

Bibliography

[1] Shin-Tson Lee, Seung Hee, Kim, Sung Min, Wu. Emerging vertical-alignment liquid-crystal technology associated with surface modification using UV-curable monomer. *Journal of the Society for Information Display*, 17(7):551–559, 2009.

[2] Jae Jin Lyu, Hirotsuku Kikuchi, Dae Hyun Kim, Jun Hyup Lee, Kyeong Hyeon Kim, Hiroki Higuchi, and Seung Hee Lee. Phase separation of monomer in liquid crystal mixtures and surface morphology in polymer-stabilized vertical alignment liquid crystal displays. *Journal of Physics D: Applied Physics*, 44(32):325104, August 2011.

[3] C. V. Rajaram, S. D. Hudson, and Liang-Chy Chien. Morphology of polymer-stabilized liquid crystals. *Chemistry of Materials*, 7(9):2300–2308, 1995.

[4] Kazunori Maruyama, Takeshi Houryu, and Yasufumi Iimura. Polymer-stabilized method for vertically aligned supertwisted nematic liquid crystal displays. *Japanese Journal of Applied Physics*, 46(2):726–728, February 2007.

[5] Volodymyr Borshch, Jeoung-Yeon Hwang, and Liang-Chy Chien. Liquid crystal-directed polymer nanostructure for vertically aligned nematic cells. *Proceedings of SPIE*, 7618:76180V–76180V–6, 2010.

[6] Czung-Yu Ho, Fa-Hsin Lin, Yu-Tai Tao, and Jiunn-Yih Lee. Improvement in device performance from a mixture of a liquid crystal and photosensitive acrylic prepolymer with the photoinduced ver-

tical alignment method. *Science and Technology of Advanced Materials*, 12(6):065002, December 2011.

[7] Julita S. Gasowska, Stephen J. Cowling, Martin C. R. Cockett, Michael Hird, Robert A. Lewis, E. Peter Raynes, and John W. Goodby. The influence of an alkenyl terminal group on the mesomorphic behaviour and electro-optic properties of fluorinated terphenyl liquid crystals. *Journal of Materials Chemistry*, 20(2):299, 2010.

[8] Rafael Verduzco, Neal R. Scruggs, Samuel Sprunt, Peter Palffy-Muhoray, and Julia A. Kornfield. Director dynamics in liquid-crystal physical gels. *Soft Matter*, 3(8):993, 2007.

[9] Michael D. Kempe, Neal R. Scruggs, Rafael Verduzco, Jyotsana Lal, and Julia A. Kornfield. Self-assembled liquid-crystalline gels designed from the bottom up. *Nature Materials*, 3(3):177–82, March 2004.

[10] Matthias Bremer and Lars Lietzau. 1,1,6,7-Tetrafluoroindanes: improved liquid crystals for LCD-TV applicationw. *New Journal of Chemistry*, 29:72–74, 2005.

[11] Melanie Klasen, Matthias Bremer, and Kazuaki Tarumi. New liquid-crystal materials for active matrix displays with negative dielectric anisotropy and low rotational viscosity. *Applied Physics*, 39(11):1180–1182, 2000.

[12] H. Finkelman, H.-J. Kock, and G. Rehage. Phase studies of liquid crystalline side chain polymers mixed with low molar mass liquid crystals of similar structure. *Mol*, 89:23–26, 1982.

[13] Michael David Kempe. *Rheology and dynamics of side-group liquid crystalline polymers in nematic solvents*. Phd thesis, California Institute of Technology, 2003.

[14] R. L. Ameri David and Julia A. Kornfield. Facile, efficient routes to diverse protected thiols and to their deprotection and addition to create functional polymers by thiol–ene coupling. *Macromolecules*, 41(4):1151–1161, February 2008.

[15] J. H. Park, J. H. Lee, D. H. You, and S. D. Lee. Axially symmetric vertically-aligned (ASVA) liquid crystal display using surface relief gratings on a polymer layer. In *3rd Asian Symposium on Organized Molecular Films for Electronics and Photonics (ASOMF 3)*, pages 231–234. Taylor & Francis, 2000.

Chapter 4

Structure and Conformation of End-on and Side-on SGLCP Hompolymers in Aligned Nematic Solvents

Paul Pirogovsky and Rohan Hule contributed to the experiments discussed in this chapter. We traveled together to the NIST Center for Neutron Research (NCNR) and Oak Ridge National Laboratorys High Flux Isotope Reactor (HFIR) where we shared the responsibility of performing the neutron scattering experiments. Were grateful to Boualem Hammouda, John Barker, Lionel Porcar and Cedric Gagnon at the NCNR and Ken Littrel, Lisa Debeer-Schmit, and Kathy Bailey at HFIR for help with neutron scattering experiments. Paul Pirogovsky deuterated the starting material for the liquid crystal solvent according to a procedure he optimized. Michael D. Wand of LC Vision in Boulder, CO made some great suggestions when I was designing a new synthesis of perdeuterated 4-pentyl-4'-cyanobiphenyl.

4.1 Abstract

The spontaneous anisotropy in the local chain conformation of side-on and end-on side-group liquid crystalline polymers when dissolved in aligned nematic solvent was investigated using small angle neutron scattering. Measurements of dilute solutions of polymers in deuterated nematic solvent allowed

information about individual polymer coils to be extracted. Side-on polymers were also determined to retain local anisotropic order, even after the solvent undergoes the nematic-to-isotropic phase transition.

4.2 Introduction

Side-group liquid crystal polymers (SGLCPs) exhibit unique properties that arise from the coupling of the orientational order inherent in the LC side group to the flexible backbone of the polymer [1] [2]. When random coil polymers are dissolved in conventional (isotropic) solvents, they adopt an isotropic conformation (Figure 4.1a). On the other hand, because of the local coupling of SGLCP side groups with the nematic LCs, SGLCPs adopt an anisotropic conformation when they are dissolved in nematic solvents, leading to a synergistic ordering effect that has no counterpart in random coil polymers in conventional solvents [2] [3] [4].

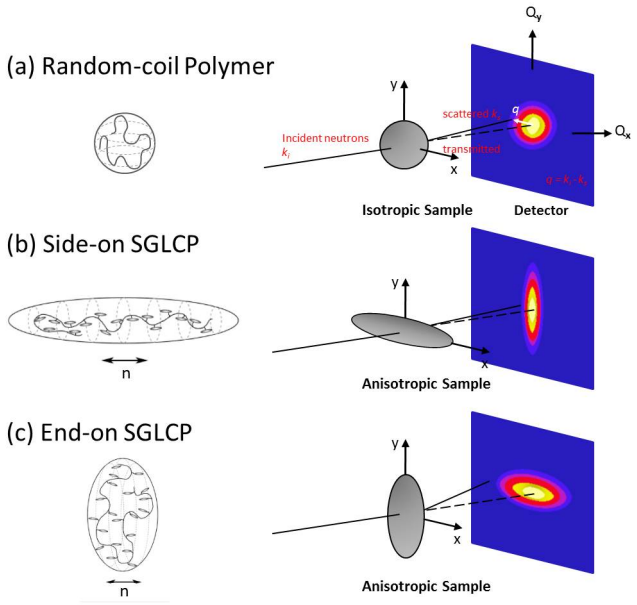

Figure 4.1. Conventional polymers in good solvents adopt isotropic conformations and give isotropic small angle scattering patterns. (b) Side-on SGLCPs in aligned nematic solvents adopt a prolate ($R_{\parallel} > R_{\perp}$) conformation, and show anisotropic scattering patterns. Because small angle scattering is an inverse spcace technique, prolate samples give oblate $R_{\parallel} < R_{\perp}$) scattering patterns, right. (c) End-on SGLCPs in nematic solvents adopt an oblate conformation and display prolate scattering patterns.

Side-on and end-on SGLCPs have profoundly different orientational coupling between their liquid crystal mesogens and their polymer backbones: laterally-attached, side-on side group typically orient perpendicular to the parallel backbone (Figure 4.1b), while terminally-attached, end-on side groups most often orient perpendicular to the polymer backbone (Figure 4.1c). When dissolved in nematic solvent, the nematic interactions between the solvent and the side groups result in the side groups aligning along the LC director (*n*), while their attachment geometry (side-on or end-on) forces the backbone to follow suit. The different attachment geometries thus affect both the chain flexibility (due to the coupling between adjacent side groups) and the orientation of the backbone relative to the director when dissolved in the nematic solvent: the side-on SGLCP, because of strong solvent/side group coupling, adopts a strongly prolate conformation relative to the direction of the director. (Figure 4.1b), while the end-on SGLCP, with weaker side group/solvent coupling, adopts a mildly oblate conformation (Figure 4.1c). The polymers equilibrium conformation is thus determined by the thermodynamic compromise between the entropic penalty of backbones deviation from a Gaussian random-walk and enthalpic benefit of side-group-solvent interactions [5].

End-on SGLCPs with cyanobiphenyl ("CB4") side groups and side-on 3,5-di(4-butoxybenoate ("BB") side groups are known to be soluble in the nematic liquid crystal 4-*n*-pentyl-4-cyanobiphenyl (5CB), as well as its perdeuterated counterpart, d_{19}5CB. Indeed, the Kornfield group has previously studied solutions of these homopolymers in the semidilute regime, finding that while the end-on polymers remain mildly oblate throughout the nematic region, side-on polymers, with stronger side group/solvent coupling leading to highly prolate structures, display strongly temperature-dependent anisotropy [4] [5]. In this concentration regime, the polymers have been shown to adopt spherical conformations after the solvent is heated past the nematic-to-isotropic phase transition temperature (T_{NI}) [4] [5].

The nematic LC solvent undergoes a discontinuous change in solvent ordering at the nematic-to-isotropic phase transition. SGLCPs are soluble in both the nematic and isotropic phases, undergoing the change

in orientational order along with the LC solvent [5]. The Kornfield group has previously demonstrated that this step change in solvent quality across the T_{NI} indeed produces an abrupt change in the conformation of SGLCP homopolymers [5], as well as in the self-assembly of SGLCP diblock copolymers, at concentrations above 5% SGLCP by weight [4] [5]. As the concentration of polymer in a polymer-LC system increases, the T_{NI} of the system shifts to higher temperatures, because of the increasing contribution SGLCP, which has higher-temperature nematic stability [6]. Indeed, at certain concentrations a synergistic effect is seen, with the T_{NI} of the system being higher than both the T_{NI} of small molecule nematic solvent and the T_{NI} of polymer [6]. In this work, we'll show that, even at temperatures above (but close to) T_{NI}, anisotropic scattering was seen in 1.0% solutions of side-on polymers in nematic solvents, indicating the presence of ordered strutcutes above the bulk isotropic phase transition (see Section 4.3).

Small angle scattering is ideal for studying the conformational anisotropy of SGLCPs. In the case of SGLCPs in liquid crystal solvent, small angle neutron scattering (SANS) is essential due to insufficient contrast between the polymer and LC solvent seen in small angle x-ray scattering (SAXS): neutrons are scattered by the samples nuclei, and can thus distinguish between light atoms (through isotopic labeling) without causing radiation damage, giving information about polymer conformation on the nanometer scale (1 – 500 nm) [7]. Specifically, SANS contrast arises from difference between scattering cross sections of the deuterated LC solvent and the undeuterated polymer chains. In dilute systems, the polymer chains can be assumed to be noninteracting, so SANS can be used to extract information related to individual polymer chains, isolating the form rather than the structure factor [8].

SANS is an oft-used tool for investigating dilute polymer solutions because contrast can be acheived by isotopic-labelling rather than chemical modification, leaving physical properties unperturbed. Typically, such contrast is achieved using deuterated solvents and hydrogenated polymers [8], or, in the case of LC solvents, because of lack of commercial availability of deuterated LCs: deuterated polymer backbones

and hydrogenated side-groups and LC solvent [9]. Unfortunately, in dilute solutions, the scattering intensity of such systems is quite low [9]. The Kornfield group has thus devised a method to perdeuterated 4'-n-pentyl-4-cyanobiphenyl (5CB) and measure the scattering of hydrogenated SGLCPs in deuterated LC solvent [10] [2] [4]. Our experiments also break isotropic symmetry and study samples that are aligned in a near-monodomain, rendering the anisotropy visible and measurable in a way that it is not polydomain samples. The same analyses as those carried out for isotropic scattering patterns can tell us about chain dimensions both parallel and perpendicular to the nematic director.

Here we examine conformational anisotropy of dilute solutions of end-on and side-on SGLCPs with matched degrees of polymerization, in aligned, nematic solvent using SANS. We show significant differences in the backbone rigidity between the side-on and end-on SGLCPs in LC solvent. Monitoring local ordering as a function of temperature also shows an interesting retention of anisotropy in the side-on SGLPs past the T_{NI} of the solvent, giving insight into the coupling between configurational entropy and orientational order.

4.3 Experimental

4.3.1 Materials and Instrumentation

4-pentylbiphenyl was purchased from TCI America, deuterium oxide from Cambridge Isotope Labs. Anionic prepolymers for the SGCLPs came from two sources: polybutadiene (98% 1,2 content) of size 1.07x10^3 g/mol and narrow molecular weight distribution (polydispersity index: 1.07) was synthesized by Dr. Steven Smith of Procter and Gamble Co, while polybutadiene (85% 1,2 content) of size 0.48x10^3 g/mol was purchased from Polymer Source (Montreal, Quebec, Canada). The prepolymer's absolute molecular weight was determined by the manufacturers using light scattering. Platinum catalysts were

obtained from United Chemical Technologies in Bristol, PA and used as received. Polished quartz plates for SANS cells were obtained from Technical Glass Products in Painesville Twp., OH. Elvamide 8023R® was obtained as a sample from DuPont Engineering Polymers. Metal Washers (1/32", $\sim$800 μm thick) were obtained from McMaster Carr. Optically activated glue, NOA68, was obtained from Norland Optical Products in Cranbury, NJ. All other reagents were purchased and used as received from Aldrich, unless otherwise noted

Reaction temperatures were controlled by an IKAmag RET basic temperature modulator. Mechanical shaking of polymer solutions was carried using a Burrell Wrist Action Shaker, Model 75. Thin-layer chromatography (TLC) was performed using J. T. Baker silica gel IB and visualized by short wave UV (254 nm), EMD Silica gel (particle size 0.040-0.063 mm) was used for flash column chromatography. The deuteration of the LC solvent for SANS experiments was carried out in a PARR 4561 stirred pressure reactor with PTFE liner.

^{1}H NMR spectra were obtained using a Varian Inova 500 (at 500 MHz) NMR; all spectra were recorded in $CDCl_3$ and referenced to tetramethylsilane.

The GPCs were carried out in tetrahydrofuran (THF) at 35°C eluting at 0.9 mL/min through four PLgel 10-μm analytical columns (Polymer Laboratories, PLgel 10 μm analytical columns, 30 cm long, 10^6 to 10^3 Å in pore size) connected to a Waters 410 differential refractometer detector (λ = 930 nm).

Liquid crystal phase transitions were observed using a Zeiss Universal Polarized Optical Microscope and a Mettler FP 82 hot stage, controlled by a Mettler FP 80 Central Processor. Optical Micrographs were taken with a Cannon EOS D30 digital camera. Differential scanning calorimetry (DSC) was performed using a Perkin-Elmer DSC 7 calorimeter. The onset temperature and latent heat of the nematic-isotropic phase transition were calculated from DSC data using Perkin-Elmers Pyris® version 3.04).

SANS experiments were conducted on the NG3 beamline at the National Institute of Standards and Technology cold neutron source in Gaithersburg, MD and on the CG2 beamline at Oak Ridge National Laboratory's High Flux Isotope Reactor. Temperature control for later SANS experiments was achieved using a home-built Peltier-based temperature environment and controller that was designed and built by Paul Pirogovsky.

4.3.2 Methods

4.3.2.1 SGLCP Homopolymers

End-on and side-on SGLCP homopolymers were synthesized using polymer analogous chemistry. This chemistry was first developed by Mike Kempe, and later optimized by Neal Scruggs and Rafael Verduzco, during each of their respective times in the Kornfield group. The end-on homopolymers used in these experiments were synthesized by myself following the procedure developed by the Kornfield group [9] [5]. while the side-on homopolymers were synthesized by both myself and Rafael Verduzco while he was in the Kornfield group, also based on procedures developed in the Kornfield group [11]. A representative synthesis of side-on SGLCPs can be found in Chapter 2. What follows is a representative synthesis of end-on SGCLP homopolymers.

Synthesis of end-on SGLCP homopolymers

4.3.2.2 Synthesis of Perdeuterated 4-Pentyl-4-Cyanobiphenyl (D5CB)

Because the coherent neutron scattering length of hydrogen (bH = -3.74 x 10^{-5} Å) is significantly different from that of deuterium (bD = 6.67 x 10^{-5} Å), the perdeuterated solvent provides scattering contrast while maintaining the liquid crystal solvents other physical properties. Perdeuterated 4-

penyl-4-cyanobiphenyl (d_{19}5CB) was synthesized according to methods described below. The nematic-isotropic transition temperature (T_{NI}) of d_{19}5CB is approximately 7 to 10°C lower than that of hydrogenated 5CB. Perdeuterated 4-pentyl-4'-cyanobiphenyl (d_{19}5CB) was synthesized from perdeuterated 4-pentylbiphenyl in two ways. First we used a modified version of our group's original perdeuterated 4-pentylbiphenyl synthesis designed by Mike Kempe while he was in the Kornfield group [10] [9] and later used and adapted by Neal R. Scruggs and Rafael Verduzco, when they were in the Kornfield group [4] [6] [11]. I've used both Kempes chemistry, with modifications, as well as a new synthesis, (see below).

Deuteration of 4-pentylbiphenyl. Just like in Michael Kempe's method, the first step in our d_{19}5CB syntheses involves multiple deuterium exchanges between hydrogenated 4-pentylbiphenyl and deuterium oxide using a heterogeneous platinum catalyst [12] [13]. For these experiments, as well as those in the next chapter, a more efficient deuterium exchange step, has been designed and carried out by Paul Pirogovsky. 4-Pentylbiphenyl (75 mL), deuterium oxide (150 g), platinum black (800 mg), and aluminum foil (1 cm^2, two squares, to reduce the free oxygen content in the reactor, thus extending the lifetime of the catalyst) were placed in a pressure reactor, which was then flushed and filled with N_2 gas (60 psig), heated to 205 °C, and stirred for 48 hrs.

After each exchange of D_2O, a small aliquot of semi- or perdeuterated 4-pentylbiphenyl was removed in order to measure deuterium content is measured by ^{1}H NMR spectroscopy: a proton NMR spectrum is collected from a solution containing known mass of 4-pentylbiphenyl ($\sim$50 mg, known mass) and hydrogenated ethylene glycol ($\sim$1 mg, known mass) in deuterated chloroform ($CDCl_3$). The ethylene glycol proton peaks are used as a standard to calculate the degree of deuteration of the sample. The process is declared complete when the 4-pentylbiphenyl is found to be $>$90% deuterated, approximately three to four exchanges. This new perdeuteration procedure enabled us to achieve highly deuterated PBP

in about one third of the time of the original method, which typically took between six and eight five-day exchanges to achieve the same amount of deuteration.

Synthesis of perdeuterated 4-pentyl-4-cyanobiphenyl from perdeuterated 4-pentylbiphenyl, (Method 1). Perdeuterated 4-pentylbiphenyl is converted to the liquid crystal (perdeuterated) 4-pentyl-4-cyanobiphenyl in two steps. First, the perdeuterated 4-pentylbiphenyl is reacted with one equivalent of elemental bromine, with $FeBr_3$ catalyzing the addition of the Br_2 to the 4 position of the biphenyl group. Second, the bromine is replaced with a nitrile group. In the first step, the perdeuterated 4-pentylbiphenyl (5.71 g, 25.4 mmol) and $FeBr_3$ (0.345 mg, 1.5 mmol,) are dissolved together in 50 mL of anhydrous chloroform, followed by the dropwise addition of $Br_{2(l)}$ (1.4 mL, 27.18 mmol) *via* a syringe at room temperature, then stirring at room temperature for 30 minutes (sometimes this step takes up to a day). The solvent was evaporated with gas pressure until it was almost gone; water was added and the reaction vessel was then shaken until the tan solid product was precipitated from the originally red/purple viscous slurry. The water was decanted off and extracted twice with methylene chloride. The solid d_{19}5Br reaction mix is dissolved with methylene chloride, combined with the organic layer of the previous extraction, and dried with magnesium sulfate. The solvent is then evaporated and the resulting perdeuterated 4'-pentyl-4-bromobiphenyl is recrystallized with hot hexanes (mass after 1 recrystallization: 1.09g, 14% yields, after 2-3 recrystallizations: $>$30%).

In the second step, 4-pentyl-4-bromobiphenyl is converted to 4-penyl-4-cyanobiphenyl using potassium cyanide. A palladium catalyst ($Pd(TPP)_2$) is synthesized by dissolving palladium (II) acetate ($Pd(OAc)_2$, 180 mg, 0.80 mmol) together with triphenyl phosphine on polymer support (TPP-polymer, 1.0 g, 1.6 mmol/gram loading) in 40 mL anhydrous toluene and heated at 50°C until the mixture turns bright red (about 30 minutes). TPP-polymer was introduced to aid in the purification of the final product. Potassium cyanide (KCN, 309mg, 4.75 mmol), 4-pentyl-4-bromobiphenyl (1.4 g, 4.34 mmol) and N,

N, N, N-tetramethylethylenediamine (TMEDA, 160 μL, 1.1 mmol) (TMEDA is used to promote the solubility of KCN in organic solvent [14]) are added directly to the reaction flask, which is then purged with inert gas, then sealed and heated at 90 °C for approximately 3 days (this process takes longer than the Kempe/Scruggs/Verduzco process, likely because the TPP is now attached to the polymer support). The product was purified on a silica gel column using 1% ethyl acetate in hexane as the mobile phase. Although using TPP on polymer support helped decrease the purification steps, this process still requires repeated column chromatography before nematic liquid crystal fractions resulted (with isotropic fractions having been discarded between each column). It is for this reason, as well as the low overall yield that I began developing another method to synthesize perdeuterated 4-pentyl-4-cyanobiphenyl (d_{19}5CB) from perdeuterated 4-pentylbiphenyl (see below).

The T_{NI} of the final product, often obtained by combining perdeuterated 4-penyl-4-cyanobiphenyl fractions purified from several separate syntheses, was usually around 25.0 and 28.0 °C, below that of hydrogenous 5CB (T_{NI} = 35 °C). The deuterium content of the product was measured by proton NMR in the same way as for perdeuterated 4-pentylbiphenyl.

Synthesis of perdeuterated 4-penyl-4-cyanobiphenyl from perdeuterated 4-pentylbiphenyl, (Method 2). The 4 hydrogen in perdeuterated 4-pentylbiphenyl is converted first to an amide using oxalyl chloride, which is then dehydrated to a nitrile group using two dehydration methods.

Carbon black is filtered via vacuum filtration. The small amount of D_2O remaining is removed by drying with magnesium sulfate, filtering, and drying under vacuum overnight.

The anhydrous aluminum chloride (5 g, 37.4 mmol)is dissolved in anhydrous $\sim$10 mL carbon disulfide in a three necked funnel and cooled in an ice bath. Oxalyl chloride (4.6 g, 37.4 mmol) is added dropwise from a syringe or an addition funnel over the course of one hour, and then the reaction is stirred for

15 minutes. Dry 4-pentylbiphenyl (8 g, 34.1 mmol) is dissolved in carbon disulfide and then added dropwise over 30 minutes (should be one hour) to the reaction mixture. The reaction mixture instantly turns black upon addition of pentylbiphenyl. After stirring for 1.5 hrs as the ice bath returns to room temperature, the reaction is refluxed at 50°C for 1.5 hrs.

The acid chloride reaction is cooled, and then quenched by pouring onto cold ammonium hydroxide/ammonia in isopropanol (in the future, because of unwanted side reactions, other quenchers should probably be used) and left sitting overnight, resulting in tan solid below a brownish supernatant liquid. The product is purified via liquid-liquid extraction with distilled water and methylene chloride. The organic layers are combined, dried, and evaporated and the resulting amide is recrystallized from hot hexanes/IPA/toluene. The amide is then reduced to the nitrile via dehydration. Two dehydration methods were attempted. First, pyridine is added to a solution of amide and para-toluensulfonyl chloride in dichloromethane and the reaction was allowed to proceed for 18 hrs, monitored by thin-layer chromatography. When the reaction was complete, saturated sodium bicarbonate was added and the resulting two-phase mixture was stirred at room temperature for 2 hrs. The aqueous and organic layers were separated and the organic layer was washed with 1N HCl followed by saturated sodium bicarbonate while the aqueous layers were back-extracted with dichloromethane and the resulting organic layers from each extraction were combined then dried and filtered. Finally, the solvent was evaporated leaving perdeuterated-4-pentyl-4-cyanobipheneyl (d_{19}5CB). In some cases the resulting mixture was passes through a plug of silica gel using a pure dichloromethane eluent to eliminate any isomeric impurities left (Pure (d_{19}5CB) was the second fraction to elute).

We also dehydrated the amide to the nitrile using the Vilsmeyer-Hack reagent as follows: A thionyl chloride-dimethyl formamide complex was formed by adding thionyl chloride was added dropwise to a solution of anhydrous dimethyl formamide under an inert gas atmosphere, while keeping the mixture cooled to 0°C. The amide was added to the complex dropwise and the resulting reaction mixture was

stirred at 0°C for four hours, then allowed to warm to room temperature and stirred again overnight. The reaction was quenched by pouring the reaction mixture onto ice cold distilled water and washed with water until the pH increased to about 5.5. The organic layer was then dried, filtered and concentrated and the resulting nitrile was purified through recrystallization.

4.3.2.3 Polymer Characterization

Proton nuclear magnetic resonance spectroscopy (^{1}H NMR). ^{1}H spectra (16 or 32 scans) of solutions of polymer (with concentrations of approximately 10 to 20 mg/mL) in $CDCl_3$ were recorded at room temperature on an Inova 500 MHz NMR spectrometer. The percent conversion of the pendent vinyl groups was determined by comparing the integrated area for the peaks corresponding to both the 1,2-polybutadiene and mesogen at 4.7-4.9 ppm, with peaks corresponding to the alkyl spacers on the mesogen.

Gel permeation chromatography (GPC). The side group liquid crystal polymers relative molecular weight and molecular weight distributions (PDI = M_w/M_n), were measured using gel permeation chromatography (GPC) calibrated with monodisperse PS standards.

2-7 mg polymer was dissolved $\sim$1 mL of tetrahydrofuran (THF) and shaken for at least 30 min with a mechanical shaker. These solutions were filtered with a 0.45 μm syringe filter prior to being injected into the GPC. The total time to traverse all four columns was approximately 45 minutes.

Polarized light microscopy. Nematic-isotropic transition temperatures were measured using polarized light microscopy. First small drops (if small molecule LC solvent) or chunks (if polymer) are sandwiched between an glass slide and a coverslip and examined using a Zeiss Universal optical microscope equipped with a Mettler FP82 hot stage and crossed polarizers. Each sample was heated from

room temperature at a rate of 1 or 2°C/min and the temperature at which the birefringent, nematic texture began to disappear was recorded as the nematic-isotropic transition temperature, T_{NI}. (Two temperatures were recorded for samples that became biphasic during the transition: the temperature at which the first circular black regions appear was recorded as the beginning of the biphasic range and the temperature at which the last birefringent region disappear was recorded as the end of the T_{NI}.

4.3.2.4 Small Angle Neutron Scattering

Solutions for small angle neutron scattering (SANS). Dilute solutions of polymers in perdeuterated liquid crystal solvent were prepared by dissolving the polymers in the perdeuterated 4-penyl-4-cyanobiphenyl using an organic cosolvent that is later evaporated away. Specifically, 1.0% by weight SGLCP homopolymers solutions in the perdeuterated liquid crystal solvent were prepared by first dissolving known masses of the polymers in volumetric amounts of tetrahydrofuran, and then shaking this mixture for greater than 30 minutes, resulting in either 5 or 2.5 mg/mL solutions. Known volumes of these known concentrations were combined (using a 500 μL syringe) with the nematic perdeuterated 4-penyl-4'-cyanobiphenyl (d_{19}5CB) mixed by hand-rotating the vials, then evaporating the organic solvent under vacuum for at least 18 hours.

Transition temperature determination. The T_{NI} of the solutions were measured, first in the lab, using a hotstage and polarized optical microscope, and then *in situ*, at the beamline.

Polarized light microscopy. Nematic-isotropic transition temperatures were measured in two ways. First small sandwiched between an unrubbed glass slide and coverslip and examined using a Zeiss Universal optical microscope equipped with a Mettler FP82 hot stage and crossed polarizers. Each sample was heated from room temperature at a rate of 1 or 2°C/min and the temperature at which the birefrin-

gent, nematic texture began to disappear was recorded as the nematic-isotropic transition temperature, T_{NI}. (Two temperatures were recorded for samples that became biphasic during the transition: the temperature at which the first circular black regions appear was recorded as the beginning of the biphasic range and the temperature at which the last birefringent region disappear was recorded as the end of the T_{NI}.)

***In situ* transition temperature measurements.** For the first set of experiments, the transition temperature was judged based on the light scattering of the red alignment laser at the NG3 beamline as we heated the sample in 0.25 and 0.5°C increments, waiting 10 minutes between each temperature change: in the nematic phase, the cloudy solution scattered the beam, while in the isotropic phase a bright red spot was visible. When the sample was undergoing its phase transition, the parts of the solution that were still nematic visible were distinguishable from the parts that were already isotropic. When we switched to using our home-built temperature controller, we measured the T_{NI} of the samples *in situ* using crossed polarizers and a flashlight

Sample cells and sample environment. Sample cells were prepared by sandwiching an $\sim$800μm aluminum spacer between quartz plates that were pretreated with a layer of rubbed polyimide or nylon to induce uniform alignment of the LC director. The alignment layer was created by either dip-coating the quartz in a 1% polyimide solution in N- methylpyrrolidone, or dip-, or spin-coating with 0.5% Elvamide8023R®in methanol (this solution was made by refluxing the Elvamide in methanol for $>$12hrs), followed by unidirectional rubbing (with either velvet or a natural hair brush) greater than 50 times. The aluminum spacer was glued between the two quartz plates using either 5-minute epoxy or optically active glue and a UV source (254 or 356 nm).

Polymer solutions were loaded into the sample cells using a syringe. These samples were then heated to

isotropic (often just using the heat of ones hand) and placed in a room-temperature vacuum oven for at least 8 hours, allowing the sample to align into a uniform monodomain and enough time for to remove any small air bubbles present in the sample. Initially, samples were heated with NCNRs single-cell holder heated with continuous flow of water whose temperature was controlled by a circulating water bath. After it was determined that a more well-controlled temperature environment was needed, Paul Pirogovsky designed a transmission-geometry, Peltier-based sample environment allowing for rapid, stable, bidirectional teperature control that was used for all subsequent SANS experiments. Thiss allowed improvement in temperature precision from $\pm 1.0^{\circ}$C to $\pm 0.05^{\circ}$C. Further details can be found in Paul Pirogovsky's forthcoming PhD dissertation.

Small angle neutron scattering. Cells containing homogeneously aligned SGLCP solutions were mounted in our home-built temperature-controlled environment which was, in turn, held closely between the pole pieces of a 0.9 T electromagnet. The magnetic field served to reinforce the planar alignment induced by the rubbed alignment layers. The LC director was thus perpendicular to the incident neutron beam. Samples were annealed at the desired temperatures for at least ten minutes before to data was collected. Experiments were performed at multiple temperatures in the both the nematic phase and in the isotropic phase.

Incident monochromatic neutrons (λ = 6 Å) were scattered by the sample and collected on 2-D detector. Two dimensional scattering patterns were collected at 3 sample-to-detector distances (1.3, 4.5, and 11 or 9m). The patterns at all detector distances were combined to produce scattering curves over nearly 2 decades in q (0.004 $\text{Å}^{-1} <$ q $<$ 0.3 Å^{-1}), where q = $4\pi\sin(\theta/2)/\lambda$, where θ is the scattering angle and is the wavelength of the incident beam. The raw data were converted to absolute coherent scattering intensities, I, as a function of q using corrections for detector inhomogeneity and sensitivity, background electronic noise, and incoherent scattering intensity according to standard procedures [15].

Two-dimensional scattering patterns collected at nematic temperatures were sector-averaged, specifically, data having the same magnitude of the scattering vector, q, in $\pm 10^{\circ}$ sectors in both the equatorial (horizontal) and meridional (vertical) directions were averaged to give the scattering parallel to the director, $I_{\parallel}$, and perpendicular to the director, $I_{\perp}$, respectively. Two-dimensional scattering patterns of the deuterated solvent, d_{19}5CB, were sector averaged in the same way, and then subtracted from each sector, to account for slight variation between the sectors (top, bottom, left, right) in the low q, in particular a strong flare in the bottom sector observed when the scattering was the lowest (*i.e.*, low concentration of polymer). Sectors without these features were chosen to represent the equatorial and meridional scattering, called "horizontal sector averages" and "vertical sector averages."

4.4 Results

4.4.1 Small Angle Neutron Scattering at Nematic Temperatures

The 2-D scattering patterns of dilute (1%) end-on (Figure 4.2a) and side-on (Figure 4.2b) SGLCP solutions in aligned nematic solvent are anisotropic, confirming that the SGLCPs adopt ellipsoidal conformations in LC solvent, as has been previously reported [4] [5] [16] [17]. As expected, side-on SGLCPs display a prolate conformation (Figure 4.2a, right), while end-on SGLCPs display an oblate conformation (Figure 4.2b, right) [4]. The amount of conformational anisotropy can be crudely estimated by determining a rough aspect ratio of the major and minor axes of the ellipse traced out by an approximate iso-intensity contour of the 2-D scattering pattern at low-q (Table 4.1). Aspect ratios found this way show a difference between end-on and side-on SGLCPs: aspect ratios change for the two molecular weights of end-on SGLCPs, while nearly doubling the molecular weight of the side-on SGLCP doesnt seem to alter the aspect ratio, at least within the uncertainty limit of this method. The aspect ratio calculated from the 2-D pattern of CB4-2000 at seven degrees below the start of the nematic-to-isotropic

phase transition (T_{NI}) is 1.85, while the aspect ratio for the lower molecular weight end-on SGLCP, CB4-880, was calculated to be 1.4. This is similar to those reported for 5% solutions of the same polymers [5]. The aspect ratio of both side-on SGLCPs at T_{NI} - 7°C calculated from the 2-D patterns at low-q was ∼3.3, lower than that found for semidilute solutions (∼4.1 to 4.5, [5]). In isotropic solvent, the end-on and side-on scattering patterns at low-q are circularly symmetric (aspect ratio equal to one), indicating that polymer conformations are spherically symmetric. (Though it should be noted that at isotropic temperatures close to the T_{NI} some anisotropic scattering is seen in both side-on SGCLPs at high-q, see Figures 4.8 to 4.10).

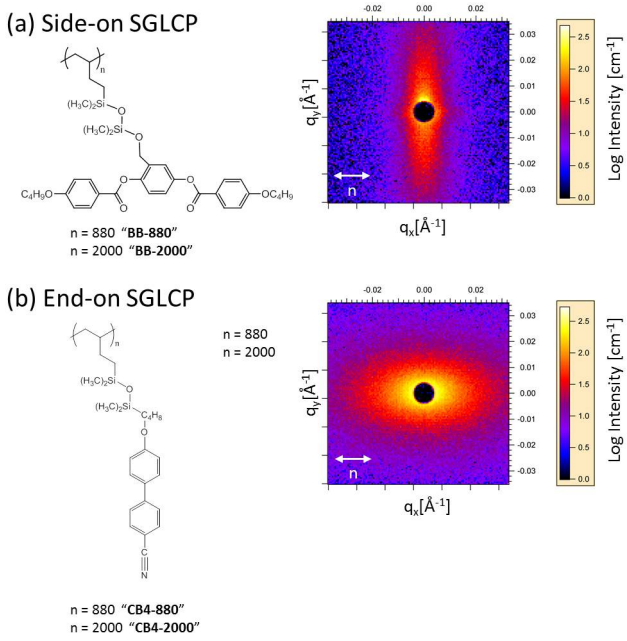

Figure 4.2. Chemical structures (left) and 2-D small angle neutron scattering patterns (right) of (a) side-on and (b) end-on SGLCPs. The SGCLPs are dissolved at 1.0% by weight in perdueterated nematic liquid crystals solvent and measured in aligned cells under a magnetic field (double-headed arrow indicates the direction of the magnetic field and hence the direction of alignment of the nematic director, *n*)

Some 2-D patterns showed a strong streak in the horizontal direction of as yet undetermined origin. This feature always appeared in the same direction (horizontal), regardless of whether the polymer sample was end-on or side-on or a homo- or diblock copolymer. The horizontal streak appeared under two different alignment layer conditions: polyimide, where it was much stronger and appeared to higher-q,

Table 4.1. Aspect ratios of end-on "CB4") and side-on ("BB") SGLCPs based on 2D scattering patterns, 1-D reduction and fitting to the shape-independent Debye function

Polymer	Aspect Ratio from 2-D	Aspect Ratio from $q_{\perp}$ vs. $q_{\parallel}$	Aspect Ratio from Debye Fits
CB4-2000	1.85	1.64	2.0
CB4-880	1.4	1.45	1.76
BB-2000	3.3	3.2	-
BB-880	3.3	3.4	-

and nylon (the data shown in this chapter), where it appeared much less intense. The streak was also determined to be, at least in some part, a filling artifact, appearing and disappearing after addition and removal of the same polymer to the same cell. This streak can, at times, overwhelm the horizontal scattering of the polymers, in particular at the low q. An example of a weak streak can be seen in figure 2b, the 2-D scattering of the side-on polymer, BB-2000. For morst samples it was possible to fit the data by avoiding the regions of the detector when scattering dominated by the "streak."

The samples tested were shown to be in the dilute regime: a concentration sweep of the lower molecular weight side-on polymer (3%, 1.5% and 1.2% by weight) at nematic temperatures (18°C) shows that the scattering of 1.5% and 1.2% have similar slopes from 0.14_{-1} Å $< q <$ 0.0047 $Å_{-1}$, differing mostly in the intensity of their scattering, indicating that 1.5% and 1.2% polymers are in the dilute regime, while 3% is not. Most of the following measurements were thus performed at 1.0% or less polymer, to ensure that we were in the dilute regime for all molecular weights of polymers studied.

Sector-averaged scattering patterns of polymer-LC solutions at nematic temperatures also show anisotropy (Figure 4.3). The scattering parallel to the nematic director ($I_{\parallel}$) of the end-on polymer is more intense than the scattering perpendicular to the director ($I_{\perp}$), while the reverse is true for the side-on polymer. It should be noted here that the horizontal sector average ($I_{\parallel}$) of the side-on polymer (Figure 4.3b, open circles, red) overlapped completely with the background starting at in the mid q range. Subtracting the background resulted in the foreshortened trace shown here. As expected from the anisotropy difference in the 2-D scattering patterns, the ratio of the scattering intensities parallel to the nematic director (hori-

zontal sector average) and perpendicular to the director (vertical sector average) is lower for the end-on polymer than for the side-on. Indeed, this difference in the 1-D sector averages can be used to obtain another measure of the conformational anisotropy: a ratio of the scattering vector, q, in the horizontal and vertical directions ($q_{||}$ and $q_{\perp}$) at the same scattered intensity was taken in the high q regime, where slopes of the two sector averages are almost parallel – a little like a one-point iso-intensity contour. This analysis was performed for all four samples (Table 4.1), though it should be noted that at both molecular weights of side-on SGLCPs, there were very limited regions where the horizontal and vertical sector averages had similar slopes, the aspect ratios so derived for the side-on polymers will thus have more error than the ones derived for the end-on SGLCPs. Aspect ratios taken this way, however, show similar trends as those taken from the 2-D scattering pattern: CB4-2000 has a slightly bigger aspect ratio than does CB4-880, while BB-2000 and BB-880 have similar aspect ratios.

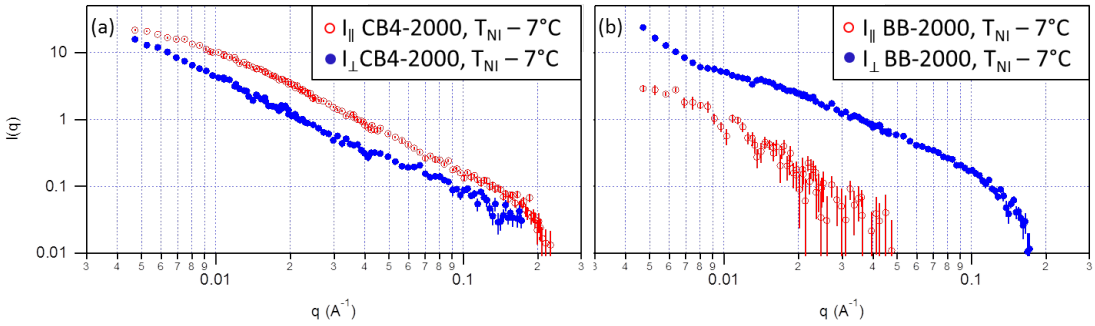

Figure 4.3. 1-D horizontal (red, open circles) and vertical (blue, closed circles) sector averages ($\pm 10^{\circ}$) of small angle neutron scattering patterns of (a) end on (CB4-2000) and (b) side-on (BB-2000) SGLCPs in aligned nematic solvent. As expected from the greater anisotropy visible in the 2-D scattering patterns, the difference in intensity between $I_{\perp}$ (scattering intensity of the vertical (perpendicular to the LC director) sector) and $I_{||}$ (scattering intensity of the horizontal (parallel to the LC director) sector) is larger in the side-on SGLCP relative to the end-on SGLCP.

In most cases, we see an upturn in both $I_{||}$ and $I_{\perp}$ at very low q of the 1-D sector averages (for example $I_{||}$, Figure 4.3b, closed circles, blue). Similar upturns at low-q have been observed in semidilute SGLCP solutions in aligned nematic solvent [5] [18], dilute SGLCP solutions in isotropic solvent [19] [20], and dilute solutions of rodlike conducting polymers [21]. Upturns such as these are generally attributed to associations between polymer chains, even in dilute solutions [5] [21]. By decreasing the concen-

tration to the dilute regime, the upturn has also decreased and only appears at the lowest-q values (q $<0.007\text{Å}^{-1}$). For systems like this, in order to extract information about the object size, it is much more reliable to fit the entire data set, rather than to try to extract radii of gyration using the Guinier regime [21].

In most of the q-range measured, the parallel and perpendicular scattering intensities ($I_{\|}$ and $I_{\perp}$) of the end-on SGLCPs both scale approximately as q^{-2}, indicating that these polymer chains adopt random -coil geometries. This is consistent with scattering seen in semidilute solutions (5%) of these same polymers. On the other hand neither $I_{\|}$ nor $I_{\perp}$ of the side-on polymers appear to scale as woukd be expected for Gaussian polymers: in the vertical direction, $I_{\perp}$ of BB-2000 scales as $q^{-1.26\pm0.22}$ and BB-880 scales as $q^{-1.08\pm0.27}$ indicating a rigid rod-like behavior at distances less than the persistence length of the SGLCP.

When Porod scaling gives an exponent of -2, as is the case with the end-on polymers it indicates scattering from a solution of Gaussian polymer chains and the Debye model can be fit to a wide region of the scattering pattern (in this case, not the very low q, where upturn deviates from the Debye prediction, and the high-q where the Debye model is not derived to fit) [21]. $I_{\|}$ and $I_{\perp}$ of the end-on SGLCPs were fit to the form:

$$I(Q) = 2A/x^2(x - 1 - e^{-x}) + B. \tag{4.1}$$

Where $x = Q^2R_g^2$ and R_g is the radius of gyration of the polymer chain. A is a scaling factor and B is the q-independent incoherent background scattering. The Debye model has been used successfully to model many polymer systems [8] [22]. Since there are only three fitting parameters, they were allowed to float freely for the nonlinear, least-squares fit of a wide range of the end-on SGLCP patterns (Figure

4). Figure 4b shows a Kratky-plot with the expected plateau for a Gaussian coil conformation, indicating the appropriateness of the Debye model, at least until q = 0.1 $Å^{-1}$. At $q > 0.1$ $Å^{-1}$ (not shown), there is some evidence of an upturn in the Kratky plot, indicating the intensity may be beginning to scale like a rigid rod (q^{-1}). Unfortunately the noise in the data makes it hard to determine if indeed this is the case.

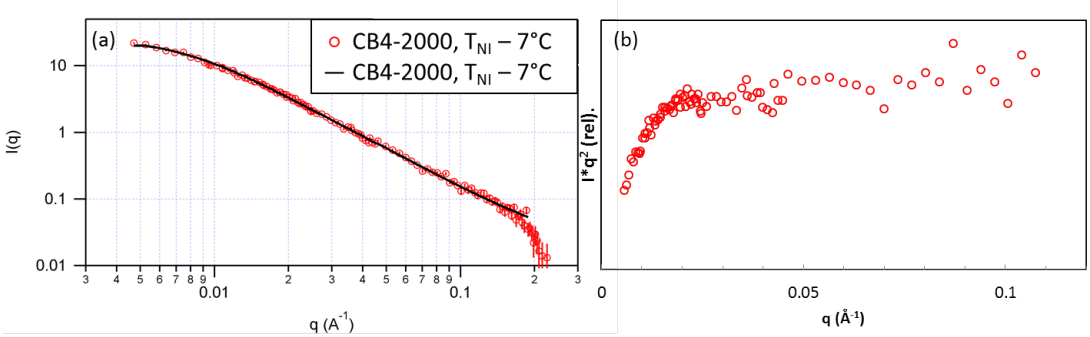

Figure 4.4. 1-D horizontal sector average of small angle neutron scattering of end-on SGLCP, CB4-2000. High-q scaling of $I \approx q^{-2}$ indicates that the Debye function can be used. (b) A Kratky plot shows a plateau, also indicating that the Debye model can be used, at least until for q <0.1 $Å^{-1}$.

Table 4.2. Aspect ratios of end-on "CB4") and side-on ("BB") SGLCPs based on 2D scattering patterns, 1-D reduction and fitting to the shape-independent Debye function

Polymer	$R_{g_\parallel}$ (T_{NI} - 7°C)	$R_{g_\perp}$ (T_{NI} - 7°C)	R_g (T_{NI} + 4°C)	Aspect Ratio (T_{NI} - 7°C)
CB4-2000	20.39 ± 0.23	40.87± 2.29	23.46 ±0.68	2.0
CB4-880	12.21 ± .022	25.25± 2.79	-	1.76

Previous SANS experiments investigating end-on SGLCPs with siloxane backbones having a degree of polymerization approximately 10x less than CB4-880 (DP of 70 vs 880) showed $R_{g_\parallel}$ ∼2.8 nm and an $R_{g_\perp}$ of ∼2.5 nm, indicating an aspect ratio of close to 1 [20]. Significantly increasing the moleculear weight, gives a more anisotropic aspect ratio, and increases $R_{g_\parallel}$ by ∼5 fold, and $R_{g_\perp}$ by about 10-fold.

Previous studies of semidilute solutions report that at 5% by weight, end-on SGLCPs in d_{19}5CB sector averages of different molecular weight polymers were virtually superimposable [5]. In the dilute regime, at 1% by weight SGLCP, scattering is no longer insensitive to M_w, though the differences remain slighter for end-on SGLCPs than for side-on SGLCPs.

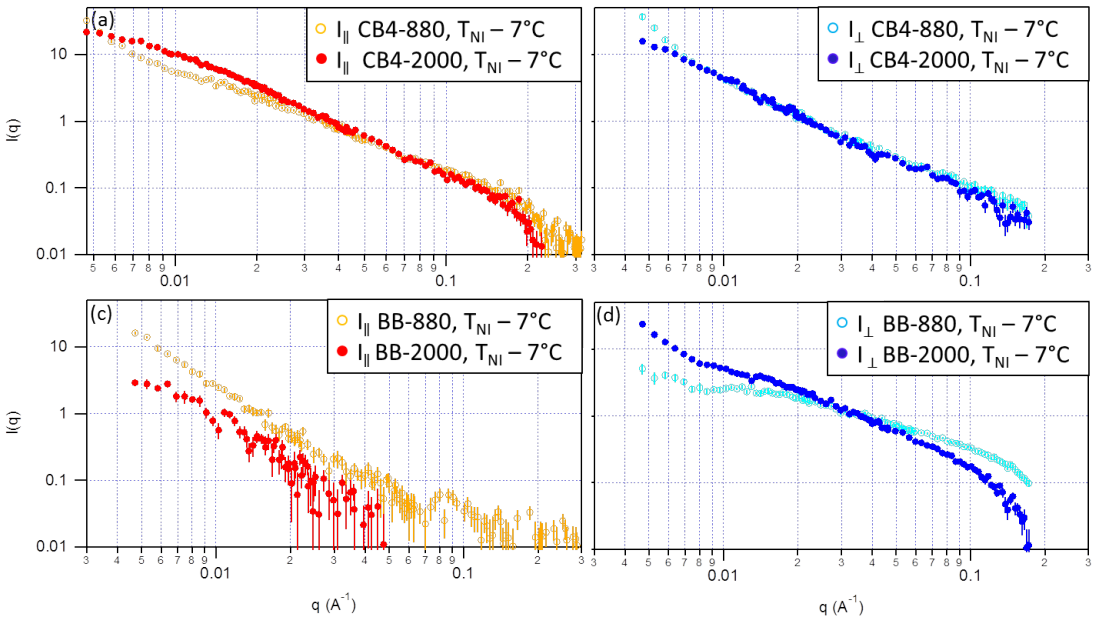

Figure 4.5. 1-D sector averages ($\pm 10°$) of small angle neutron scattering patterns of end-on SGLCPs, CB4-880 (open circles), and CB4-2000 (closed circles) (a) parallel to the nematic director (orange and red, respectively) and (b) perpendicular to the nematic director (light and dark blue, respectively). 1-D sector averages ($\pm 10°$) of side-on SGLCPs, BB-880 (open circles), and BB-2000 (closed circles), (c) parallel to the nematic director and (orange and red, respectively) (d) perpendicular to the nematic director (light and dark blue, respectively). All scattering patterns were taken at the same nematic temperature (T_{NI} - 7°C).

4.4.2 Small Angle Neutron Scattering at Isotropic Temperatures

At higher temperatures, specifically above the T_{NI}, both 1-D and 2-D scattering patterns at *low* q appear isotropic. In particular the low-q upturns vanish, indicating associations between polymers have ceased at these temperature/solvent conditions (Figure 4.6). As one would expect, the molecular weight increases, the size of the isotropic polymer also increases (Figure 4.7)

Debye fits to isotropic CB-2000 shows that after the T_{NI} the more extended dimension ($R_{g_\perp}$), decreases to approximately match the size in the parallel direction, which, already a Gaussian coil, remains about the same (Table 4.2).

At the smallest detector distance (1.3 m) a very interesting feature is seen in scattering of the side-on polymers: at temperatures just after the solvent has transitioned to the isotropic phase: some anisotropy

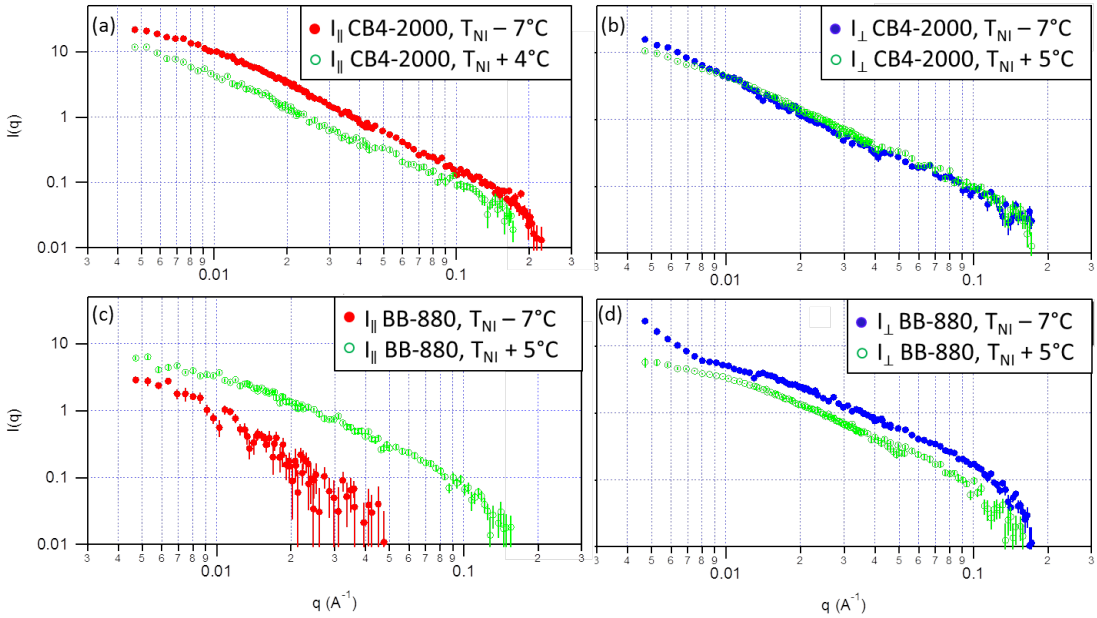

Figure 4.6. 1-D sector averages ($\pm 10°$) of end-on SGLCP, CB4-2000 (a) parallel to the nematic director and (b) perpendicular to the nematic director at both nematic (T_{NI} - 7°C, filled circles) and isotropic (T_{NI} + 4°C, green open circles) temperatures. 1-D sector averages ($\pm 10°$) of side-on SGLCP, BB-2000 (c) parallel to the nematic director and (d) perpendicular to the nematic director at both nematic (T_{NI} - 7°C, filled circles) and isotropic (T_{NI} + 5°C, green open circles) temperatures.

still remains in the high-q scattering (Figure 4.8). This effect is only apparent when a magnetic field is applied 2-D scattering patterns of BB-880 and BB-2 thresholded to remove low intensity scattering show that anisotropy is clearly retained to T_{NI} + 5°C in BB-880, and to at least T_{NI} + 2°C in BB-2000. 2-D scattering patterns of the end-on SGLCPs, on the other hand, show that they lose their anisotropy at all detector distances a few degrees below the solvents phase transition temperature, as has been reported in the literature for other SGLCPs [23].The side-on scattering in the mid-and high-q regions essentially overlap, as well. This effect is therefore confined to regions of local order of the polymer with the global structure remaining isotropic.

1-D sector averages confirm this anisotropy: at high-q the vertical and horizontal sector averages of BB-880 and BB-2000 at these temperatures do not overlap (at low q and mid q, the vertical and horizontal sector averages *do* overlap) (Figures 4.9 and 4.10). The 1-D sector averages also give us a more detailed picture of this anisotropy: while it is unclear if any anisotropy remains as the BB-2000 is heated up

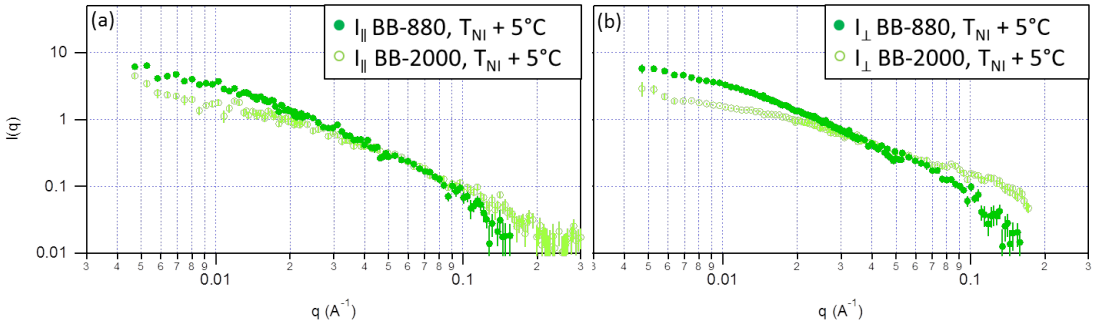

Figure 4.7. 1-D sector averages at T_{NI} + 5°C side-on SGLCPs, BB-880 (light green open circles) and BB-2000 (dark green, closed circles).

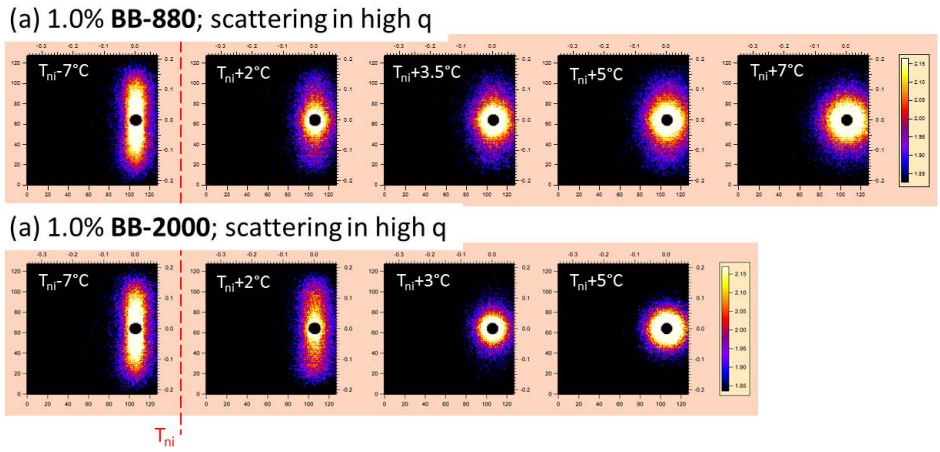

Figure 4.8. 2-D scattering patterns at the smallest detector distance (high-q range) of (a) BB-880 and (b) BB-2000 at a variety of temperatures. Scattering patterns are thresholded to remove low intensity scattering for clarity. Some degree of anisotropy appears to remain in BB-880 to T_{NI} + 5°C and in BB-2000 to at least T_{NI} + 2°C. The anisotropy retained at T_{NI} + 2°C is stronger for BB-2000 than for BB-880.

to T_{NI} + 3°C, the 1-D sector average show that vertical sector average, does not overlap with the horizontal scattering at this temperature (Figure 4.10 (d)). 1-D sector averages also confirm that the retained anisotropy in BB-2000 is stronger initially, but is retained for a smaller temperature window past the nematic-to-isotropic phase transition temperature of the solvent. In both BB-880 and BB-2000, it is clear that the horizontal sector averages (red) remain similar in slope and intensity at all temperatures studied, while the vertical sector average changes as the temperature increases (Figures 4.9 and 4.10). 1-D sector averages of end-on polymers overlapped in this whole region at all temperatures above the T_{NI} of the solvent.

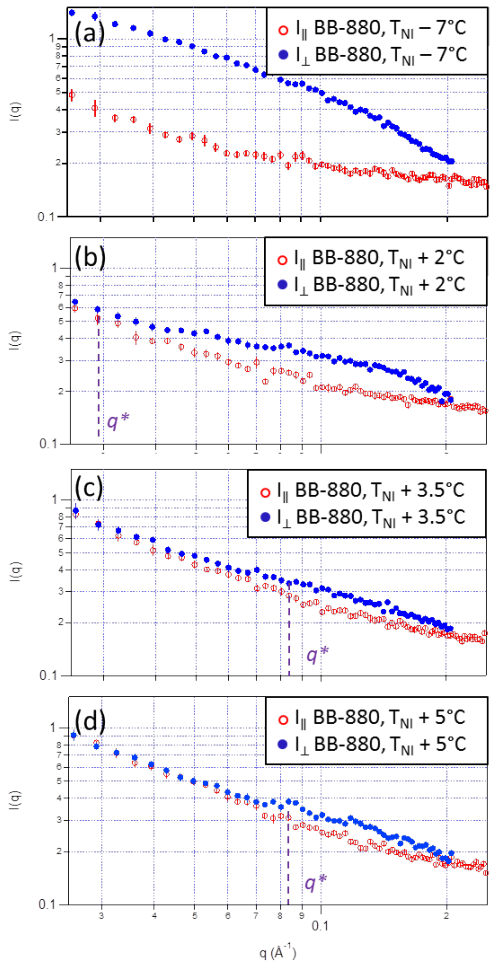

Figure 4.9. 1-D horizontal (red) and vertical (blue) sector averages of BB-880 (a) in the nematic phase, and at three temperatures above the solvents T_{NI} (b) T_{NI} + 2°C, (c) T_{NI} + 3.5°C and (d) T_{NI} + 5°C. The point at which the horizontal and vertical scattering ceases to overlap, "q*," is marked on each graph. At T_{NI} + 6°C (not shown) the horizontal and vertical scattering at this detector distance finally begins to overlap at all q, within the margin of error for these patterns.

The strength of the magnetic field doesnt affect this anisotropic scattering: 1-D sector averages of BB-880 do not change, for magnetic fields of 0.23, 0.45, and 0.9T (all of the rest of data shown here was taken under a 0.9T field). The magnetic field thus appears to simply break isotropic symmetry such that this effect is able to be seen.

We defined q* as the point at which the anisotropy begins. Specifically, we designated it as the q in which the difference between the vertical and horizontal scattering intensities ($I_{\perp}$ and $I_{||}$, respectively) was more than 20% of the horizontal scattering intensity. To reduce noise, the difference was taken as

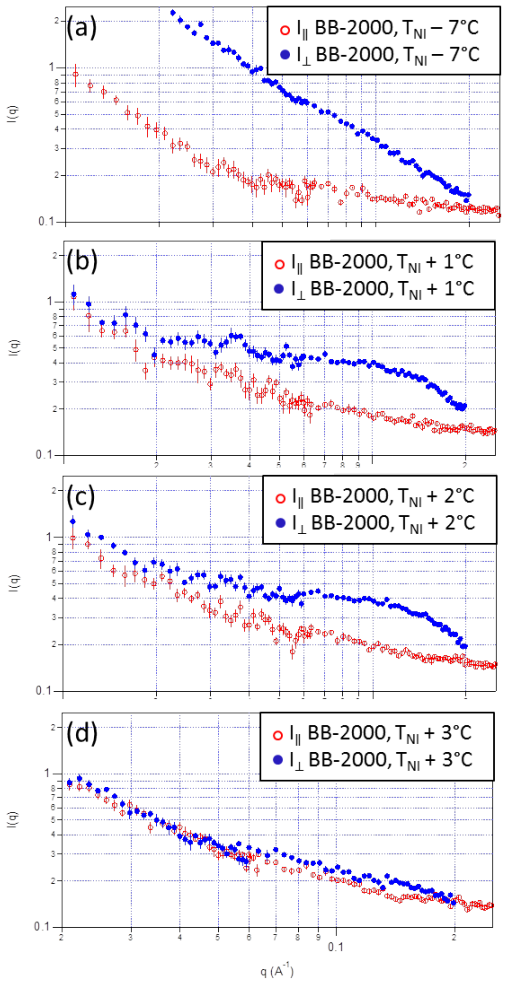

Figure 4.10. 1-D horizontal (red) and vertical (blue) sector averages of BB-2000 (a) in the nematic phase, and at three temperatures about the solvents T_{NI} (b) T_{NI} + 1°C, (c) T_{NI} + 2°C and (d) T_{NI} + 3°C. The point at which the horizontal and vertical scattering ceases to overlap, q*, harder to find in this q range for this polymer since the anisotropy is larger than in the case of BB-2000. At T_{NI} + 3°C (not shown) the horizontal and vertical scattering finally overlaps at all q, within the margin of error for these patterns.

a three point running average of $I_{\parallel}$ - $I_{\perp}$. This point for each temperature of the 1-D sector averages of BB-880 is marked in Figure 4.9, but was more difficult to find in the case of BB-2000, first because the anisotropy was so large and then because it was quite small. As temperature increases, q* for BB-880 appears about the same for T_{NI} + 1°C and T_{NI} + 2°C, then jumps discontinuously at T_{NI} + 3.5°C and remains there at T_{NI} + 5°C (Figure 4.11).

To get a better idea of the amount of anisotropy present at high q, we subtracted $I_{\parallel}$ (the scattering intensity in the horizontal sector) from $I_{\perp}$ (the scattering intensity in the vertical sector) at $0.06 < q < 0.01$

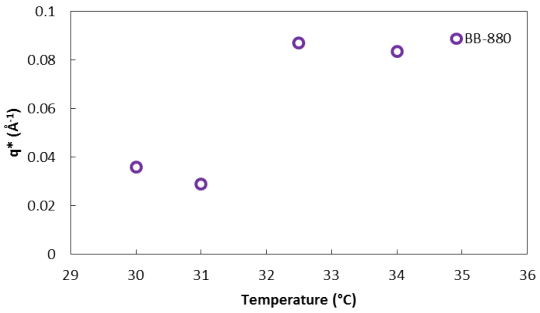

Figure 4.11. The point at which the anisotropy begins (q*) at each temperature appears to jump discontinuously with increasing temperature.

$Å_{-1}$, the q range of interest. Summing across of each subtracted point is a way to get a numberical value representing the difference between $I_{||}$ and $I_{\perp}$ while reducing the noise (it also takes into account any negative differences). Figure 4.12 shows this measure for both BB-880 (open circles) and BB-2000 (filled circles) in both nematic and isotropic solvent. While the $I_{||}$ - $I_{\perp}$ in BB-880 appears to decrease continuously after the nematic isotropic transition, $I_{||}$ - $I_{\perp}$ in BB-2000 changes discontinuously after T_{NI} + 2°C.

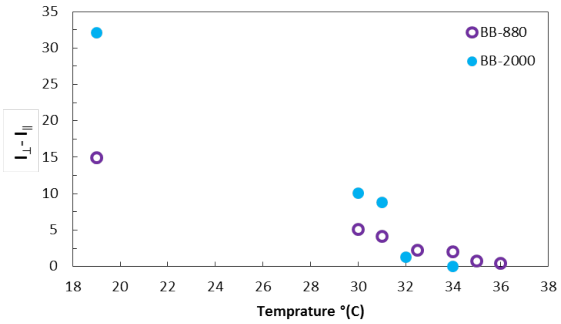

Figure 4.12. A numerical representation of the anisotropy in BB-880 (open, purple circles) and BB-2000 (closed, light blue circles). The anisotropy retained in BB-800 appears to decrease continuously with increasing temperature, while the originally larger aniostropy retained in BB-2000 decreases discontiuously witn increasing temperature above the T_{NI}.

It should be noted that although this effect was seen clearly to at least T_{NI} + 2°C in multiple polymers and two separate batches of perdueterated LC solvent, d_{19}5CB, in a third experiment the effect was much more subdued. This third batch of d_{19}5CB solvent had a much lower transition temperature (25°C *vs.* 29°C), indicating the presence of impurities. This local anisotropy retention appears very sensitive to

solvent chemistry and purity.

4.5 Discussion

Although solutions of 1 wt.% end-on and side-on SGLCPs were found to be in the dilute regime, interactions between chains were still present, as evidenced by the upturns in the low q scattering patterns. This upturn at low q prevented us from using Guinier's law to extract size information, however decreasing polymer concentration from the semi-dilute regime lead to this upturn being only apparent at very low q. End-on SGLCPs were determined to behave like Gaussian coils when dissolved in aligned nematic solvent, while side-on SGLCPs behave more like rigid rods. The scaling exponents determined for side-on SGLCPs were different in the horizontal and vertical directions, potentially indicating an anisotropy of excluded volume effects.

Scattering from dilute solutions enables us to get information about single polymer coils. Indeed, Debye fits to both molecular weights of end-on SGLCPs gave R_gs both parallel and perpendicular to the nematic director. These R_gs make intuitive sense when compared to sizes previously determined from SGLCPs with degrees of polymerization about tenfold smaller than our SGLCPs and confirmed our more rough aspect ratio measurements.

Retention in anisotropy at high q is seen at temperatures above the solvent's T_{NI} for both molecular weights of side-on polymer. This retained anisotropy is limited to short length scales that are less than the radius of a single polymer coil, with no long range order being seen at larger length scales.

This retention was not seen in end-on polymer samples, and it varied as d_{19}5CB batches varied, indicating strong solvent sensitivity. Additional experiments indicated that the magnetic field does not induce the effect; it breaks symmetry – making it possible to observe the effect

Although the LC solvent is isotropic at these temperatures, the polymer, itself liquid crystalline, has a T_{NI} far above the solvents ($\sim$80°C). Though the majority of the solvent is isotropic, inside the side-on polymer coils the polymer may be creating an internal nematic field, resulting in local ordering of the small molecule LC within/around the polymer, similar to the way certain boundary conditions can locally condense isotropic LC into the nematic phases above the bulk T_{NI} (*e.g.*, capillary condensation). It should be noted here that the end-on polymers also have T_{NI}s greater than that of the solvent, but these temperatures ($\sim$60°C) along with the initial anisotropy of these polymers is smaller in magnitude than for the side-on SGLCPs.

To our knowledge this effect has not been reported in SGLCPs, but we liken it to two other situations in which local anisotropy has been seen: swollen nematic elastomers and solutions of carbon nanotubes in LC solvent. When cross-linked liquid crystal polymers (a "nematic elastomer") are swollen with LC solvent (7 mol% elastomer) and heated past the TNI of the solvent, but not that of the LC polymer network, nematic order persisted in the gel, though the bulk solvent was isotropic, resulting in, in this case, an increase in volume (nematic order increasing the swelling of the elastomer with LC) [24]. Very dilute solutions (0.007% by weight) of carbon nanotubes, anisotropic by definition, have also been shown to produce local nematic ordering in isotropic 5CB, creating a measurable dielectric anisotropy at isotropic temperatures (measured to at least T_{NI} + 2°C) (In this case the symmetry was broken by an electric, rather than magnetic field) [25]. The authors here suggest coupling of the small molecule LCs to the CNT though $\pi - \pi$ stacking, gives rise to short range order (on the order of a few molecules thick), calling them "pseudo nematic domains."

4.6 Conclusions

The conformation of side-on and end-on SGCLPs in aligned nematic solution was studied using small angle neutron scattering. Even at dilute concentrations, the SGLCPs were seen to associate together. End-on SGLCPs were determined to obey Gaussian statistics and were fit using the Debye model. On the other hand side-on SGLCP appear to scale like rigid rods. The presence of local ordering at small length scales leads to an apparent retention of anisotropy in the high q scattering of side-on SGLCPs, at temperatures above the nematic-to-isotropic transition temperature of the LC solvent.

Bibliography

[1] Michael D. Kempe and Julia A. Kornfield. Shear alignment behavior of nematic solutions induced by ultralong side-group liquid crystal polymers. *Physical Review Letters*, 90(11):19–22, March 2003.

[2] Michael D. Kempe, Julia A. Kornfield, and Jyotsana Lal. Chain anisotropy of side-group liquid crystalline polymers in nematic solvents. *Macromolecules*, 37(23):8730–8738, 2004.

[3] L. Hardouin, F., Leroux, N., Mery, S., Noirez. Small angle neutron scattering experiments on "side-on fixed" liquid crystal polysiloxanes. *Journal de Physique. II*, 2(3):271–278, 1992.

[4] Michael D Kempe, Neal R Scruggs, Rafael Verduzco, Jyotsana Lal, and Julia A Kornfield. Self-assembled liquid-crystalline gels designed from the bottom up. *Nature Materials*, 3(3):177–82, March 2004.

[5] Neal R. Scruggs. *Coupling polymer thermodynamics and viscoelasticity to liquid crystalline order: self-assembly and relaxation dynamics of block copolymers in a nematic solvent*. Phd thesis, California Institute of Technology, 2007.

[6] Neal R. Scruggs and Julia A. Kornfield. Synergistic ordering of side-group liquid crystal polymer and small molecule liquid crystal: order and phase behavior of nematic polymer solutions. *Macromolecular Chemistry and Physics*, 208(1920):2242–2253, October 2007.

[7] David Burgess. NG3–Small Angle Neutron Scattering. http://www.nist.gov/ncnr/ng3-sans-small-angle-neutron-scattering.cfm.

[8] Julia S. Higgins and Henri C. Benoit. *Polymers and Neutron Scattering*. Oxford Univeristy Press, Oxford, 1994.

[9] Michael David Kempe. *Rheology and dynamics of side-group liquid crystalline polymers in nematic solvents*. Phd thesis, California Institute of Technology, 2003.

[10] Shin-Tson Wu, Qiong-Hua Wang, Michael D. Kempe, and Julia A. Kornfield. Perdeuterated cyanobiphenyl liquid crystals for infrared applications. *Journal of Applied Physics*, 92(12):7146, 2002.

[11] Rafael Verduzco. *Self-assembled liquid crystal polymer gels*. Phd thesis, California Institute of Technology, 2007.

[12] Michael D. Kempe, Julia A. Kornfield, Christopher K. Ober, and Steven D. Smith. Synthesis and phase behavior of side-group liquid crystalline polymers in nematic solvents. *Macromolecules*, 37:3569–3575, 2004.

[13] A. F. Thomas. *Deuterium Labeling in Organic Chemistry*. Appleton-CenturyCrofts, New York, 1971.

[14] Mark Sundermeier, Alexander Zapf, and Matthias Beller. Palladium-catalyzed cyanation of aryl halides: recent developments and perspectives. *European Journal of Inorganic Chemistry*, 19:3513–3526, October 2003.

[15] S. R. Kline. Reduction and Analysis of SANS and USANS data using IGOR Pro. *Journal of Applied Crystallography*, 39:895–900, 2006.

[16] Hedi Mattoussi and Raymond Ober. Conformation of comblike liquid-crystalline macromolecules. *Macromolecules*, 23(6):1809–1816, November 1990.

[17] Gustavo A. Carri and M. Muthukumar. Configurations of liquid crystalline polymers in nematic solvents. *The Journal of Chemical Physics*, 109(24):11117, 1998.

[18] Neal R Scruggs, Rafael Verduzco, David Uhrig, Waliullah Khan, Soo-Young Park, Jyotsana Lal, and Julia A Kornfield. Self-assembly of coil–liquid-crystalline diblock copolymers in a liquid crystal solvent. *Macromolecules*, 42(1):299–307, 2009.

[19] Karin Viertler, Alf Wewerka, Franz Stelzer, George Fytas, and Dimitris Vlassopoulos. Macromolecular anisotropic association in isotropic solutions of a liquid crystal side chain polymer. *Macromolecular Chemistry and Physics*, 202(16):3174–3179, November 2001.

[20] Yiqiang Zhao, Alex M Jamieson, Brian G Olson, Ning Yao, Shaosheng Dong, Sergei Nazarenko, Xuesong Hu, and Jyotsana Lal. Conformation of comb-like liquid crystal polymers in isotropic solution probed by small-angle neutron scattering. pages 2412–2424, 2006.

[21] Bryan McCulloch, Victor Ho, Megan Hoarfrost, Chris Stanley, Changwoo Do, William T. Heller, and Rachel A. Segalman. Polymer chain shape of poly(3-alkylthiophenes) in solution using small-angle neutron scattering. *Macromolecules*, 46(5):1899–1907, March 2013.

[22] Michael Rubinstein and Ralph. H. Colby. *Polymer Physics*. Oxford Univeristy Press, New York, 2003.

[23] Soo-Young Park, Thangavelu Kavitha, Tahseen Kamal, Waliullah Khan, Taegyu Shin, and Baek-seok Seong. Self-assembly of dPS-liquid crystalline diblock copolymer in a nematic liquid crystal solvent. *Macromolecules*, 45(15):6168–6175, August 2012.

[24] Sawa Yoshiki, Kenji Urayama, and Toshikazu Takigawa. Temperature-responsive bending of nematic elastomers with hybrid molecular alignment. *Molecular Crystals and Liquid Crystals*, 549(1):106–112, October 2011.

[25] Rajratan Basu and Germano S. Iannacchione. Orientational coupling enhancement in a carbon nanotube dispersed liquid crystal. *Physical Review E*, 81(5):051705, May 2010.

Chapter 5

Self-Assembly of Coil-SGLCP Diblock Copolymers

Paul Pirogovsky and Rohan Hule contributed to the experiments discussed in this chapter. We traveled together to the NIST Center for Neutron Research (NCNR) and Oak Ridge National Lab's High Flux Isotope Reactor (HFIR), where we shared the responsibility of performing the neutron scattering experiments. We're grateful to Boualem Hammouda, John Barker, Lionel Porcar, and Cedric Gagnon at the NCNR and Ken Littrel, Lisa Debeer-Schmit, and Kathy Bailey at HFIR for with neutron scattering experiments. We thank Boualem Hammouda, in particular, for his help with interpretation of our SANS data.

We are grateful to the Macromolecular Complex Systems group at Oak Ridge National Laboratorys Center for Nanophase Material Sciences (CNMS), especially David Uhrig, for synthesizing our diblock prepolymers and Neal R. Scruggs and Rafael Verduzco for synthesizing the end-on and side-on polymers, respectively, from the diblock prepolymers. Paul Pirogovsky deuterated the starting material for the liquid crystal solvent according to a procedure that he optimized and Michael D. Wand, of LC Vision in Boulder, CO, made some great suggestions when I was designing a new synthesis of perdeuterated 4-pentyl-4'-cyanobiphenyl.

Paul Pirogovsky designed the temperature-controlled environment and the new sample cells we used at the beamline. Rohan Hule used diblock solutions that I made to prepare TEM samples and to carry out the unstained TEM measurements shown in this chapter. Stained TEM measurements were carried out on a trip I made to Professor Soo-Young Parks lab at in Kyungpook National University in Daegu, Korea with Waliullah Khan and several of his labmates at KNU. We're also grateful to the Tirrell lab for use of their spin-coater (and Larry Dooling, in particular for training and spin-coating troubleshooting) and the Haw lab at the University of Southern California for use of their pressure reactor for liquid crystal deuteration.

5.1 Abstract

The local chain conformation and self-assembled morphology of diblock copolymers consisting of a Side-Group Liquid Crystalline Polymer (SGLCPs) block and a random coil (polystyrene) block were investigated using Small Angle Neutron Scattering (SANS) and Transmission Electron Microscopy (TEM). SANS measurements of coil-SGLCP diblocks reveal the formation of anisotropic, self-assembled microstructures, substantiated by TEM observations. Size scales of the morphological features at both at the network ($>$100 nm) and intrachain (5-100 nm) levels were examined.

5.2 Introduction

In contrast to random coil polymers, SGLCPs adopt an anisotropic conformation when they are dissolved in a small-molecule LC solvent, because the side-group LC moieties couple locally to the director of the nematic solvent, leading to a synergistic ordering effect that has no counterpart in random coil polymers in conventional solvents [1] [2] [3]. We chose a flexible coil polymer that is generally insolu-

ble in LC solvent to provide a driving force for phase segregation when covalently linked to an SGLCPs block [4]. Coil-SGLCP block copolymers (BCPs) thus exhibit ordered morphologies that reflect the interplay of microphase segregation and LC order.

In solution, the thermodynamic interactions between polymer blocks and solvent determine the self-assembled structure: the same BCP, at the same concentration can adopt various morphologies, depending on the solvent [2] [4]. When a block copolymer is dissolved in a solvent that preferentially solvates one block, in this case, the LC block, in order to minimize the contact of the less soluble block with the solvent, block copolymers typically assemble into aggregates like micelles or vesicles. The solvents' "selectivity" or preference for one block over the other is determined by the Flory-Huggins thermodynamic interaction parameters χ between the solvent and each polymer block [5]. A nonselective solvent ($\chi_{A-solvent}$ = $\chi_{B-solvent}$), will partition more or less equally between the both blocks (A and B) of an A-B block copolymer, while a solvent strongly selective for one block (say, the A-block, $\chi_{A-solvent} >> \chi_{B-solvent}$), will partition strongly into this block, for example: into the corona of a diblock copolymers micelle, with the micelle core almost completely devoid of solvent [5].

LC gels formed by coil-SGCLP BCPs acquire the anisotropy inherent to the host solvent [2]. If the coil block is soluble in isotropic LC solvent, the morphology of the system will change significantly across the nematic-to-isotropic phase transition (T_{NI}). In contrast to conventional solvents, this large structural change occurs over a narrow temperature range (1-2°C) – a discontinuous first order phase transition with each phase having substantially different thermodynamic properties. Coil-SGLCP BCPs thus have potential applications as additive in small molecule LCs as rheology modifiers, surfactants [6] [7], alignment aids [3] [8], self-assembled charge transfer materials [9], and sensors. Swelling polymers with small molecule LC solvents can also improve the polymers response time upon application of an electromagnetic stimulus, making them good candidates for displays, where both long range order and fast response times are required [3].

The coupling between the LC solvents orientational order and the polymer backbone conformation is mediated by the side groups. End-on and side-on SGLCPs have profoundly different orientational coupling: the end-on SGLCP (Figure 5.1a) adopts a mildly oblate conformation, while the side-on SGLCP (Figure 5.1b) adopts a strongly prolate conformation (in both cases the symmetry axis coincides with the director). Because of the entropic penalty of dissolving isotropic PS in a nematic liquid crystal phase, PS is insoluble in the small molecule liquid crystal solvent 5CB at nematic temperatures [10] [11]. Thus, covalently attaching increasing molecular weight polystyrene (PS) coil blocks to end-on and side-on SGLCP blocks increases the complexity of the architecture and thus increases availability of new nanostructures; and controlling such nanostructures is necessary for molecular design of actuators and sensors and other SGLCP block copolymer applications.

Small angle scattering is ideal for studying the conformational anisotropy of SGLCPs themselves as well as the self-assembly of SGLCP-coil BCPs. In the case of SGLCPs in liquid crystal solvent, small angle neutron scattering (SANS) is essential first because insufficient contrast between the polymer and LC solvent seen in small angle x-ray scattering (SAXS) and second because SANS allow us to access the length scales (100s of nm) that are of interest to this study. Dilute solutions are characterized by scattering from single polymer chains, enabling us to get information about polymer size and self-assembly [12]. Scattering measurements are performed in Fourier space, also called reciprocal space to differentiate it from real space techniques such as microscopy [12]. Scattering data thus need to be either inverted back to real space or fitted reciprocal space-based models. It is not possible to reconstruct a complete image of the sample structure by scattering alone, complimentary techniques such as transmission electron microscopy (TEM), are necessary to investigate self-assembled architecture.

We have prepared matched pairs of end-on and side-on diblock copolymers using polymer analogous synthesis [3]: anionic prepolymers of polystyrene-1,2-polybutadiene (prepared at Oak Ridge National Laboratory's Center for Nanophase Materials) with systematically varied PS length (from 400 to 1150

units) and nearly constant 1,2-PB length (1050 $\pm$ 150 units) were converted to end-on (Figure 5.1, left) and side-on diblocks (Figure 5.1 center), to investigate the interplay between inherent LC order and diblock self-assembly using SANS and TEM.

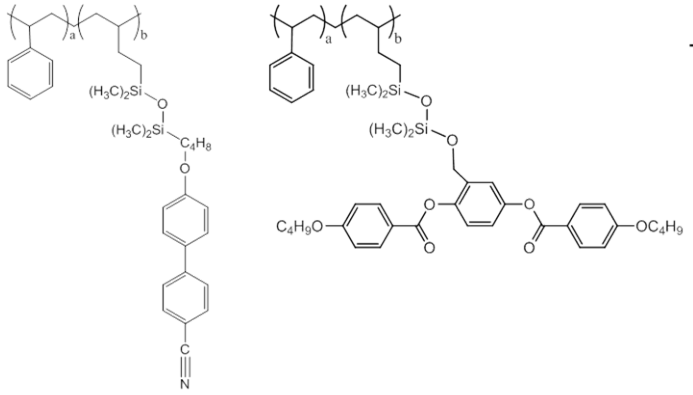

a	b
400	1250
550	1050
800	1100
1150	900

Figure 5.1. Our diblocks are made up of a polystyrene coil block and either a terminally attached, or "end-on" or laterally attached, or "side-on" SGLCP block. The diblocks have approximately constant SGCLP content, b, while their polystyrene content, a, varies across the series from less than that of the SGLCP to more than that of the SGLCP [4].

5.3 Experimental

5.3.1 Materials and Instrumentation

4-pentylbiphenyl was purchased from TCI America, deuterium oxide from Cambridge Isotope Labs. Anionic prepolymers for the SGCLPs were obtained from the Center for Nanophase Materials at Oak Ridge National Labs, in Oak Ridge, Tennessee (see below). Polished quartz plates for SANS cells were obtained from Technical Glass Products in Painesville Twp., OH. Elvamide 8023R® was obtained as a sample from DuPont Engineering Polymers. Metal Washers (1/32", $\sim$800 μm thickness) were obtained from McMaster Carr. Optically active glue, NOA68, was obtained from Norland Optical Products in Cranbury, NJ. All other reagents were purchased and used as received from Aldrich, unless otherwise noted.

Reaction temperatures were controlled by an IKAmag RET basic temperature modulator. Mechanical shaking of polymer solutions was carried using a Burrell Wrist Action Shaker, Model 75. Thin-layer chromatography (TLC) was performed using J. T. Baker silica gel IB and visualized by short wave UV (254 nm), EMD Silica gel (particle size 0.040-0.063 mm) was used for flash column chromatography. The deuteration of the LC solvent for SANS experiments was carried out in a PARR 4561 stirred pressure reactor with PTFE liner.

^{1}H NMR spectra were obtained using a Varian Inova 500 (at 500MHz) NMR; all spectra were recorded in $CDCl_3$ and referenced to tetramethylsilane.

The GPCs were carried out in tetrahydrofuran (THF) at 35°C eluting at 0.9 mL/min through four PLgel 10-μm analytical columns (Polymer Laboratories, PLgel 10 μm analytical columns, 30 cm long, 10^6 to 10^3 Å in pore size) connected to a Waters 410 differential refractometer detector (λ = 930 nm).

Liquid crystal phase transitions were observed using a Zeiss Universal Polarized Optical Microscope and a Mettler FP 82 hot stage, controlled by a Mettler FP 80 Central Processor. Optical Micrographs were taken with a Cannon EOS D30 digital camera.

Differential scanning calorimetry (DSC) was performed using a Perkin-Elmer DSC 7 calorimeter. The onset temperature and latent heat of the nematic-isotropic phase transition were calculated from DSC data using Perkin-Elmers Pyris® version 3.04).

SANS experiments were conducted on the NG3 beamline at the National Institute of Standards and Technology cold neutron source in Gaithersburg, MD and on the CG2 beamline at Oak Ridge National Laboratory's High Flux Isotope Reactor. Temperature control for later SANS experiments was achieved using a home-built Peltier-based temperature environment and controller that was designed and built by Paul Pirogovsky.

Transmission Electron Microscopy was taken on Hitachi H-7600 transmission electron microscope operating at 100 kV and FEI Technai-12 transmission electron microscope at an accelerating voltage of 120 kV.

5.3.1.1 Polymers

Matched pairs of "end-on" and "side-on" SGLCP-coil diblock copolymers, with polystyrene (PS) as coil blocks were prepared by former Kornfield Group members, Neal Scruggs and Rafael Verduzco using polymer analogous synthesis [3]. The anionic prepolymers, a series of four poly[styrene-*b*-1,2-polybutadiene diblock copolymers having approximately equally sized PB blocks and variably sized PS blocks were prepared using living anionic polymerization by David Uhrig at Oak Ridge National Laboratorys Center for Nanophase Material Sciences (CNMS). This prepolymer series, with systematically varied PS length (from 400 to 1150 units) and nearly constant 1,2-PB length (1050 $\pm$ 150 units). In each case, the polybutadiene (PB) block contained greater than 95 mol % 1,2-butadiene, the PB-type that is amenable to functionalization with LC side groups (the remainder of the PB block consisted of unreactive 1,4-butadiene).

Table 5.1. Diblock prepolymers with near-constant polybutadiene (PB) and polystyrene (PS) blocks that vary from 40 to 120 kg/mol (DP = 380 to 1140) were synthesized by the Center for Nanophase Materials at ORNL.

Prepolymer	PS Block Mn (kg/mol)	PB Block Mn (kg/mol)	Mole Fraction 1,2-PB	Mole Fraction 1,4-PB	Number of PS units (n)	Number of 1,2-PB units (m)	PS:PB Ratio
PS(400)-b-PB(1250)	43	68	0	0.01	380	1270	0.3:1
PS(550)-b-PB(1050)	59	55	0.15	0.05	570	1030	0.55:1
PS(800)-b-PB(1100)	83	59	0.05	0.03	760	1100	0.7:1
PS(1150)-b-PB(900)	121	45	0.22	0.01	1140	840	1.4:1

The reactive polybutadiene groups of each backbone were functionalized with either a terminally-attached cyanobiphenyl side group, or a laterally-attached butoxy-benzoate side group, resulting in "end-on" and "side-on" diblock copolymers, respectively. The end-on diblock copolymers were synthesized by Neal Scruggs and the side-on diblock copolymers were synthesized by Rafael Verduzco while they were both in the Kornfield Group.

Table 5.2. End-on and side on coil-SGLCP diblock copolymers were synthesized from prepolymers with polystyrene ("PS") and polybutadiene ("PB") blocks: end-on polymers are named "CB4" for the cyanobiphenyl side group, while side-on are labeled BB, for the 3,5-di(4-butoxybenoate side group and the numbers in the brackets correspond to the degree of polymerization (DP) of each of the blocks (*a* or *b*, Figure 6.1).

Prepolymer	End-on Diblock	Side-on Diblock
PS(400)-b-PB(1250)	PS(400)-b-CB4(1250)	PS(400)-b-BB(1250)
PS(550)-b-PB(1050)	PS(550)-b-CB4(1050)	PS(550)-b-BB(1050)
PS(800)-b-PB(1100)	PS(800)-b-CB4(1100)	PS(800)-b-BB(1100)
PS(1150)-b-PB(900)	PS(1150)-b-CB4(900)	PS(1150)-b-BB(900)

5.3.2 Methods

5.3.2.1 Polymer Fractionation

Some amount of cross-linking of these polymers (some of which were prepared as early as 2006 then stored under inert gas at -4°C) was unavoidable and when needed, these high molecular weight fractions were removed: first by filtration through at 0.45 μm PTFE syringe filter, followed, in the cases of the end-on homopolymers and diblock copolymers by solvent fractionation using a tetrahydrofuran-toluene mixture (60:40, THF:Toluene) as the good solvent and methanol (containing 10 ppm BHT) as the poor solvent. (The side-on polymers turned out to be difficult to fractionate via this method and were instead used as is.)

The polymer fractionation was carried out as follows: methanol was added at room temperature to solution of 0.5 wt.% polymer in good solvent until the cloud point is reached (generally, this turned out

to be an equal part methanol as good solvent). More methanol (about 5-15 mL) was added to ensure the separation of the high molecular weight fraction. The cloudy solution was then heated to 70°C until it became clear, whereupon it was poured into an oven-hot, insulated separatory funnel and allowed to separate slowly, overnight, protected from air currents. The next day, a viscous syrup composed largely of high molecular weight polymer sat at the bottom of the separatory funnel, and was easily drained off, precipitated with methanol, and dried in vacuum. The low molecular weight polymer remained in the dilute solution (above the high molecular weight fraction after cooling) and was recovered by evaporating the solvent, precipitating with methanol then drying in vacuum overnight.

5.3.2.2 Polymer Characterization

Proton nuclear magnetic resonance spectroscopy (^{1}H NMR). ^{1}H spectra (16 or 32 scans) of solutions of polymer (with concentrations of approximately 10 to 20 mg/mL) in $CDCl_3$ were recorded at room temperature on an Inova 500 MHz NMR spectrometer. The percent conversion of the pendent vinyl groups was determined by comparing the integrated area for the peaks corresponding to both the 1,2-polybutadiene and mesogen at 4.7-4.9 ppm, with peaks corresponding to the alkyl spacers on the mesogen.

Gel permeation chromatography (GPC). The side group liquid crystal polymers relative molecular weight and molecular weight distributions (PDI = M_w/M_n), were measured using gel permeation chromatography (GPC) calibrated with monodisperse PS standards.

2-7 mg polymer was dissolved in $\sim$1 mL of tetrahydrofuran (THF) and shaken for at least 30 min with a mechanical shaker. These solutions were filtered with a 0.45 μm syringe filter prior to being injected into the GPC. The total time to traverse all four columns was approximately 45 minutes.

Polarized light microscopy. Nematic-isotropic transition temperatures were measured using polarized light microscopy. First small drops (if small molecule LC) or chunks (if polymer) are sandwiched between an glass slide and a coverslip and examined using a Zeiss Universal optical microscope equipped with a Mettler FP82 hot stage and crossed polarizers. Each sample was heated from room temperature at a rate of 1 or 2 °C/min and the temperature at which the birefringent, nematic texture began to disappear was recorded as the nematic-isotropic transition temperature, T_{NI}. (Two temperatures were recorded for samples that became biphasic during the transition: the temperature at which the first circular black regions appear was recorded as the beginning of the biphasic range and the temperature at which the last birefringent regions disappear was recorded as the end of the T_{NI}.)

5.3.2.3 Transmission Electron Microscopy (TEM)

Polymer solutions in (hydrogenated) liquid crystal solvent for TEM. Dilute solution conditions were employed to ensure accurate measurements of morphological dimensions. Specifically, solutions of 0.5%, 1.0%, and 2.0% by weight SGLCP diblock copolymers in 5CB were prepared by dissolving known masses of the polymers and known masses of 5CB in organic solvent (tetrahydrofuran or dichloromethane), followed by mechanical shaking for at least one hour. The organic solvent was evaporated, first using gas pressure then completing the evaporation process by holding the nematic solutions under vacuum for at least 18 hours.

Stained TEM sample preparation. Stained TEM samples were prepared in three ways. In each case, the polymer solutions were prepared as above. In the first preparation method, droplets of the polymer-5CB solutions were spread on water at 40°C (above the T_{NI} of the 5CB) in a petri dish. Copper TEM grids were submerged in the water and then pulled up through the thin, spread-out 5CB layer. The grids were then dried overnight.

In the second preparation method, droplets of polymer-5CB solutions were again spread on water at 40°C (above the T_{NI} of the 5CB) in a petri dish. These LC films were then thinned by adding methylene chloride. Copper TEM grids were submerged in the water and then pulled up through the thinner, spread-out organic layer. The grids were then dried overnight. In the third preparation method, droplets of the polymer-5CB solutions were spread on water at 80°C in a petri dish. These LC films were physically thinned with a toothpick. Copper TEM grids were submerged in the water and then pulled up through the thin, spread-out 5CB layer. The grids were then dried overnight. All of the grids were then stained with ruthenium oxide vapor for 10 min.

Transmission electron microscopy (Stained TEMs). RuO_4-stained grids were imaged using a Hitachi H-7600 transmission electron microscope operating at 100 kV. TEM images were analyzed using the ImageJ software [13]. The diameters of at least 30 micelles with well-defined boundaries were measured.

Unstained TEM sample preparation. Unstained TEM sample preparation began with the preparation of 0.5 wt.% polymer solutions in 5CB. A 10 μL aliquot of each polymer solution was placed on a 300 mesh carbon-coated Copper grid using a syringe. The excess was blotted by Whatman filter paper. All grids were dried under ambient conditions for a minimum of 1 hr prior to imaging. At least three grids were prepared for each sample, and multiple images from each grid were used in image analysis.

Transmission Electron Microscopy (Unstained TEMs). Bright-field images of diluted, unstained SGLCP samples in 5CB were obtained using a FEI Technai-12 transmission electron microscope at an accelerating voltage of 120 kV with a Gatan CCD camera. TEM images were analyzed using the ImageJ software [13]. The diameters of around 50 micelles with well-defined boundaries were measured.

5.3.2.4 Small Angle Neutron Scattering

Solutions for small angle neutron scattering (SANS). Dilute solutions of polymers in perdeuterated liquid crystal solvent were prepared by dissolving the polymers in the perdeuterated 4-penyl-4-cyanobiphenyl using an organic co-solvent that is later evaporated away. Specifically, solutions of 1.0 weight percent SGLCP homopolymers and diblock copolymers in the perdeuterated liquid crystal solvent were prepared by first dissolving known masses of the polymers in volumetric amounts of tetrahydrofuran, and then shaking this mixture for greater than 30 minutes, resulting in either 5.0 or 2.5 mg/mL solutions. Known volumes of these known concentrations were combined (using a 500 μL syringe) with the nematic perdeuterated 4-pentyl-4'-cyanobiphenyl (d_{19}5CB) mixed by hand-rotating the vials, then evaporating the organic solvent under vacuum for at least 18 hrs.

Transition temperature determination. The T_{NI} of the solutions were measured, first in the lab, using a hotstage and polarized optical microscope, and then *in situ*, at the beamline.

Polarized light microscopy. Nematic-isotropic transition temperatures were measured in two ways. First small sandwiched between a glass slide and coverslip were examined using a Zeiss Universal optical microscope equipped with a Mettler FP82 hot stage and crossed polarizers. Each sample was heated from room temperature at a rate of 1 or 2 $^{\circ}$C/min and the temperature at which the birefringent, nematic texture began to disappear was recorded as the nematic-isotropic transition temperature, T_{NI}. (Two temperatures were recorded for samples that became biphasic during the transition: the temperature at which the first circular black regions appear was recorded as the beginning of the biphasic range and the temperature at which the last birefringent regions disappear was recorded as the end of the T_{NI}.)

***In situ* transition temperature measurements.** For the first set of experiments, the transition temperature was judged based on the light scattering of the red alignment laser at the NG3 beamline as we heated the sample in 0.25 and 0.5°C increments, waiting 10 minutes between each temperature change: in the nematic phase, the cloudy solution scattered the beam, while in the isotropic phase a bright red spot was visible. When the sample was undergoing its phase transition, the parts of the solution that were still nematic visible were distinguishable from the parts that were already isotropic. When we switched to using our home-built temperature controller, we measured the T_{NI} of the samples in situ using crossed polarizers and a flashlight

Sample cells and sample environment. Sample cells were prepared by sandwiching an $\sim$800μm aluminum spacer between quartz plates that were pretreated with a layer of rubbed polyimide or nylon to induce uniform alignment of the LC director. The alignment layer was created by either dip-coating the quartz in a 1% polyimide solution in N- methylpyrrolidone, or dip-, or spin-coating with 0.5% Elvamide8023R® in methanol (this solution was made by refluxing the Elvamide in methanol for $>$12 hrs), followed by unidirectional rubbing (with either velvet or a natural hair brush) greater than 50 times. The aluminum spacer was glued between the two quartz plates using either 5-minute epoxy or optically active glue and a UV source (254 nm).

Polymer solutions were loaded into the sample cells using a syringe. These samples were then heated to isotropic (often just using the heat of ones hand) and placed in a room-temperature vacuum oven for at least 8 hours, allowing the sample to align into a uniform monodomain and enough time for to remove any small air bubbles present in the sample. Initially, samples were heated with NCNR's single-cell holder heated with continuous flow of water whose temperature was controlled by a circulating water bath. After it was determined that a more well-controlled temperature environment was needed, Paul Pirogovsky designed a transmission geometry, Peltier-based sample environment that was used for all

subsequent SANS experiments. This enabled precise bidirectional temperature control ($\pm$ 0.05°C) over a range of $\pm$ 50°C from reference and nearly insantaneous temperature changes ($\sim$30 ms from minimum to maximum acheivable temperature). Further details can be found in Paul Pirogovsky's forthcoming PhD dissertation.

Small angle neutron scattering. Cells containing homogeneously aligned SGLCP solutions were mounted in our home-built temperature-controlled environment which was, in turn, held closely between the pole pieces of a 0.9 T electromagnet. The magnetic field served to reinforce the planar alignment induced by the rubbed alignment layers. The LC director was thus perpendicular to the incident neutron beam. Samples were annealed at the desired temperatures for at least ten minutes before to data was collected. Experiments were performed at multiple temperatures in the both the nematic phase and in the isotropic phase.

Incident monochromatic neutrons (λ = 6 Å) were scattered by the sample and collected on 2D detector. Two dimensional scattering patterns were collected at 3 sample-to-detector distances (1.3, 4.5, and 9 or 11 m). The patterns at all detector distances were combined to produce scattering curves over nearly 2 decades in q ($0.004\text{Å}^{-1} < \text{q} < 0.3$), where q = $4\pi\sin(\theta/2)/\lambda$, where θ is the scattering angle and is the wavelength of the incident beam. The raw data were converted to absolute coherent scattering intensities, I, as a function of q using corrections for detector inhomogeneity and sensitivity, background electronic noise, and incoherent scattering intensity according to standard procedures [14].

Two-dimensional scattering patterns collected at nematic temperatures were sector-averaged, specifically, data having the same magnitude of the scattering vector, q, in $\pm 10^{\circ}$ sectors in both the equatorial (horizontal) and meridional (vertical) directions were averaged to give the scattering parallel to the director, Ipar, and perpendicular to the director, Iperp, respectively. Two-dimensional scattering patterns of the deuterated solvent, d_{19}5CB, were sector averaged in the same way, and then subtracted from

each sector, to account for slight variation between the sectors (top, bottom, left, right) in the low q, in particular a strong flare in the bottom sector observed when the scattering was the lowest (*i.e.*, low concentration of polymer). Sectors without these features were chosen to represent the equatorial and meridional scattering, called "horizontal sector averages" and "vertical sector averages."

5.4 Results

2-D scattering of PS-SGLCP diblock copolymers in aligned nematic solvent show anisotropic patterns at nematic temperatures (Figure 5.2a and c). End-on diblocks display oblate conformations: the long axis of the scattering pattern is parallel to the director (Figure 5.2a), indicating that, in real space, the long axis of the polymer is perpendicular to the director. Side-on polymers, on the other hand, display prolate conformations: with the long axis of the scattering perpendicular to the director (Figure 5.2c), indicating the long axis of the polymer is parallel to the director. When heated to a temperature above the T_{NI} of the solvent, both side-on and end-on diblocks lose their conformational anisotropy and adopt spherical conformations (Figure 5.2b and d).

5.4.1 End-on Coil-SGCLP Diblock Copolymers.

2-D SANS patterns from all four end-on diblocks (having near-constant SGLCP DP and varying polystyrene lengths: from DP = 400 (40 kg/mol) to DP = 1150 (121 kg/mol)) reveal that at all polystyrene molecular weights, the end-on coil-SGLCP diblocks show oblate scattering at low-q (close to the beamstop) (Figure 5.3). Although the intensity and shape of the scattering in the horizontal direction does not appear to change much with increasing polysterene length, at least to first approximation, an interesting feature appears to develop in the *vertical* direction in the mid q range, as the polystyrene molecular weight increases: higher scattering intensity with an orientation that is perpendicular the low q scattering is

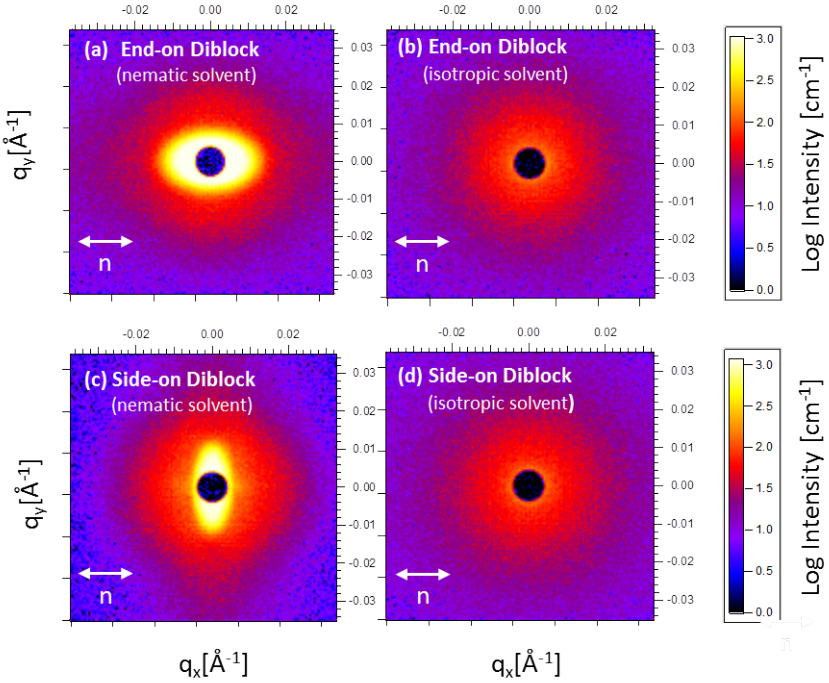

Figure 5.2. Representative 2-D small angle neutron scattering patterns of (a) an end-on SGLCP-polystyrene diblock copolymer (PS(550)-b-CB4(1050)) and (c) a side-on SGLCP-polystyrene diblock copolymer (PS(550)-b-BB(1050)) in aligned nematic solvent. The double-headed arrows indicate the orientation of the nematic director this alignment is created by a rubbed polymer alignment layer and reinforced by a 0.9T magnetic field. When the samples are heated above the nematic-isotropic transition temperature of the LC solvent, the scattering patterns of both the end-on (b) and the side-on (d) diblocks become circularly symmetric, indicating that the polymers adopt a spherical conformation.

observed in the mid q region. In each case, appearing in the merdional direction for end-on diblocks PS(550)-b-CB4(1050) (weakly), PS(800)-b-CB4(1100) (more obviously), and PS(1150)-b-CB4(900) (very strongly) (Figure 5.3). Given the length scale at which it appears, and its orientation, this diffuse scattering is ascribed to polystyrene-rich regions of the self-assembled objects.

The intermediate q scattering feature is also visible in 1D sector averages: a "bump" is seen at mid-q (0.009 Å $<$ q $<$ 0.04 Å) in the vertical sector average of the end-on diblocks (Figure 5.4). In fact, though the scattering feature is hard to discern in the 2-D scattering pattern of the diblocks with the smaller polystyrene M_w, PS(400)-b-CB4(1250), the feature appears, if weakly, in the 1-D sector averages (Figure 5.4a). Scattering in the vertical direction is complex. At lower q than the "bump" feature, scattering profiles display Porod-like (power law) features that arise from the periphery/interface of

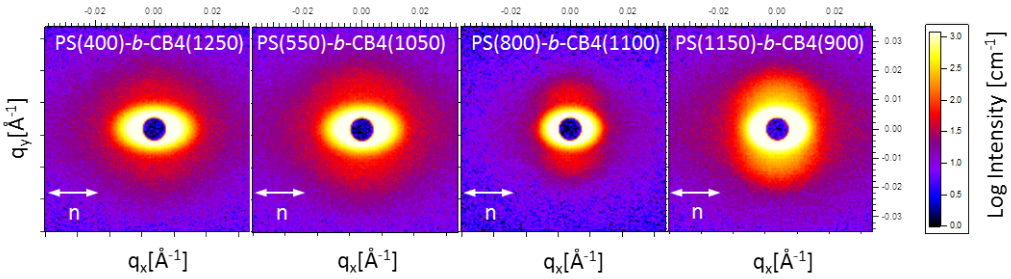

Figure 5.3. 2-D small angle neutron scattering patterns of end-on SGLCP-polystyrene diblock copolymers with near-constant SGLCP block length and increasing (from left to right) polystyrene block length.

the self-assembled morphologies, at very low q, it appears as though the scattering may be reaching a Guinier plateau (Figure 5.4). However, more points would be needed at lower q than was accessible to determine this conclusively. It thus appears that the full size of the objects formed by the self-assembly of the coil-SGCLP diblock copolymers in aligned nematic solution, at least in the vertical direction, is out of the measurement range of the SANS instrument. The size scale of the intermediate q feature in the vertical sector average, however, can be determined (see below). The horizontal sector averages of the end-on diblock copolymers in aligned nematic solvent are less complicated: a Guinier plateau is seen, from which sizes of self-assembled morphologies can be extracted.

Because of the apparent superposition of scattering from real-space features in the 1-D vertical sector averages, in particular the "bump" at mid q, the vertical sector average of the end-on diblock copolymers cannot be adequately described by a single expression over the entire q-range. Vertical sector averages were thus fit to the form:

$$I(Q) = Ge^{-Q^2R_g^2/3}, \qquad Q < Q_1, \tag{5.1}$$

$$I(Q) = A/Q^n + C/[1 + QL]^m + B, \qquad Q > Q_1, \tag{5.2}$$

a combination of the shape-independent Guinier and Lorentzian models. Models such as this have been

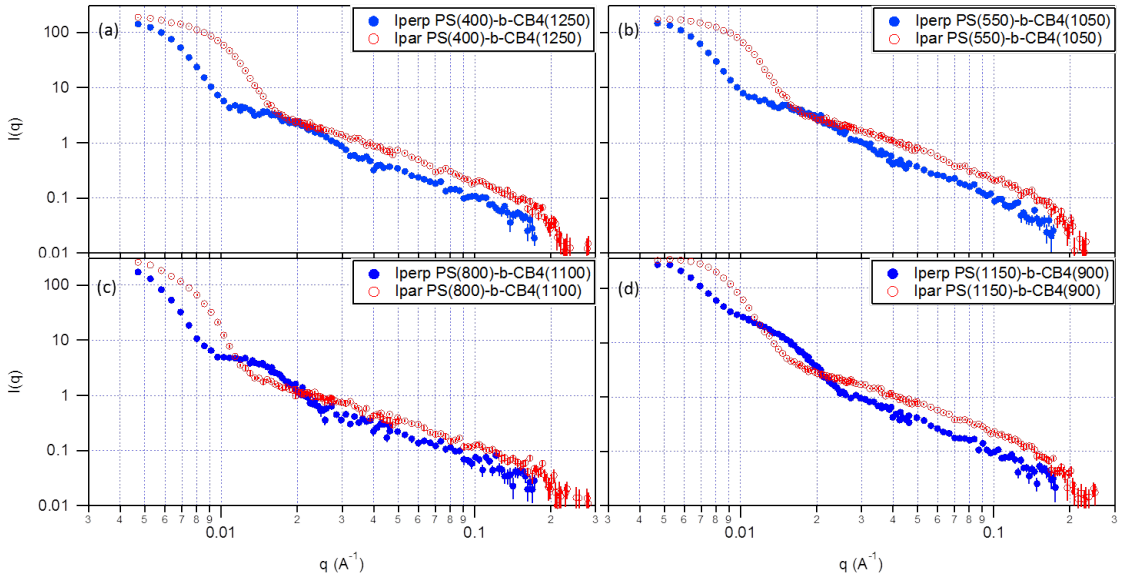

Figure 5.4. 1-D horizontal (red, open circles, Ipar) and vertical (blue, filled circles, Iperp) sector averages (10°) of small angle neutron scattering patterns of end-on coil-SGLCP diblocks with increasing polystyrene molecular weights, specifically, (a) PS(400)-b-CB4(1200), (b) PS(550)-b-CB4(1050), (c) PS(800)-b-CB4(1100) and (d), and PS(1150)-b-CB4(900).

used to fit many systems, including self-assembled peptide-based fibrillar hydrogel networks, [15] [16] semidilute solutions of SGLCP homopolymers [17] and a number of other systems [12]. Scattering in the low-q region is described by the first equation, the Guinier model (in this case the "low q region" is fit until q $<$ 0.01 Å, stopping where the scattering becomes power law at very-low q, the Guinier R_g that we extract in this manner will thus give us size of the "bump"). The first term in the second equation, A/Q^n corresponds to Porod scattering from the surface where the exponent, *n*, is predicted to be 4 when there is a sharp interface, and between 3 and 4 when there is less defined interface. The second term is a Lorentzian function describing the scattering from the polymer chains at high q, where L is a Lorentzian screening length, and *m* is predicted to be 2 when the polymer is in a theta solvent and 1.7 for an expanded polymer in good solvent. The third term, *B*, is the q-independent incoherent background scattering, while A and C are weighting factors for the first two terms. In this case, when fitting, B was set to near-zero, since the incoherent background did not appear to contribute much to the diblock copolymer scattering.

Preliminary fitting gave similar values of *n* and *m* for both end-on and side-on diblocks, regardless of polystyrene molecular weight or temperature. These values were therefore fixed, *n*, to 4, and *m* to 2, and a second round of fitting was carried out. A low-q exponent of 4 indicates a very sharp interface, while a high q exponent of 2 indicates Gaussian polymer chains in good solvent and is in good agreement with experimentally observed exponent for end-on homopolymer SGLCPs solutions. The extracted fitting parameters $R_{g\perp}$ and $L_{\perp}$ are shown in table 5.3.

Table 5.3. Chain shape parameters for end-on coil-SGLCP diblock copolymers in the parallel direction ($R_{g\|}$) are derived from Guinier fits and in the perpendicular direction ($R_{g\perp}$ and $L_{\perp}$) are derived by fitting a combination of the Guinier and Lorentzian shape-independent models.

End-on Diblock	$R_{g\|}$ (Gunier) (nm)	$R_{g\perp}$ (Gunier-Lorentzian) (nm)	$L_{\perp}$ (Gunier-Lorentzian) (nm)
PS(400)-b-CB4(1250)	21.08 ± 0.20	9.43 ± 0.17	2.19 ± 0.16
PS(550)-b-CB4(1050)	18.01 ± 0.37	9.78 ± 0.13	2.15 ± 0.16
PS(800)-b-CB4(1100)	31.9 ± 0.22	13.37 ± 0.19	1.88 ± 0.13
PS(1150)-b-CB4(900)	27.35 ± 0.36	15.80 ± 0.11	1.64 ± 0.04

Rather than the combined Guinier- and Lorentzian model, a simple Guinier fit was carried out on the horizontal sector averages of the end-on polymers, their shape being qualitatively different than the vertical sector average. A wide Guinier plateau can be seen in each 1-D scattering pattern (Figure 4, red open circles). A good linear fit was obtained over the q range $0.005\text{Å} < q < 0.008\text{Å}$, indeed this linear fit could extend to at least $q > 0.01\text{Å}$, but the condition $qR_g < 1.2$ was not satisfied for the higher q values, and the larger range was not used (values obtained for both fits were very similar). The extracted $R_{g\|}$ for all end-on coil-SGLCP diblock copolymers are shown in table 5.3.

Transmission electron micrographs (TEMs) positively-stained with ruthenium tetroxide (Figure 5.5a and c) are consistent with self-assembly into micelles composed of polystyrene-rich cores and diffuse SGLCP-rich coronas. Ruthenium tetroxide preferentially stains phenyl rings, which are present in both blocks of the diblock copolymers. Core-shell micelles are visible in TEM micrographs of all but the smallest polystyrene molecular weight end-on diblocks. On the other hand, unstained TEMs of the same

diblocks (Figure 5.5b and d), show spherical objects without visible distinction. Based on the size of these objects, we believe that the unstained TEMs show the dense polystyrene cores, while the more diffuse SGLCP corona has lower electron contrast in these images. Unstained TEM image analysis allows us to extract morphological dimensions without staining artifacts. Micelle diameters determined from both stained and unstained TEMs are summarized in table 5.4.

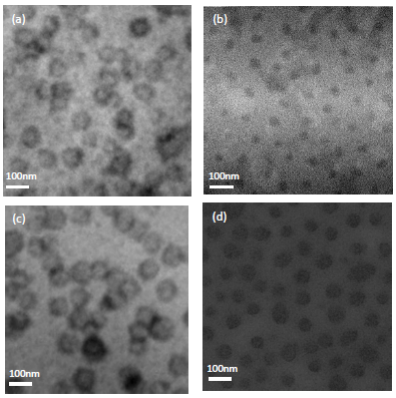

Figure 5.5. TEM micrographs of end-on SGLCPs PS(550)-b-CB4(1050) (a) stained with RuO_4 and (b) unstained, and PS(1150)-b-CB4(900) (c) stained with RuO_4 and (d) unstained. The scale bar in all cases is 100nm.

Table 5.4. Micelle diameters determined from ImageJ analysis of stained and unstained TEM micrographs of end-on coil-SGLCP diblock copolymers.

End-on Diblock	Diameter (Unstained TEM) (nm)	Inner Diameter (Stained TEM) (nm)	Outer Diameter (Stained TEM) (nm)
PS(400)-b-CB4(1250)	-	-	67.2 ± 20
PS(550)-b-CB4(1050)	28.1 ± 5.3	47.2 ± 7.4	102.1 ± 13.1
PS(800)-b-CB4(1100)	44.7 ± 7.1	53.9 ± 10.2	94.0 ± 12.2
PS(1150)-b-CB4(900)	48.9 ± 8	57.2 ± 8.8	93.0 ± 8.8

5.4.2 Side-on Coil-SGCLP Diblock Copolymers.

2-D scattering patterns of *side-on* coil-SGCLP diblock copolymers are qualitatively similar to the end-on diblocks, albeit with their aspect ratios reversed (Figure 5.6). In this case, scattering is more intense in the vertical direction at low q, with a diffuse feature appearing in the horizontal scattering at the mid q, with increasing polystyrene molecular weights. It should be noted here, that the vertical scattering of

PS(800)-b-BB(1100) appears to decrease in intensity, a phenomenon that we have yet to explain.

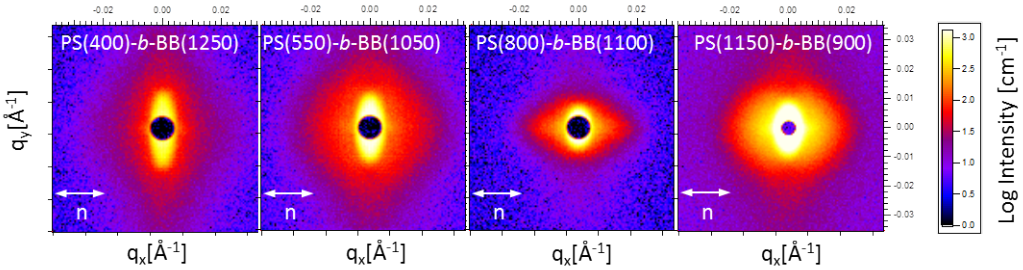

Figure 5.6. 2-D scattering patterns of side-on SGLCP-polystyrene diblock copolymers with near-constant SGLCP block length and increasing polystyrene block length (from left to right).

1-D sector averages of the side-on diblocks also show similar trends relative to the end-on diblock copolymers. In the horizontal sector averages (Figure 5.7, red open circles), a similar intermediate-q "bump" appears, followed by what appears to be the beginning of a power law regime at lower q. This power law is particularly visible in the scattering pattern of PS(1150)-b-BB(900), the polymer with the largest polystyrene molecular weight (Figure 5.7d, red open circles). This scattering pattern was was taken under slightly different experimental conditions that gave access to lower q data, making visible the beginnng of the low q power law region. Since the horizontal sector average (Ipar) of this highest molecular weight diblock at low-q is qualitatively similar to the vertical sector averages of the end-on SGLCPs, we assume that the horizontal scattering of the other side-on diblocks will also be similar, if lower q scattering data were available for these samples. This bump feature appears at lower q for the side-on SGLCP diblocks than for end-on diblocks, indicating a larger length scale. Again, it also appears that the overall self-assembled structure of the coil-SGLCP diblock copolymers, at least in the horizontal direction, cannot be determined by SANS alone.

The horizontal sector averages (Ipar) of the side-on on diblocks were fit with the Guinier-Lorentzian model, as above, while the vertical sector averages (Iperp) were fit with a simple Guinier approximation. Although the condition $qR_g < 1.2$ is not satisfied for all points of the Guinier approximation, particularly for the highest molecular weights, a good linear fit is obtained, as has also been reported for solutions

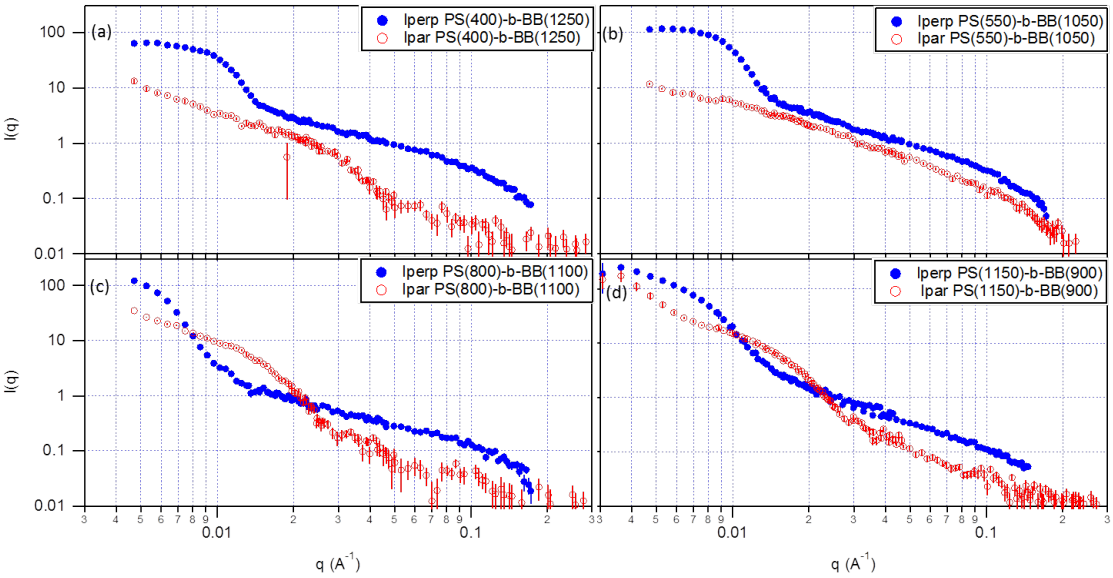

Figure 5.7. 1-D horizontal (red, open circles, Ipar) and vertical (blue, filled circles, Iperp) sector averages ($\pm 10^{\circ}$) of small angle neutron scattering patterns of side-on coil-SGLCP diblocks with increasing polystyrene molecular weights, specifically, (a) PS(400)-b-BB(1200), (b) PS(550)-b-BB(1050), (c) PS(800)-b-BB(1100) and (d), and PS(1150)-b-BB(900).

of SGLCP homopolymers [18]. Table 5.5 summarizes the parameters extracted from these fits.

Table 5.5. Chain shape parameters for side-on coil-SGLCP diblock copolymers in the parallel direction ($R_{g\|}$ and $L_{\|}$) are derived from Guinier fits and in the parallel direction ($R_{g\perp}$) are derived by fitting a combination of the Guinier and Lorentzian shape-independent models.

Side-on Diblock	$R_{g\|}$ (Gunier-Lorentzian) (nm)	$R_{g\perp}$ (Gunier) (nm)	$L_{\|}$ (Gunier-Lorentzian) (nm)
PS(400)-b-BB(1250)	8.34 ± 0.14	14.79 ± 0.90	1.40 ± 0.32
PS(550)-b-BB(1050)	10.65 ± 0.13	18.25 ± 0.69	3.91 ± 2.12
PS(800)-b-BB(1100)	15.88 ± 0.14	41.47 ± 0.14	1.50 ± 0.33
PS(1150)-b-BB(900)	15.81 ± 0.09	32.02 ± 0.57	1.11 ± 0.88

Unstained TEM images were obtained for side-on coil-SGCLP diblocks. The polystyrene core appears to give rise to the visible electron density contrast, while ensuring that staining artifacts do not interfere with data analysis.

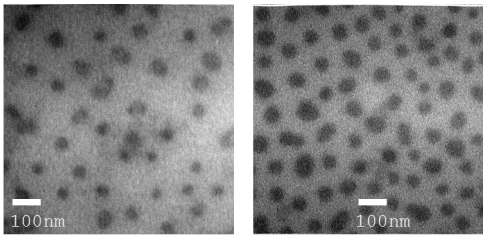

Figure 5.8. TEM micrographs of unstained side-on SGLCPs (a) PS(550)-b-CB4(1050), and (b) PS(1150)-b-CB4(900). The scale bar in all cases is 100 nm.

Table 5.6. Micelle diameters determined from ImageJ analysis of stained and unstained TEM micrographs of end-on coil-SGLCP diblock copolymers.

Side-on Diblock	Diameter (Unstained TEM) (nm)
PS(550)-b-BB(1050)	45.6 $\pm$ 6.2
PS(1150)-b-CB4(900)	55.1 $\pm$6.8

5.5 Discussion

The self-assembly of side-on and end-on coil-SGLCP diblock copolymers with near constant SGLCP block lengths and increasing polystyrene block lengths (40 kg/mol to 120 kg/mol) was investigated using SANS and TEM. Chain conformations were observed using SANS, a global tool for quantitatively measuring polymer conformation and morphology. 1-D sector averages show complex architecture, indicating, anisotropic self-assembly in aligned nematic solvent. Although the length scale of the entire self-assembled object was determined to be too large to be entirely observed within the q-range of the SANS experiments, positively-stained TEM micrographs gave the length scales of approximately 100 nm. Unstained TEM micrographs show dense objects, approximately correlated in size with the inner diameter of the core-shell micelles shown in the stained TEM (Figure 5.5). The size of this core also seems to correlate well with the Guinier-derived R_g in the horizontal direction for the end-on diblocks and the horizontal direction for the side-on diblocks.

When they studied polystyrene-b-polyisoprene diblocks of comparable molecular weights in selective solvents, Lodge [19] and Register [20] found micelle diameters in the range of 10-20 nm, but TEM micrographs of both side-on and end-on PS-SGLCP diblock copolymers show diameters on the order

of 60 to 100 nm (Figures 5.4 and 5.8), when dissolved in 5CB, too large for the PS to span a micelle.

We thus propose that the structure formed by the self-assembly of coil-SGLCP diblock copolymers in deuterated nematic solvent consists of anisotropic micelles. The micelles appear to be made up of dense, anisotropic PS-rich cores, surrounded by relatively diffuse, swollen SGLCP-rich coronas. Due to the lower degree of solvation (and therefore greater hydrongen density) of the core, the SANS intensity appears to be dominated by the scattering from the core. This anisotropic structure is directly observable in algined SANS experments because of the uniform director oerientation provided by a rubbed alignment layer and reinforced by a magnetic field. That the TEM micrographs do not show anisotropic structures can be explained by the known homeotropic alignement of 5CB in a suspended film.

Scattering exponents describing local and "network" chain conformations at two length scales were studied using SANS and corroborated in real space using TEM: at larger length scales, the Porod exponent of 4 seen for all polymers, corresponds to a sharp interface, corroborating what appears to core-shell micelles with dense polystyrene cores in the TEM micrographs.

A diffuse scattering feature appears in the vertical direction for end-on diblocks and in the horizontal direction for side-on diblocks and increases with polymer molecular weight and is ascribed to polystyrene packing. Sizes of this feature determined by fitting to a correlation length model were smaller than both the inner diameter of the core-shell micelles seen in the stained TEMs, and the diameters determined from the unstained TEMS, though these calculated sizes, too, in general increase in length scale with increasing polystyrene molecular weight (from 20 to 30 nm in the end-on diblocks and from $\sim$8.5 nm to 16 nm in the side-on diblocks). The correlation lengths determined from the fit were all on the order of 2 nm, potentially corresponding to the approximate distances between adjacent side groups.

For the end-on coil-SGLCP diblock, the shape and anisotropy of the core appears to depend on both

the SGLCP and polystyrene block length. Although, SGLCP backbones were designed to be close in molecular weight, some variation was inevitable. While the core dimensions determined from SANS to increase with increasing polystyrene M_w (Table 5.3), in the perpendicular direction this trend is monotonic, while in the parallel direction the $R_{g\|}$ of PS(550)-b-CB4(1050) is small than that of PS(400)-b-CB4(1250) and $R_{g\|}$ of PS(1150)-b-CB4(900) is small than that of PS(800)-b-CB4(1100). In these cases the, the *SGLCP* M_w is smaller for the polymers displaying smaller $R_{g\|}$, even though the polystyrene M_w is greater. The SGLCP block thus contribution to the size of the assembly is not insignificant.

5.6 Conclusions

The structure and self-assembly of side-on and end-on coil-SGLCP diblock copolymers in aligned nematic solvent was investigated using small angle neutron scattering and transmission electron microscopy. Polymers with liquid crystal blocks with near-constant molecular weight, and four different lengths of amorphous polystyrene blocks were examined. Nematic solvent is strongly selective for the SGLCP block driving the self-assembly into large anisotropic objects, as indicated by the complex small angle neutron scattering patterns. Combining SANS with both positively-stained and nonstained TEM enabled direct correspondence between structural features found in the anisotropic scattering and micelle sizes.

Increased morphological and conformational comprehension of these coil-SGLCP diblocks can open opportunities for design of responsive LC interfaces with in-built functionality of the coil domain.

Bibliography

[1] Leroux N. Mery S. Noirez L. Hardouin, F. Small angle neutron scattering experiments on "side-on fixed" liquid crystal polysiloxanes. *Journal de Physique. II*, 2(3):271–278, 1992.

[2] Michael D. Kempe, Julia A. Kornfield, and Jyotsana Lal. Chain anisotropy of side-group liquid crystalline polymers in nematic solvents. *Macromolecules*, 37(23):8730–8738, 2004.

[3] Michael D. Kempe, Neal R. Scruggs, Rafael Verduzco, Jyotsana Lal, and Julia A. Kornfield. Self-assembled liquid-crystalline gels designed from the bottom up. *Nature Materials*, 3(3):177–82, March 2004.

[4] Neal R. Scruggs, Rafael Verduzco, David Uhrig, Waliullah Khan, Soo-Young Park, Jyotsana Lal, and Julia A. Kornfield. Self-assembly of coil–liquid-crystalline diblock copolymers in a liquid crystal solvent. *Macromolecules*, 42(1):299–307, 2009.

[5] Michael Rubinstein and Ralph. H. Colby. *Polymer Physics*. Oxford Univeristy Press, New York, 2003.

[6] Dong-Yul Lee, Jung-Min Seo, Waliullah Khan, Julia A. Kornfield, Zuleikha Kurji, and Soo-Young Park. pH-responsive aqueous/LC interfaces using SGLCP-b-polyacrylic acid block copolymers. *Soft Matter*, 6(9):1964, 2010.

[7] Waliullah Khan, Jin Ho Choi, Gyu Man Kim, and Soo-Young Park. Microfluidic formation of pH responsive 5CB droplets decorated with PAA-b-LCP. *Lab on a Chip*, 11(20):3493–8, October 2011.

[8] Pola Goldberg-Oppenheimer, Dinesh Kabra, Silvia Vignolini, Sven Hüttner, Michael Sommer, Katharina Neumann, Mukundan Thelakkat, and Ullrich Steiner. Hierarchical orientation of crystallinity by block-copolymer patterning and alignment in an electric field. *Chemistry of Materials*, 25(7):1063–1070, April 2013.

[9] Zlatka Stoeva, Zhibao Lu, Malcolm D. Ingram, and Corrie T. Imrie. A new polymer electrolyte based on a discotic liquid crystal triblock copolymer. *Electrochimica Acta*, 93:279–286, March 2013.

[10] Hironobu Hori, Osamu Urakawa, and Keiichiro Adachi. Dielectric Relaxation in Phase-Segregated Mixtures of Polystyrene and Liquid Crystal 5CB. *Macromolecules*, 37(4):1583–1590, February 2004.

[11] Neal R. Scruggs, Julia A. Kornfield, and Jyotsana Lal. Using the switchable quality of liquid crystal solvents to mediate segregation between coil and liquid crystalline polymers. *Macromolecules*, 39(11):3921–3926, May 2006.

[12] Julia S. Higgins and Henri C. Benoit. *Polymers and Neutron Scattering*. Oxford Univeristy Press, Oxford, 1994.

[13] C. A Schneider, W. S Rasband, and K. W. Eliceiri. NIH Image to ImageJ: 25 years of image analysis. *Nature Methods*, 9:671–675, 2012.

[14] S. R. Kline. Reduction and analysis of SANS and USANS data using IGOR Pro. *Journal of Applied Crystallography*, 39:895–900, 2006.

[15] Rohan A. Hule, Radhika P. Nagarkar, Ayesegul Altunbas, Hassna R. Ramay, Monica C. Branco, Joel P. Schneider, and Darrin J. Pochan. Correlations between structure, material properties and bioproperties in self-assembled B-hairpin peptide hydrogels. *Faraday Discussions*, 139:251–264, 2008.

[16] Rohan A. Hule, Radhika P. Nagarkar, Boualem Hammouda, Joel P. Schneider, and Darrin J. Pochan. Dependence of self-assembled peptide hydrogel network structure on local fibril nanostructure. *Macromolecules*, 42(7137-7145), 2009.

[17] Neal R. Scruggs and Julia A. Kornfield. Synergistic ordering of side-group liquid crystal polymer and small molecule liquid crystal: order and phase behavior of nematic polymer solutions. *Macromolecular Chemistry and Physics*, 208(1920):2242–2253, October 2007.

[18] Yiqiang Zhao, Alex M Jamieson, Brian G Olson, Ning Yao, Shaosheng Dong, Sergei Nazarenko, Xuesong Hu, and Jyotsana Lal. Conformation of comb-like liquid crystal polymers in isotropic solution probed by small-angle neutron scattering. pages 2412–2424, 2006.

[19] Timothy P Lodge, Bryant Pudil, and Kenneth J Hanley. The full phase behavior for block copolymers in solvents of varying selectivity. *Macromolecules*, 35(12):4707–4717, 2002.

[20] Chiajen Lai, William B. Russel, and Richard A. Register. Phase behavior of styrene-isoprene diblock copolymers in strongly selective solvents. *Macromolecules*, 35(3):841–849, 2002.